UNIVERSITÀ DEGLI STUDI FIRENZE

DOTTORATO DI RICERCA IN
SCIENZE BIOMEDICHE
CICLO XXVI

COORDINATORE Prof. Persio Dello Sbarba

Electromechanical and energetic dysfunction in HCM mouse models carrying troponin T mutations.

Settore Scientifico Disciplinare BIO/09

Dottorando

Dott.ssa Tosi Benedetta

Tutori

Prof. ssa Chiara Tesi

Prof. Corrado Poggesi

Coordinatore
Prof. Persio Dello Sbarba

Anni 2011/2014

Electromechanical and energetic dysfunction in HCM mouse models carrying troponin T mutations.

TABLE OF CONTENTS

1: Aims and introduction

1.1 Hypertrophic Cardiomyopathy (HCM): a sarcomere disease.

1.1.1 HCM genetic, clinical and therapeutic features.

Hypertrophic cardiomyopathy (HCM) is a dominant disease of the cardiac sarcomere, occurring in 1:500 people (Maron, 2002). HCM is the most prevalent cardiovascular single gene disorder and it is characterized by the presence of left ventricular hypertrophy (LVH)- left ventricular wall and septal hypertrophy- in the absence of other cardiac or systemic disease, such as pressure overload (systemic hypertension, aortic stenosis) or other multisystem illness (storage or infiltrative diseases). LVH is typically asymmetric (Klues et al, 1995) and usually involves the basal anterior septum and anterolateral free wall, where, generally, maximum wall thickness values are observed (Olivotto et al, 2006). The degree of hypertrophy may be mild (13-15 mm) or extreme (> or =30 mm) with an average wall thickness of 23 ± 5 mm (Goldman et al, 1984a) (Goldman et al, 1984b) see **Fig 1.1.1a**. Obstruction of the left ventricular outflow tract is present at rest in approximately 25% of patients. Although HCM is a very heterogeneous disease, the diagnosis is based on the two-dimensional echography identification of an otherwise unexplained LVH (Goldman et al, 1984a), however, it is important to treat HCM not solely as a hypertrophic disease but as a progressive cardiac pathology that leads to complex changes in ventricular geometry and function. Although the underlying gene mutation is present before birth, the age at onset varies widely, the disease penetrance can in fact remain incomplete through the age of 60 years or can develops at puberty(Kokado et al, 2000; Maron, 2002; Niimura et al, 1998).

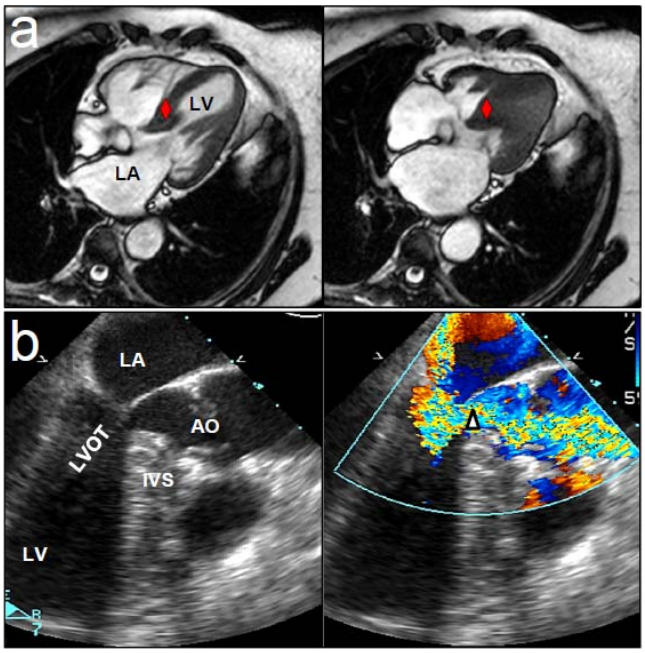

Fig 1.1.1a The HCM features. Representative MRI images at end-diastole (left) and end-systole (right) showing asymmetric upper septal hypertrophy. ◊ indicates the septum. **(b)** Trans-esophageal echo section showing obstructed left ventricular outflow tract (left) and corresponding color-doppler image (right), displaying accelerated turbulent blood flow during systole (Δ). LV= left ventricle; LA=left atrium; AO=ascending aorta; LVOT=LV outflow tract; IVS= inter ventricular septum. Modified from Coppini et al, 2013.

The first disease-causing missense mutation was the R403Q in the β-cardiac myosin heavy chain (*β-MyHC*), identified in 1990 (Geisterfer-Lowrance et al, 1990). This discovery and the further confirmations of a prevalence of mutations in sarcomeric proteins established the paradigm that HCM is primarily a "disease of the sarcomere". Molecular genetics has revealed that HCM is a complex molecular disease, exhibiting both gene and allele heterogeneity (multiple disease genes and multiple mutations), and it is caused by more than 400, predominantly missense, mutations in any 1 of the 10 genes each encoding sarcomere proteins. The HCM-causing mutant genes encode: β-MyHC, cardiac myosin binding protein-C (cMyBP-C) both regulatory (RLC) and essential (ELC) myosin light chains,

α-tropomyosin (α-Tm), cardiac troponin I (cTnI) cardiac troponin T (cTnT), cardiac troponin C (cTnC), cardiac actin and the giant structural protein titin (Belus et al, 2008; Marian & Roberts, 2001; Seidman & Seidman, 2001; Thierfelder et al, 1994). Three genes account for most known mutations: *MYH7* (β-MyHC), *MYBPC3*(cMyBP-C) and cardiac troponin T (*TNNT2*) (Olivotto et al, 2011) see **Fig 1.1.1b**. The 60-70% of HCM affected individuals is considered to have myofilament-positive HCM. The remaining patients show no discernible myofilament mutations and are considered to have myofilament-negative HCM; of note, with the wider availability of genetic screening for HCM-related mutations, the number of detected genotype-positive mutation carriers without cardiac hypertrophy is increasing: in the Florence cohort of HCM patients' relatives, 200 undiseased mutation carriers have been already recognized.

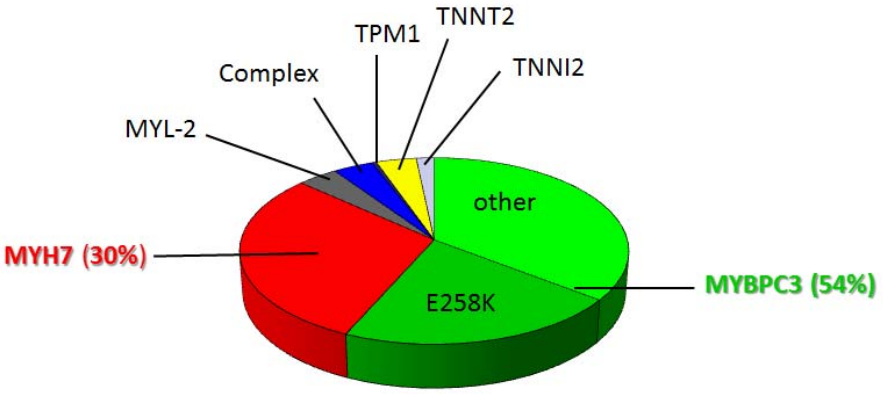

Mutational analysis	N= 384
Myofilament negative	**141 (36.7%)**
Myofilament positive	**243 (63.3%)**
Thick filament	**218 (90%)**
MYBPC3 (Protein C)	**137 (56.4%)**
MYBPC3 (E258K)	**49 (20.2%)**
MYH7 (Myosin Heavy Ch.)	**72 (29.6%)**
MYL2 (Myosin Light Ch.)	**9 (3.7%)**
Thin filament	**17 (7%)**
TNNT2 (Troponin T)	**12 (4.9%)**
TNNI3 (Troponin I)	**2 (0.8%)**
TPM1 (Tropomyosin)	**2 (0.8%)**
ACTC (Actin)	**1 (0.4%)**
Complex (multiple genes)	**8 (3.2%)**

Figure 1.1.1b Mutational analysis and distribution of mutations in myofilament–positive HCM population. The study included 384 unrelated index patients in Florence, with a confirmed clinical diagnosis of HCM, consecutively enrolled at the Azienda Ospedaliera-Universitaria Careggi, in Florence. The most frequent disease-associated gene was *MYBPC3* (36.4%; including 9 patients with double mutations in this gene). The *MYBPC3* E258K mutation, which was found in 49 index patients, suggested a founder effect and was associated with heterogeneous cardiac morphology and clinical presentation. 21% had mutations in other thick-filament protein genes (72 in *MYH7* and 9 in *MYL2*) and 4.5% in thin filament protein genes (12 in *TNNT2*, 2 in *TPM1*, 2 in *TNNI3*, and 1 in *ACTC*). Eight patients (2%) were double heterozygous (i.e. carried mutations in 2 different genes). Modified from (Olivotto et al, 2008).

Histologically, **myocyte disarray** and interstitial fibrosis are pathognomonic of the disease (see **Fig1.1.1c**). Myocyte disarray is defined as a profound derangement of myocyte alignment, with loss of the physiological, parallel orientation of the cells, arranged in a chaotic pattern and forming a typical disorganized architecture (Basso et al, 2000; Maron, 2002). The functional consequences of disarray may affect LV mechanics by interfering with the physiological homogeneity of contraction and relaxation (Ho et al, 2002) and represent a potential substrate for ventricular arrhythmias (Basso et al, 2000).

Variable and sometimes striking patterns of **intra-myocardial fibrosis** have been described in HCM hearts based on pathological studies (Basso et al, 2000) and, more recently, by cardiac magnetic resonance (CMR) techniques allowing in vivo visualization of areas of late gadolinium enhancement (LGE)(Olivotto et al, 2006; Olivotto et al, 2008). CMR late gadolinium enhancement is present in about two-thirds of HCM patients, varying from very limited to large, confluent, infarct-like patches occupying significant proportions of the LV (Olivotto et al, 2008). LGE localizes preferentially to the most hypertrophied regions of the ventricle, often represented by the basal and mid-septum, and are more often found in patients with diffuse and severe hypertrophy. Preliminary evidences points to LGE areas as a potential substrate of ventricular arrhythmias (Adabag et al, 2008).

Another pathophysiological hallmark of HCM is **microvascular dysfunction**. In the past decade, a number of studies have demonstrated that in HCM patients the coronary vasodilator reserve is markedly impaired not only in the hypertrophied septum, but also in the least hypertrophied LV free wall (Camici & Crea, 2007; Olivotto et al, 2006). In the absence of epicardial coronary stenosis, this finding is indicative of diffuse microvascular dysfunction, in line with pathologic evidence of marked and widespread remodeling of the intramural coronary arterioles (Basso et al, 2000), which show smooth muscle hyperplasia and disorganized elastic fibers, causing deformation and irregular narrowing of the vessel lumen. Microvascular dysfunction is the most important substrate for recurrent ischemia in HCM, and has been shown to represent an important predictor of long-term prognosis and adverse LV remodeling (Camici & Crea, 2007; Olivotto et al, 2006). Although systolic contractility is preserved and features of hypercontractility are observed at the whole heart level, outflow obstruction and impaired relaxation can cause progressive forward and backward heart failure and an increased incidence of ventricular arrhythmia can lead to sudden cardiac death.

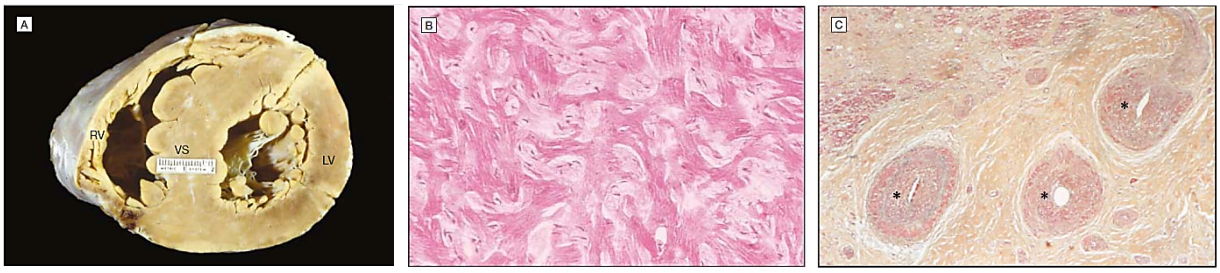

Figure 1.1.1c Pathophysiological hallmark of HCM. (A) Gross heart specimen from a 13-year-old male competitive athlete showing a disproportionate ventricular septum hypertrophy (VS) with respect to le left ventricular (LV) free wall (RV, right ventricle). (B) Myocardial disarray in the thickened VS. Bizarre hypertrophied cardiomyocytes forming the typical disorganized architecture of HCM (C) micro-vascular dysfunction, abnormal intramural coronary arteries dispersed within replacement fibrosis. (Modified from (Maron, 2002)

There is substantial variation in clinical manifestations, cardiac morphology, symptom burden, and prognosis (Gersh et al, 2011). Although most patients with HCM have a normal life expectancy, symptoms of pulmonary congestion, chest pain, and exercise intolerance result in substantial limitations despite medical or surgical therapy. HCM can also result in striking events, including the

development of end stage heart failure leading to death or cardiac transplantation, or a high risk of sudden cardiac death.

Diastolic dysfunction with an impaired LV filling seems to be the first change in myocardial function in HCM mutation carriers without hypertrophy, both in animal models and in patients (Ho et al, 2002; Nagueh et al, 2003). The origin of diastolic dysfunction in HCM is multifactorial and complex, with changes at the cellular level (e.g. impaired sarcomeric function and Ca^{2+} handling) and also abnormalities at the tissue level (myocyte disarray, interstitial fibrosis, microvascular dysfunction). Diastolic dysfunction is the main determinant of symptoms in HCM patients: reduced exercise capacity, chest pain and discomfort, dyspnea episodes, are all associated with impaired myocardial relaxation, which leads to increased ventricular filling pressure and increased atrial pressure (Goldman et al, 1984a).

Sudden Death (SD) occurs in 1-2 % of HCM patients and identifying high-risk patients remains a very challenging task. SD in HCM is arrhythmia-based due to primary ventricular tachycardia/fibrillation (VT/VF) (Maron et al, 2007) with a relationship to patient age (Maron, 2002). SD may occur at a wide range of ages with the highest rate during adolescence and young adulthood, most commonly less than about 25 to 30 years of age. Indeed, HCM is now recognized as the most common cause of SD in young people (Maron, 2003). The predisposition of HCM patients to arrhythmias is well established, and may include virtually all known rhythm disturbances. Sustained ventricular arrhythmias bear the greatest prognostic relevance, as the most frequent cause of sudden death in this population (McLeod CJ et al.2009). A major goal in treatment of HCM is to limit the life-threatening consequences of arrhythmia. The greatest limitation to this however is the relative lack of knowledge about the molecular and cellular mechanisms determining HCM-related pro-arrhythmic substrate. While tissue fibrosis and microvascular dysfunction might provide a substrate for the maintenance of ventricular automaticity by favoring establishment of reentry circuits, to date no knowledge of the cellular triggers for arrhythmias initiation in HCM is present. In spite of considerable advances in understanding HCM genetics and pathophysiology, current pharmacological treatment of patients with HCM has remained largely empiric and unchanged over the past two decades.

Recently, a simple framework for systematic clinical staging of the disease has been proposed. Four clinical stages have been identified, with special emphasis on diagnosis, potential mechanisms, challenges for management, and targets for future investigation: these are defined as *nonhypertrophic HCM*, *classic* phenotype, *adverse remodeling*, and *overt dysfunction* and Issues HCM).

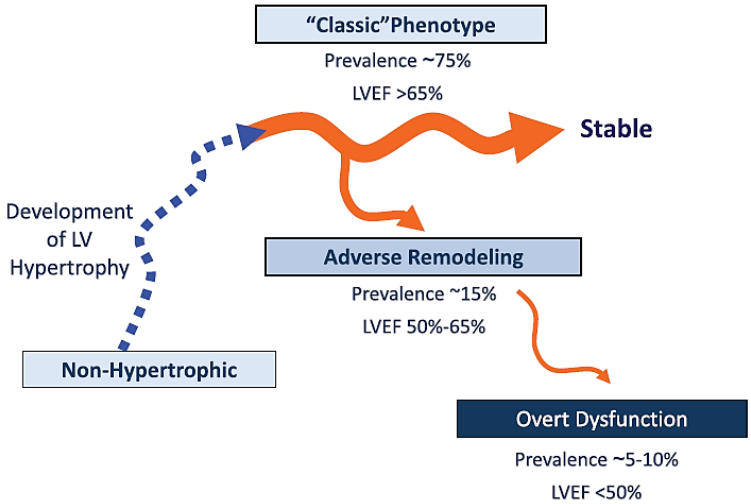

Figure 1.1.1d Stages of hypertrophic cardiomyopathy. Thickness of the **orange lines** reflects prevalence of each stage in HCM cohorts. Prevalence of nonhypertrophic HCM is unknown. LVEF indicates left ventricular ejection fraction.

Nonhypertrophic HCM is a state characterized by the absence of LV hypertrophy in individuals harboring HCM-causing mutations, investigated in the course of systematic family screenings. Subtle echocardiographic abnormalities may be found, such as impaired LV relaxation, mitral valve or subvalvar abnormalities, and mild degrees of left atrial (LA) dilatation, all of which are not diagnostic per se but may be instrumental to suspecting HCM in a familial context. Furthermore, elevated levels of type I collagen precursors has been found and coronary microvascular function may be altered in genotype-positive individuals. The whole spectrum of abnormalities may be present in individuals with nonhypertrophic HCM.

Classic HCM phenotype is defined as the phase in which the hypertrophic phenotype is fully expressed and the LV is hyperdynamic (as defined by an ejection fraction [EF] >65%), in the absence of extensive fibrotic changes suggesting unfavorable progression. The majority of HCM patients in cross-sectional studies belong to this stage.

Adverse remodeling is defined by the presence of unfavorable structural modifications, superimposed to the "classic" HCM phenotype, translating into increasing LV fibrosis and worsening function (ie, an LVEF in the low-normal range of 50% to 65%), with relatively preserved clinical and hemodynamic balance. Rather than being an "average" process, this seems to represent a selective pathway followed by about 15% to 20% of HCM patients, a smaller proportion of whom will ultimately progress to overt dysfunction and heart failure.

Overt dysfunction is an uncommon clinical evolution of HCM and represents about 5% of patients in most cohorts. It is characterized by severe functional deterioration of the LV (defined by an LVEF <50%), subtended by extreme degrees of fibrosis and remodeling and generally associated with hemodynamic decompensation and adverse. This subset coincides with so-called "end-stage" HCM.

The effective **treatment of HCM**, whether pharmacological or not, has to target the underlying mechanism(s) responsible for the clinical phenotype. Current pharmacological treatment of human HCM, while effective for symptomatic improvement, has not been established to prevent, attenuate, or reverse cardiac hypertrophy in humans with HCM or even impact the prognosis (Marian, 2008). The most commonly used pharmacological agents are the β-blockers, which are the mainstay of therapy and the first choice in the absence of a contraindication. The proposed mechanisms of effects include improved ventricular relaxation and increased diastolic filling time and, hence, improved left ventricular end diastolic pressure as well as perfusion (Ostman-Smith et al, 1999). Otherwise, the benefits of β-blockers on mortality and the risk of SCD in patients with HCM and their impact on prevention or reversal of cardiac hypertrophy in HCM remain to be established.

Verapamil and diltiazem have been used for over two decades though not proven to impart significant effects on cardiac hypertrophy or prognosis in patients with HCM (McTaggart, 2004).

Patients with LV outflow tract obstruction comprise up to 70% of the patients with HCM (Ommen et al, 2008). Apart from obstruction relief with surgical myectomy, drugs are used to attenuate obstructive symptoms. Disopyramide, a class I anti-arrhythmic drug, is used in conjunction with β-blockers to attenuate left ventricular outflow tract (LVOT) obstruction and improve symptoms (Sherrid et al, 2005). The beneficial effects of disopyramide are largely due to its negative inotropic effects. Disopyramide does not reverse or attenuate cardiac hypertrophy in patients with HCM. Alterations of intracellular Ca^{2+}-handling are probably the earliest and most important changes leading to hypertrophy development and diastolic dysfunction and all other changes might be secondary to those. With the exception of I_{CaL}, no potential therapeutic targets directly affecting HCM-related E-C coupling alterations have been identified. Consequently, one major pathogenic mechanism in HCM still remains devoid of an effective therapeutic measure. Moreover, none of the aforementioned drugs is specific for reverting changes occurring in HCM heart and bear significant undesired effects that may impact their effectiveness in patients. Therefore, the need for an effective and specific drug is still unmet.

1.1.2 **HCM caused by mutation in the thin filament regulatory proteins of the sarcomere**

Thin filament mutations occur in only 6-8% of patients with hypertrophic cardiomyopathy, making thin-filament HCM a relatively rare condition. However, several clinical and preclinical studies pointed out that HCM associated with thin-filament mutations is in many ways a disease on its own, since both the clinical course and the molecular pathophysiology are different from the much more common thick-filament HCM. To date, a wide array of nearly 100 independent mutations in all components of the cardiac thin filament have been identified (Tardiff, 2011). Although the clinical heterogeneity observed in this group of patients, compared with patients carrying thick filament mutations, thin-filament patients appear to suffer from a higher risk of sudden cardiac death, even in the absence of the "classical" risk factors such as the presence of massive hypertrophy. Moreover, these patients are more likely to develop severe diastolic dysfunction, systolic abnormalities and refractory heart failure. Thin-filament HCM has been much less studied due to its rarity and no specific preventive therapeutic option exists to address the increase risk of arrhythmias and clinical progression. From this stems the need of detailed studies on the molecular and cellular basis of myocardial alterations in the presence of thin filament mutations, which may prompt to the development of selective therapeutic strategies.
In 1994, mutations in cardiac α-tropomyosin (Tm) and troponin T (cTnT) were shown to cause familial hypertrophic cardiomyopathy (HCM) (Thierfelder et al, 1994). In a considerable subgroup of patients, HCM is determined by mutations of the sarcomere thin-filament regulatory protein genes, including cTnT, cardiac troponin I (cTnI) and Tm (Tardiff, 2011) . Albeit mutations in cTnT are the most common thin filament mutations, they account for only 3-5% of all cases of HCM; nonetheless, HCM patients with cTnT mutations have an increased likelihood of suffering a sudden cardiac death (Moolman et al, 1997) at least 26 known mutations have been found in the human cardiac TnT gene that are linked to HCM, including 23 missense mutations, one deletion mutation, and one splicing donor site mutation (Varnava et al, 2001). Patients who present TnT mutations often show no or mild hypertrophy, myocardial disarray, and have a malignant phenotype associated with a high incidence of sudden death (SD). The deletion of the 160 glutamic acid codon of the troponin T gene (Δ160E) was reported to be associated with a high incidence of SD in Caucasian patients (Watkins et al, 1995).

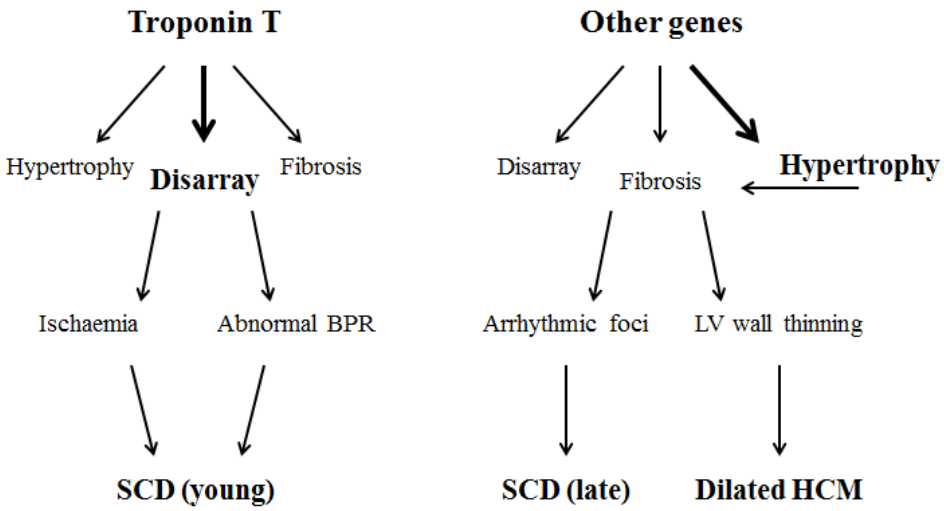

Fig1.1.2a Relation between genotype, histology, phenotype, and sudden death. Diagram showing the genotype-phenotype correlation proposed for HCM associated cTnT mutation versus HCM With Unknown Genotype. BPR indicates blood pressure response to exercise; LV, left ventricle; and SCD, sudden cardiac death.

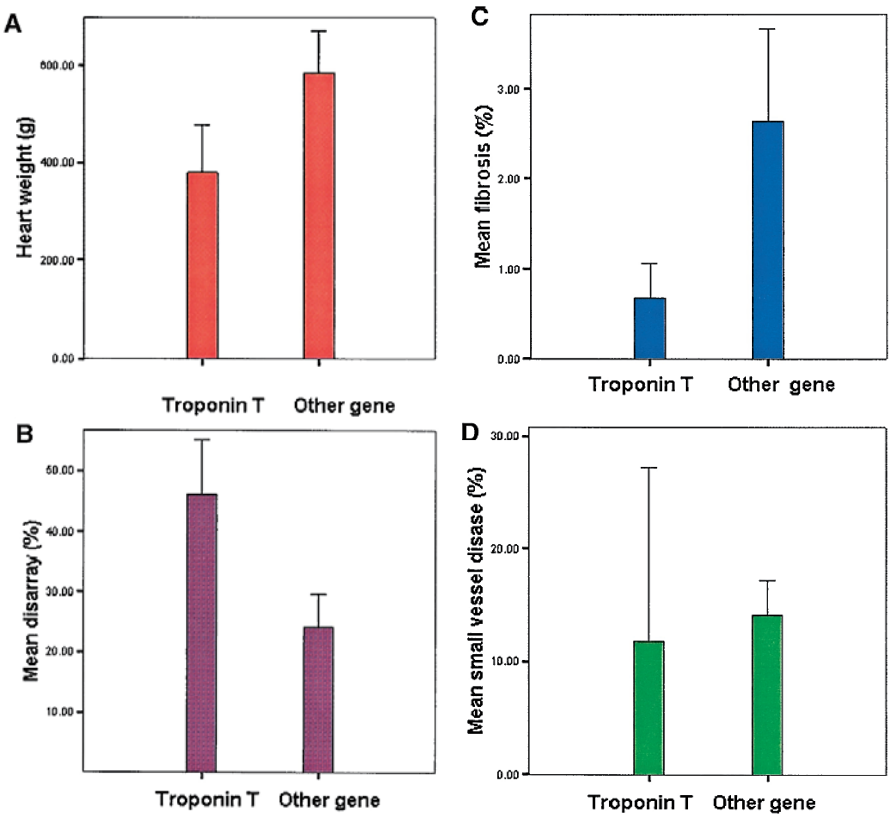

Fig1.1.2b Histology (A) Mean heart weight of patients with troponin T gene vs other gene mutations. (B) Mean disarray of patients with troponinT gene vs other gene mutations. (C) Mean fibrosis of patients with troponin T gene vs other gene mutations. (D) Mean small-vessel disease of patients with troponin T gene vs other gene mutations. Modified fromVarnava et al, 2001.

Cardiac troponin I (cTnI) mutations account for 2-3% of all cases and are similarly associated with poor outcome in patients (Doolan et al, 2005). Tm mutations are less common (1-2%) (Van Driest et al, 2003) and are also associated with high risk of arrhythmias (Karibe et al, 2001). Thin-filament HCM is characterized by a low degree of hypertrophy, despite large myocytes disarray and interstitial fibrosis (Varnava et al, 2001). A seminal study (Watkins et al, 1995) showed that the clinical features associated with 3 different cTnT mutations were remarkably similar, comprising a reduced ventricular wall thickness and an increased prevalence of sudden death compared with patients with thick filament mutations.

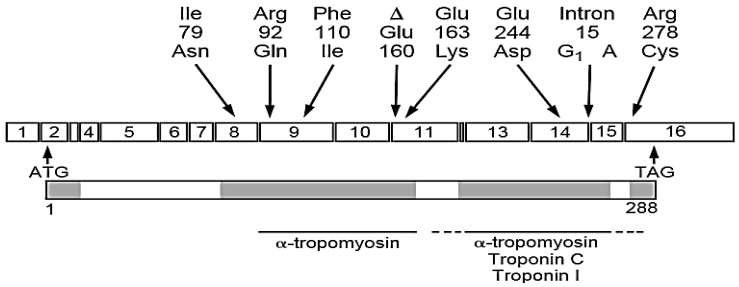

Fig1.1.2c Eight Mutations in Cardiac Troponin T that Cause Familial Hypertrophic Cardiomyopathy. The schematic illustration of the cardiac troponin T gene is based on the rat genomic structure. Exons are indicated by boxes; the location of each mutation is shown. The initiation (ATG) and termination (TAG) codons are indicated. The peptide is represented below; shaded areas indicate high levels of conservation between cardiac and skeletal isoforms. The postulated binding sites are indicated for tropomyosin, troponin C, and troponin I. Modified fromWatkins et al, 1995.

This apparent uniformity was subsequently challenged (Van Driest et al, 2002). The direct genotype-phenotype correlation established by early studies may have suffered from the pitfalls of mutations clustering due to founder effect (Moolman-Smook et al, 1999). In a Japanese study, where HCM patients with MHC or troponin T mutations were enrolled, sudden death has been found to be less frequent from what expected in both groups. Patients with charge change mutations, including Glul60del (Δ160E), showed general trends to develop systolic dysfunction. In **Figure 1.1.2d** is shown a family with a Glu163Arg mutation where a proband died of heart failure at age 47, while two children have developed septal hypertrophy. In patients with a non-charge change mutation (Phe110Ile), the clinical course was benign, although the number of patients was small (Koga et al, 1996). Two subsequent reports identified a second independent mutation at residue 92 of cTnT (Arg92Trp) (Moolman et al, 1997; Varnava et al, 2001). In the study by Moolman, 64 the patient profile was similar to the previously described cTnT mutations, with minimal LVH, low disease penetrance via echocardiogram, and a high frequency of SD especially in males, late-onset (>35 years of age), hypertrophy of the interventricular septum with no evidence of progression to a dilated phenotype

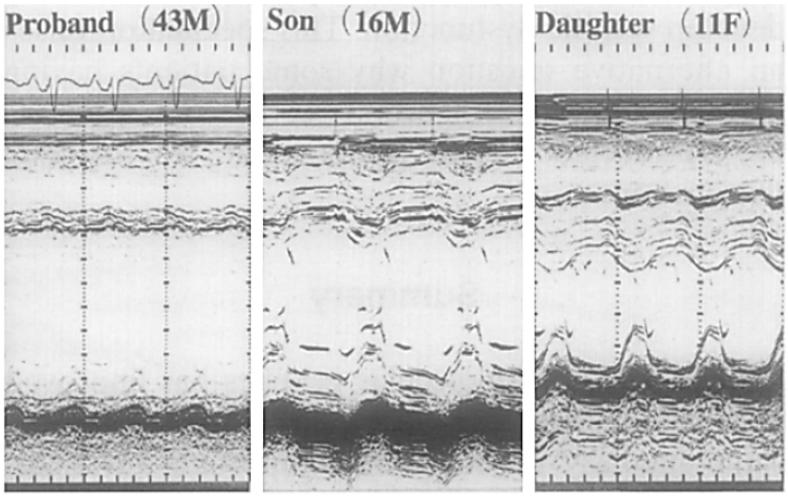

Figure 1.1.2d A family of cardiac troponin T mutation (Glu163Arg, charge change [+]). The proband is a 43 years old male who showed severe left ventricular dilatation and systolic dysfunction at the time of diagnosis. His son (16- years-old) presented with mild septal hypertrophy, while his daughter (11 years-old) manifested typical asymmetric septal hypertrophy.

However, no studies so far have assessed on a large population whether the clinical course and outcome of patients with thin filament mutations differ from those bearing mutations in the thick filament.

Numerous preclinical studies pointed out that the causal biophysical abnormalities leading to disease manifestations in presence of thin filament mutations may be different from the "classical" thick filament mutations. Early studies on skinned cardiac preparations identified the increased Ca^{2+} sensitivity of myofilaments as a common alteration in thin filament mutations (Lin et al, 1996; Redwood et al, 2000). Studies on animal models have shown that selected mutations in cTnT in mouse can result in a cardiomyopathy that includes hypertrophy and fibrosis (Tardiff et al, 1998) as well as an increased tendency for ventricular rhythm disturbances and Ca^{2+}-dependent changes in action potential morphology (Knollmann et al, 2003). Moreover, cardiac muscle from mutant mice shows specific alterations of contractile function with increased force production and slowed kinetics of contraction (Miller et al, 2001) that is directly associated with the increased Ca^{2+} sensitivity of myofilaments with mutant TnT. Furthermore, it was demonstrated that the increased susceptibility to arrhythmia in mutant hearts is related with the increased Ca^{2+} sensitivity induced by thin filament

mutations and can be observed early, even in the absence of any detectable cardiac hypertrophy or fibrosis (Baudenbacher et al, 2008). (see also Introduction, section 1.3).

Despite the widespread investigations related to HCM pathophysiology, the medical management of the disease has been largely unchanged over the past decades (Spoladore et al, 2012). So far, therapeutic approaches to HCM are based on the expertise of single clinicians; no evidence-based therapy, supported by studies on the pathogenic mechanisms of disease, is available. Moreover, none of the presently employed drug therapies has been shown capable of preventing arrhythmias and modifying disease progression in patients. The need of an effective preventive therapy is particularly required for thin filament mutation carrying patients.

1.2 The functional contractile unit on striated muscle: the sarcomere.

1.2.1 Structure of the sarcomere.

The striation pattern in muscle cells, of which a sarcomere is one repeat, is the result of the alternating ordered arrays of thick and thin filaments into myofibrils (Squire, 1997). The sarcomere is the elementary contractile unit from which all striated muscles are made. These are about 2-2.5 µm long and link end-to-end to form long thin strands known as myofibrils. Myofibrils form the contractile apparatus inside each muscle fiber in which every myofibril has a parallel, longitudinal disposition and cylindrical shape of diameter around 1 µm.

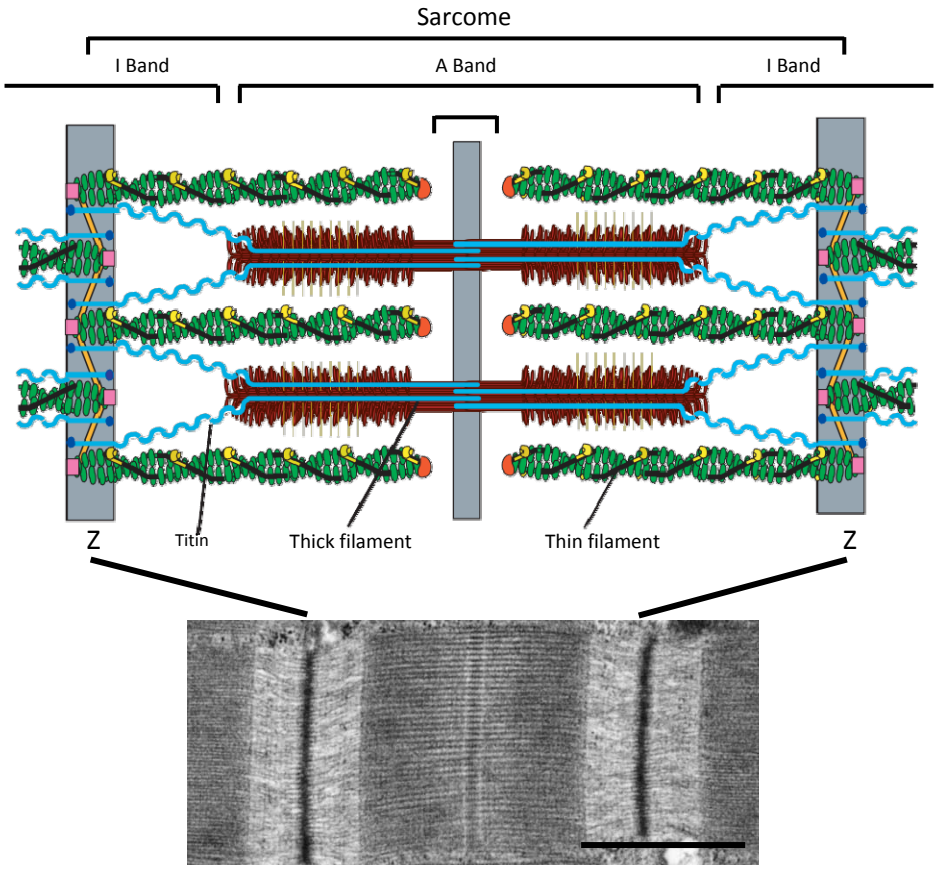

Fig 1.2.1a Major components of a cardiac muscle sarcomere. *Top:* Actin in green and myosin in red. Tropomyosin molecules (black lines) are associated with each other head to tail, forming two polymers per thin filament. Each tropomyosin molecule binds one troponin complex (troponins T, I and C; yellow). Thin filaments are polarized in muscle sarcomeres with the barbed ends anchored at the Z disk (edge of the sarcomere) by the crosslinking protein α-actinin (gold) and are capped by CapZ (pink squares). The C terminus of nebulette (a protein that shares sequence homology with the C-terminal domain of the skeletal muscle protein nebulin) extends partially into the Z disk. The third filament system is formed by titin (blue), single molecules of titin reach from the Z line to the centre (M line) of the sarcomere. Titin interacts directly with several thick filament-associated proteins, such as myosin-binding-protein C (MyBP-C; yellow transverse lines). The N-terminal regions of titin molecules from opposite sarcomeres overlap in the Z lines, and the C-terminal regions of titin molecules from opposite half sarcomeres overlap in the M lines. Therefore, in myofibrils composed of many sarcomeric units, the titin filaments form a contiguous filament system. (Modified from Gregorio & Antin, 2000) *Bottom*: Electronmiscroscopic photograph of the ultrastructural organization of cardiac sarcomeres, unpublished data from our laboratory. Bar indicates 1000nm.

Sarcomeres consist of parallel arrays of ~ 1 µm -long thin filaments that interdigitate with 1.6 µm long thick filaments. The striations that characterize both cardiac and skeletal muscle and determine the

repeating pattern of the sarcomere, are formed by alternating regions of higher and lower optical density, due to thick and thin filaments arrangement in each myofibril, named A and I bands, respectively. The sarcomere is bounded by optical dense Z-discs at the center of each I-band. The A-band is positioned around the lighter H-zone (Gregorio & Antin, 2000) (**Fig. l.2.1a**). The muscle shortening is associated to the reduction of width of I-band and H-zone, without any variation of A-band width (Squire, 1997). So, when sarcomere shortens, reduction of the distance between neighboring Z-line is related to the sliding of actin thin filaments towards the center of the sarcomere, causing the increase of overlapping of thin and thick filament, without any variation in the length of both filaments (Huxley, 1957; Huxley, 1969; Squire, 1997). Thick and thin filaments are formed by polymerization of the two principal contractile proteins, myosin and actin, respectively. Actin and myosin form the 'molecular motor' in muscles. Myosin works as an enzyme performing ATP hydrolysis under the allosteric control of actin such that actin binding initiates ATP product release and force generation in the myosin power stroke. (see **Fig1.2.1b)**. There are different isoforms for many sarcomeric proteins in cardiac and skeletal muscles, specifically, cardiac isoforms are indicated with a "c" prefix (i.e. cardiac TnT).

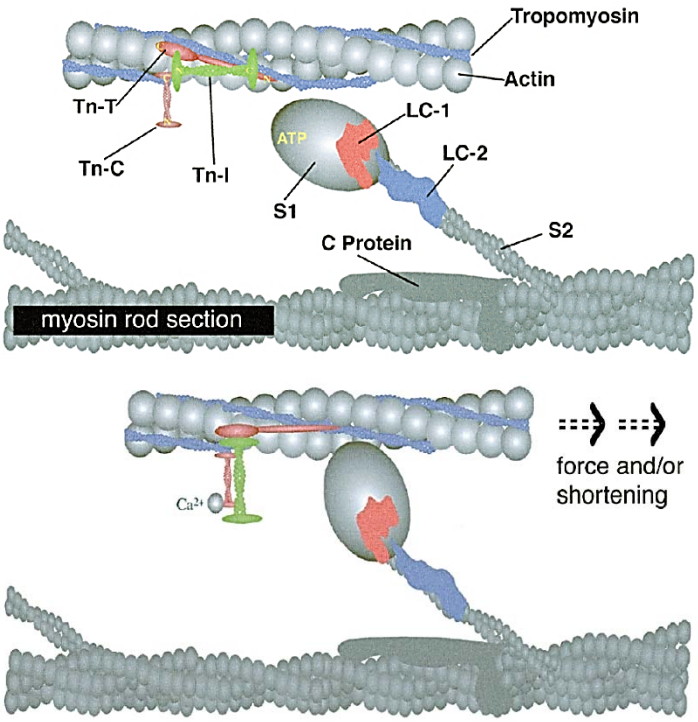

Fig 1.2.1b: Thin and thick filaments interaction. The major proteins that are involved in contractile activation and regulation are shown in diastole (top panel) and systole (bottom panel) Myosin Heavy Chain (MyHC), the motor of contraction (it is a dimer but in the scheme is depicted as a single headed monomer) is made of different domains: the *myosin rod* composing the backbone of thick filaments, *S2*, connecting the rod to the myosin head, and the myosin head *S1* comprising the actin-binding, catalytic domain and the light chain binding domain (the lever arm of the motor protein). The other thick filament-associated proteins are the essential (ELC or LC-1, in red) and the regulatory (RLC or LC-2, in blue) myosin light chains, bound to the lever arm of *S1*, and C-protein (or cardiac Myosin Binding Protein-C, cMyBP-C in dark grey), a protein with poorly understood regulatory and structural functions. Thin filament proteins comprises, besides actin, the troponin complex (troponin C, TnC, troponin I, TnI, and troponin T, TnT) and tropomyosin. Modified from de Tombe; 2002.

The thick filaments are mainly composed by the motor protein myosin II. Myosin II is a polymer (6 chains) which is composed of two heavy chains (Myosin Heavy Chain, MHC of ≈ 200 kDa each), interconnected by a long twisted tail domain, and 4 light chains (LC). The extending domains of the myosin heavy chain are called the two myosin 'heads'. Two myosin light chains (MLC-1 and MLC-2)

of ≈ 20 kDa are bound to the neck region of each head. The myosin 'head' is also called cross-bridge, since it bridges the gap between the thick myosin filaments and the thin actin filaments in muscle. The four light chains consist of two essential light chains (ELC, the MLC-1) and two regulatory light chains (RLC, the MLC-2)(Gordon et al, 2000) see **Fig 1.2.1b**. Each cross-bridge has an ATP binding site. Force and filament movement, in fact, depend on the energy released from ATP hydrolysis. In the presence of Ca^{2+}, the myosin cross-bridges bind to actin, promoting the release of Pi and then ADP. During this process a structural transition in the cross-bridge, suggested to be a change of tilt or change of shape, is thought to produce a relative sliding force between thin actin and thick myosin filaments. The cross-bridge can be released from actin when it binds another ATP molecule. In the heart, two different isoforms of MHC are present: α-myosin heavy chain (α-MHC) and β-myosin heavy chain (β-MHC). Human myosin is mainly composed of β-MHC and up to 5% of α-MHC.
Another important component of the thick filament is Myosin Binding Protein C (MyBP-C), a sarcomeric protein associated with the thick filaments, located in the cross-bridge containing A-band of the sarcomere (**Figure 1.2.1b**). To MyBP-C has been assigned a role in assembly and stability of the sarcomere as well as in the modulation of contraction (Oakley et al, 2004). In the myocardium, it has been demonstrated that cMyBP-C knockout mice are viable but show significant cardiac hypertrophy, myocyte disarray and fibrosis (Harris & Foord, 2000). Two models have been proposed for the arrangement of cMyBP-C in the sarcomere. In the first 'collar' model it is suggested that cMyBP-C molecules form a ring around the thick filament (Moolman-Smook et al, 2002). The second model proposes that the C-terminal of the molecule runs parallel to the myosin backbone, while the N-terminal domain interacts with neighboring actin filaments (Squire et al, 2003; Whitten et al, 2008). The C-terminal region of MyBP-C also contains binding sites for the giant protein titin.

The thin filament comprises F-actin helices, together with the so called "regulatory proteins": tropomyosin (Tm) and troponin (Tn) proteins in a 7:1:1 ratio.
The thin filament consists mostly of the ≈ 45 kDa globular protein G-actin. G-actin monomers polymerize spontaneously to form the backbone of the thin filament, a double helix F-actin. Muscle thin filaments. The actin helix appears as two right-handed helices which twin slowly around each other (Holmes et al, 1990; Squire, 1997) . In striated muscle, tropomyosin (Tm) is wrapped around the F-actin backbone as a α-helical coiled-coil dimer. Tm modulates the actin-myosin interactions and functions to stabilize the actin structure. It comprises 284 aminoacid chains each spanning seven actin monomers and containing seven quasi-repeating regions. The Tm molecules are linked together through a head-to-tail association, which allows adjacent Tm molecules to function as a cooperative unit that spans 7 actin monomers. The Ca^{2+} binding protein complex, troponin (Tn), is bound to Tm (Kobayashi & Solaro, 2005; Wolska & Wieczorek, 2003). Troponin is a trimeric complex consisting of three subunits: troponin C (TnC), the Ca^{2+} binding subunit; Troponin I (TnI), the inhibitor of the acto-myosin reaction that shuttles between tight binding to actin and tight binding to the Ca^{2+}-TnC; and troponin T (TnT), the Tm binding subunit. Troponin subunits are present in different isoforms which distribution is tissue specific (fast skeletal muscle and slow skeletal muscle; miocardial) and also depend on development stage(Schiaffino & Reggiani, 1996). In cardiac muscle specific isoforms are present for all three subunits: cTnC, cTnI and cTnT.

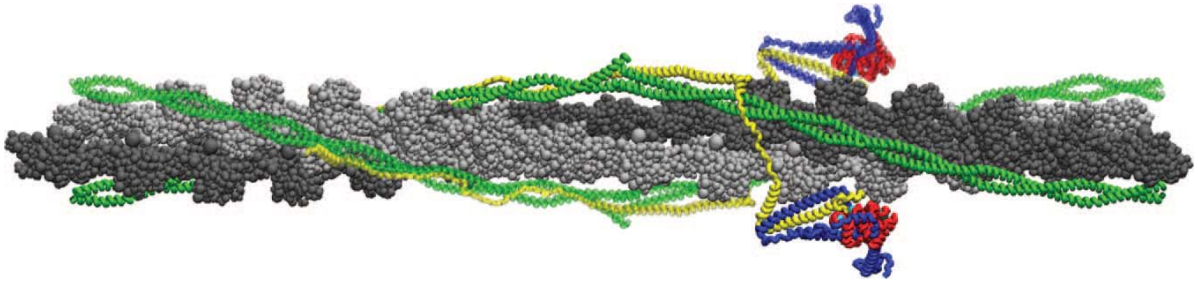

Fig 1.2.1c: An atomistic model of the human cardiac thin filament. cTnT is indicated in yellow, cTnI in blue, cTnC in red, Tm in green and actin filament in silver/gray. Modified from Tardiff, 2011.

1.5 Giant structural proteins

Titin is the largest protein found in mammals (Labeit et al, 1990) with a molecular weight of ≈ 3700 kDa depending on isoform composition. At the N-terminus titin is anchored in the Z-disc and to the thin filament and at the C-terminus it is bound to the thick filament. This molecule centers thick filaments in the sarcomere and acts as an elastic spring element during muscle contraction. The region of titin located in the I-band is a complex molecular spring element, which consists of a PEVK domain (rich in proline (P), glutamate (E), valine (V) and lysine (K)), tandem Ig segments and variable N2B and N2A elements (LeWinter et al, 2007). Titin is a major determinant of passive tension in cardiomyocytes. The passive tension results from extension of the I-band region of titin, which elongates as sarcomere length increases. The N2B element alone is present in the stiffer N2B isoform, while both the N2A and N2B elements make up the more compliant N2BA isoform. Both isoforms are co-expressed within the cardiac sarcomere and their ratio determined the passive stiffness of cardiomyocytes (LeWinter & Granzier, 2010).
Like titin, also nebulin is a giant sarcomeric protein (~800 kDa) involved in structure stability and contractile performance. A single nebulin molecule spans nearly the entire length of the thin filament. Nebulin is present only in skeletal muscle. In cardiac muscle it is replaced by a related protein, Nebulette, which is shorter and has lower MW, around a sixth the size of nebulin, and only localizes in the Z-disc (Pappas et al, 2011).

1.2.2 Chemo-mechanical cycle

The interaction of actin, myosin and nucleotides consists of a cycle in which myosin alternates between tight bonds with actin or with nucleotides. The sliding filament mechanism, i.e. the shortening of muscle due to sliding of thin on thick filaments, is coupled to the development of force along the sarcomere longitudinal axis and is driven by the myosin molecular motor, which hydrolyzes ATP and cyclically interacts with the actin thread, forming “cross-bridges”. **Fig1.2.2a** illustrates the cross-bridge chemo-mechanical cycle (Cooke, 1995; Gordon et al, 2000). The reaction pathway can be described as a series of coupled biochemical and mechanical events. The myosin head, as showed in **Fig 1.2.1b** with his light chain binding domain can move like a lever arm relative to the actin-binding, catalytic domain. Thus, myosin structure is designed to achieve the efficient conversion of biochemical energy into force production.

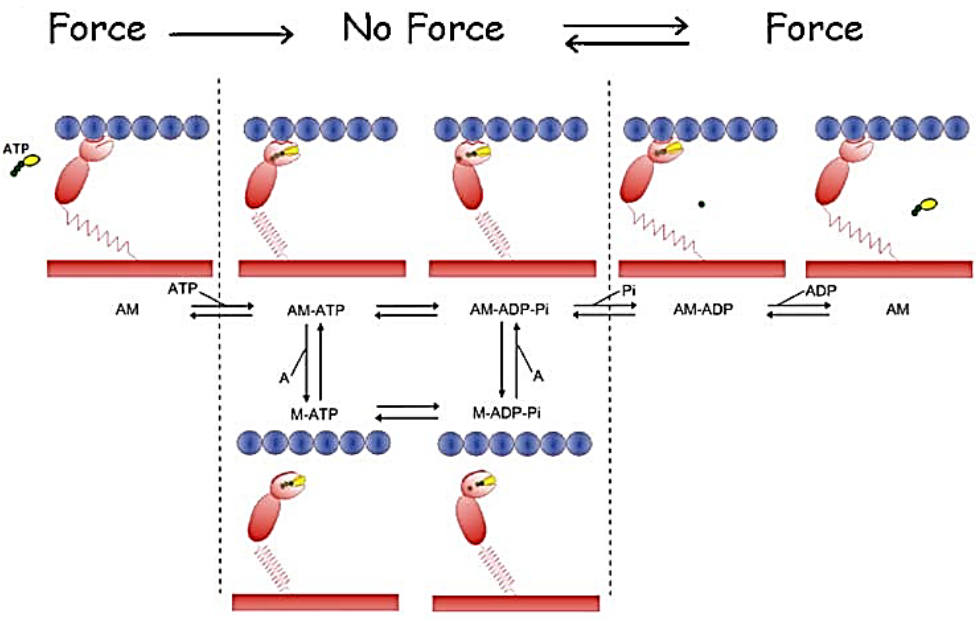

Fig 1.2.2a Reaction pathway for acto-myosin ATPase and energy transduction cycle.

ATP binding to a myosin head (M) causes a rapid, almost irreversible dissociation of the myosin head from actin (A). Following detachment from actin, the ATP is hydrolyzed to ADP and inorganic phosphate (Pi) both remaining tightly bound to the myosin head. The free energy of ATP hydrolysis is not released but remains within the structure of the M.ADP.Pi complex. The hydrolysis is, in fact, accompanied by a major conformational change that represents a "repriming" of the power stroke; both the hydrolysis and the conformational change are reversible. ADP and Pi will remain bound to the myosin head until the myosin binds again to an actin site. The affinity of M.ADP.Pi for actin is significantly higher than that of M.ATP. If an actin site is within the reach of the myosin head, this will bind rapidly and reversibly to the actin site in the presence of ATP. The interaction of the M.ADP.Pi complex with actin can promote a major change in conformation (the power stroke) which is accompanied by the dissociation of Pi (Tesi et al, 2002). If the filaments carry an external load (e.g., isometric conditions) then the power stroke results in the distortion of an elastic element. The location of the elastic element is unknown and is described in **Fig1.2.2a**, for simplicity, as part of the S2 region connecting the myosin head to the rod. The dissociation of Pi is a reversible event and Pi can rebind to reverse the power stroke. The final step of the chemo-mechanical coupling is a strain-dependent mechanism of ADP release leading to an AM complex which is rapidly dissociated by new ATP binding. ADP release can be very fast if the external load on the sarcomeres is small, while it is much slower for high loads (isometric conditions). The features of this transition likely differ between myosin designed for efficient fast shortening vs efficient load bearing. In this generally accepted scheme, transitions of crossbridges from force-generating to nonforce- generating states involved in isometric force relaxation comprise both forward (ADP release and ATP binding) and backward (Pi rebinding and reversal of the power stroke) steps.

1.2.3 Regulation of contraction: thin filament regulatory mechanism and E-C coupling.

Regulation of actomyosin cross-bridge cycling by Tm and the Tn subunits is described by the three-state model of myofilament activation, whereby the position of the Tm coiled-coil dimer is in dynamic equilibrium between three position on actin (Lehrer & Geeves, 1998; Maytum et al, 1999; McKillop & Geeves, 1993). Ca^{2+} is the physiological activator of the contractile machinery. The interactions among the Tn subunits, Tm and actin are Ca^{2+} sensitive and allow Ca^{2+} induced conformational

changes within the troponin complex, modification of the Tm position on the actin filament and the initiation of contraction (Gordon et al, 2000). During relax phase (or diastolic phase in the myocardium), the intracellular Ca^{2+} concentration is low and under these conditions TnI binds to actin-Tm and inhibits the binding of myosin and thereby force generation. During activation (or systole, in the myocardium), intracellular Ca^{2+} concentration rises and triggers the contractile machinery by binding with the Ca^{2+} sensor: the TnC. As shown in **Fig1.2.3a** skeletal muscle TnC contains two high affinity and two low affinity binding sites (Potter & Gergely, 1975), whereas, the cardiac TnC isoform (cTnC) has two high affinity sites, but only one low affinity binding site. The activation of the sarcomere occurs when Ca^{2+} binds to the low affinity site in cTnC, as the high affinity sites are always occupied by the ion.

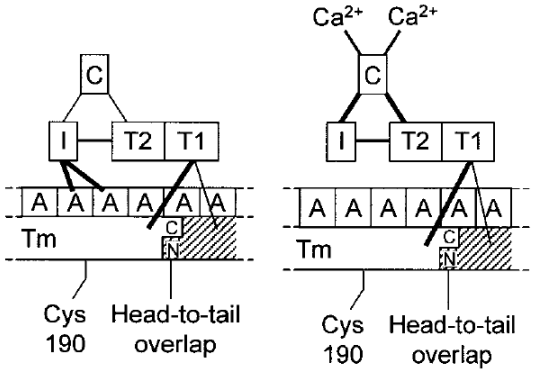

Fig 1.2.3a A model for molecular arrangement of Tn complex and Tm on the thin filament. The effect of Ca^{2+} binding to TnC on the interaction between the various thin filament proteins. A is actin, I is TnI, C is TnC, T1 is the NH_2-terminal (1–158) portion of TnT, T2 is the COOH-terminal (159 –259) (*see below*) portion of TnT, Tm is tropomyosin with the NH_2 and COOH terminals indicated in the head-to-tail overlap region and the Cys-190 region indicated. Thicker lines imply stronger binding, and thinner lines imply weaker binding. No Ca^{2+} activating state where the ion is not bound to TnC triggering sites is shown on the left; whereas the state with Ca^{2+} bound to TnC sites is shown on the right. Note that Ca^{2+} binding to TnC enhances the TnC-TnI and TnC-TnT2 interactions and weakens the TnI-A interactions. This presumably allows the Tm to move on the surface of the actins opening up myosin binding residues. Modified from Gordon et al, 2000.

The relationship between free Ca^{2+} and isometric tension is very steep, much greater than would be expected on the basis of equilibrium binding of Ca^{2+} to the binding site on TnC (Shiner and Solaro, 1984). The transduction processes induced by Ca^{2+} binding that lead to activation of muscle contraction clearly involve cooperative interactions along the thin filament. Ca^{2+} binding induces a conformational change in TnC such that a hydrophobic region becomes exposed allowing interaction with TnI (Gagne et al, 1995; Slupsky & Sykes, 1995). In the absence of Ca^{2+}, this 'signaling pathway' is not triggered and Tn constrains Tm in a position that sterically hinders myosin-S1 binding (Lehman et al, 1994; Xu et al, 1999). The movement of the troponin complex induces a conformational change in Tm, increasing its binding to actin, thereby revealing myosin-S1 binding sites on actin. Furthermore, upon forming strongly bound cross-bridges, the binding of additional cross-bridges is greatly enhanced in a cooperative manner, presumably by initiating the movement of tropomyosin to a third, more favorable position (Lehman et al, 2000; Lehrer & Geeves, 1998; Swartz & Moss, 1992; Tobacman & Butters, 2000).

A three-state model of the thin filaments has been proposed by Geeves et al. (1984) to explain the regulation of the interaction between actin, Tn, Tm and myosin (Figure 6). Tm can occupy three distinct positions on actin filament. Under relaxing condition, in absence of Ca^{2+}, Tm sterically blocks the interaction between actin and myosin heads in a 'blocked state'. Herein, not even weak myosin binding is possible. When Ca^{2+} starts to be present, Ca^{2+} starts to bind to TnC. This causes serial structural changes in all the components of Tn that allows movement of Tm to another position on actin filament and thereby the probability of formation of strong cross-bridges starts to increase. This

is called ‘closed or activated state’. Further increasing of Ca^{2+} concentration and the transition from weak to strong cross-bridges pushes Tm further to the ‘open or activated state’, further increasing the probability of strong mechanical transition and allowing full activation of thin filament and force generation by strong cross-bridges formation (Gordon et al, 2000; Lehman et al, 1997; Lehman et al, 1995).

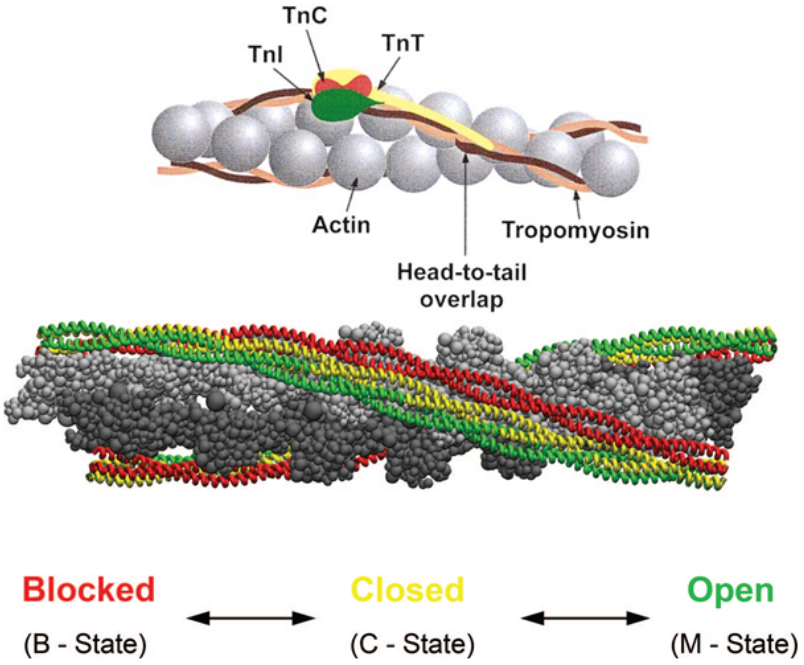

Figure 1.2.3b. The 3-state model of myofilament activation. (A) model of molecular arrangement of Tn , Tm and actin in the thin filament. The various troponin subunits are indicated TnC (red), TnT (yellow), and TnI (green) as they lie along the two stranded tropomyosin shown as an a- (brown) and b -heterodimer (orange). (B) The 3 average positions of Tm are depicted. Tm residues at the outer actin domain in the blocked state (red), Ca^{2+} binding to cTnC results in an azimuthal shift to the weakly bound closed state (yellow) in the actin inner domain, and myosin binding drives the final shift to the force-producing open state (green).

In the myocardium, activation of the contractile apparatus is initiated upon a transient increase in the cytosolic Ca^{2+} concentration. Under normal physiological conditions, calcium entry during the plateau phase of the cardiac action potential is not sufficient to directly activate the myofilaments, but instead serves as a trigger to release calcium from the sarcoplasmic reticulum (Calcium Induces Calcium Release, CICR) (Bers, 2002). Collectively, this process is defined excitation–contraction coupling (E–C coupling). The key proteins involved in E-C coupling, such as DiHydro-Pyridine-Receptors (DHPR) and Sodium-Calcium-Exchangers (NCX) are located predominantly on the t-tubular membranes (Orchard et al. 2009,Yang Z. et al. 2002, Pásek M. et al. 2008), adjacent to Ca^{2+} release-units in the Sarcoplasmic Reticulum (SR). Briefly, during the cardiac action potential, Ca^{2+}enters the cell through depolarization-activated Ca^{2+} channels as inward Ca^{2+} current (I_{Ca}), which contributes to the action potential plateau. Ca^{2+} entry triggers Ca^{2+} release from the sarcoplasmic reticulum (SR). The combination of Ca^{2+}influx and release raises the free intracellular Ca^{2+} concentration ($[Ca^{2+}]_i$), allowing Ca^{2+} to bind to the myofilament protein TnC, which then switches on the contractile machinery as previously described. For relaxation to occur $[Ca^{2+}]_i$ must decline, allowing Ca^{2+} to dissociate from Tn. This requires Ca^{2+} transport out of the cytosol by four pathways involving SR Ca^{2+}-ATPase, sarcolemmal Na^+/ Ca^{2+} exchange, sarcolemmal Ca^{2+}-ATPase or mitochondrial Ca^{2+} uniport. (see Fig **1.2.2d.)**

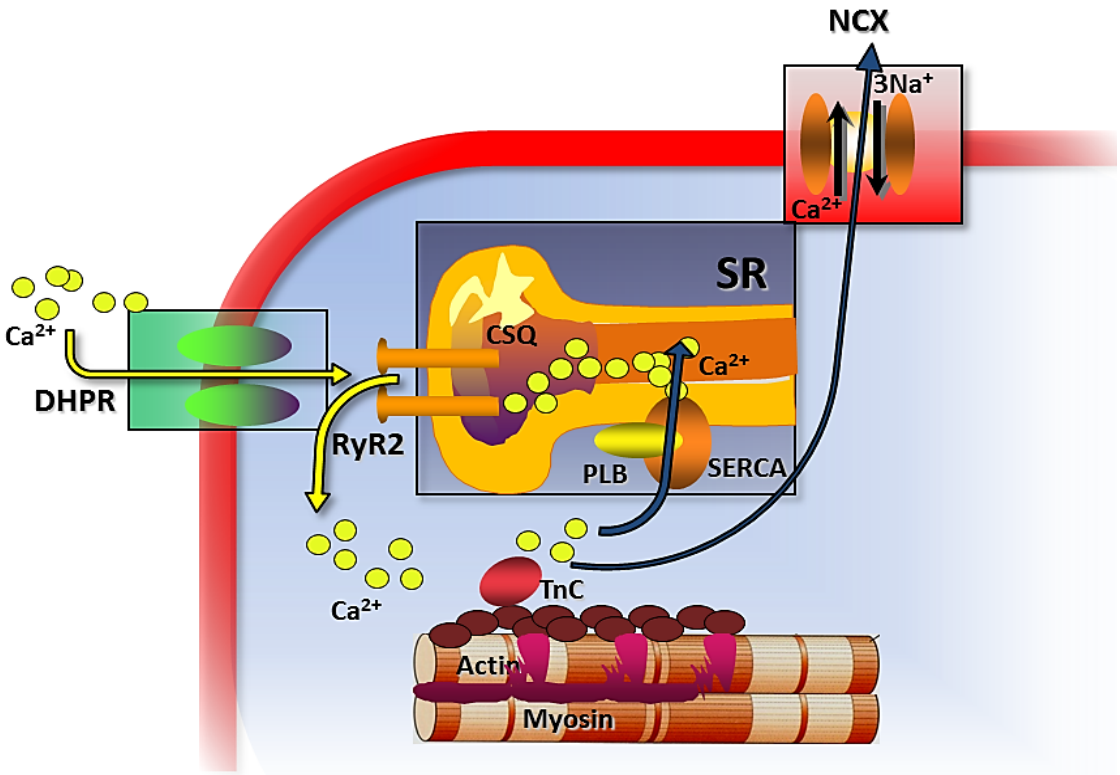

Figure 1.2.3c. Cardiac Excitation-Contraction Coupling. During the cardiac action potential, Ca^{2+} enters the cell through depolarization-activated Ca^{2+} channels (DHPR) as inward Ca^{2+} current ($I_{Ca\text{-}L}$), which contributes to the action potential plateau. Ca^{2+} entry triggers Ca^{2+} release from the sarcoplasmic reticulum (SR), where a large amount of Ca^{2+} is stored bound to calsequestrin (CSQ). The Cardiac Ryanodine Receptor (RyR2) is the main SR Ca^{2+} release channel. The combination of Ca^{2+} influx and release raises the free intracellular Ca^{2+} concentration ($[Ca^{2+}]_i$), allowing Ca^{2+} to bind to the myofilament protein troponin C (TnC), which then switches on the contractile machinery. For relaxation to occur $[Ca^{2+}]_i$ must decline, allowing Ca^{2+} to dissociate from troponin. This requires Ca^{2+} transport out of the cytosol, that occurs mainly by two pathways: SR Ca^{2+}-ATPase (SERCA) and sarcolemmal Na^+/Ca^{2+} exchange (NCX). Other pathways participate to cytosolic Ca^{2+} rise (e.g. reverse mode NCX, IP3receptor) and Ca^{2+} removal (e.g. sarcolemmal Ca^{2+}-ATPase or mitochondrial Ca^{2+}uniport), although with a minor contribution.

1.2.4 cTnT: the "glue" of the thin filament: structure and localization of the main cardiomyopathies-associated mutation

As explained above, the activation and inhibition of muscle contraction are primarily achieved by cTnC and cTnI respectively; however, these events cannot occur without cTnT. cTnT, in fact, anchors the Tn complex to the thin filament and also contributes to the Ca^{2+}dependent regulation of muscle contraction. Therefore, any functional and structural defects in cTnT may cause alteration of the Ca^{2+}regulation of muscle contraction. In his review of 1996, Tobacman described cTnT as "the glue" of the thin filament, because it links the cTnI:cTnC complex to TM-actin :"it touches them all" (Tardiff, 2011). Despite the cTnT linker's role in calcium signal propagation, little is known about its structure due to its hypervariability (Jin & Chong, 2010; Manning et al, 2012). cTnT consists of 298 aminoacids and is also named as TNNT2 from the name of gene that encode the cardiac isoform. cTnT is organized into 2 major functional domains TNT1 and TNT2. This classical organization is based on chymotryptic digest studies (Ohtsuki, 1979). The **TNT2** domain is directly bound to cTnI: cTnC and comprises a significant portion of the rigid IT arm (residues 203 to 271) (see F**ig 1.2.4a**). The I-T arm is a coiled coil consisting of two helices, one from cTnI and the other from cTnT. It plays a key role in calcium signaling and represents the most stable region of the cTn complex in terms of subunit–subunit interactions.

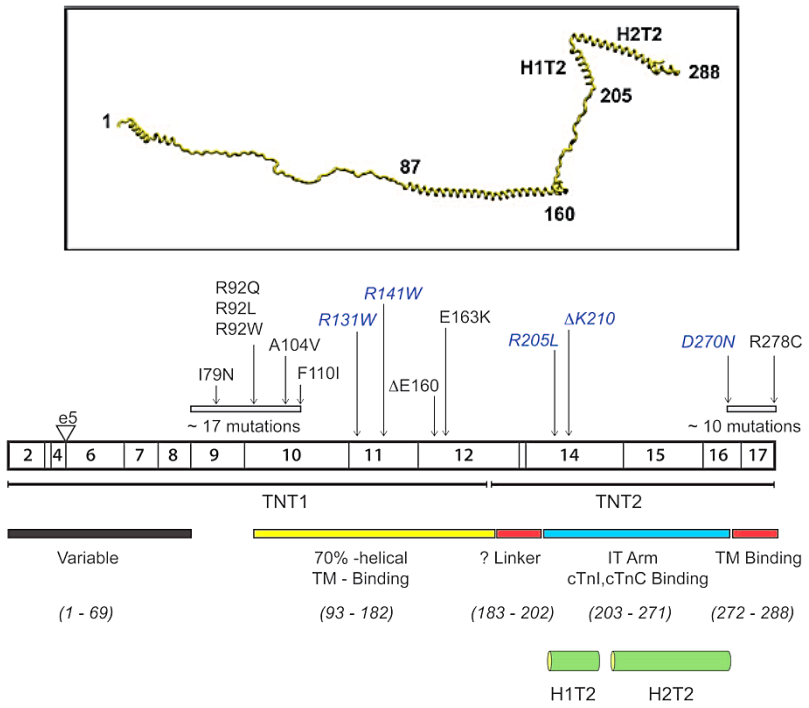

1.2.4a. Distribution of HCM- and DCM-linked mutations in the cTnT N-terminal domain. This region of cTnT is highly conserved and the structure of the protein between residues 150 to 200 is poorly defined. Mutations that lead to hypertrophic or non-dilated ventricular remodeling are shown in *black* and are contiguous to DCM-causing mutations (*blue*). The disease-causing mutations in cTnT are highly clustered within 2 primary locations, all located in regions of the protein that are predicted to be highly mobile (modified from Tardiff, 2011).

TNT2 consists of 2α-helices (H1: 204 to 220; H2: 226 to 271) connected via a short 5-aa linker sequence (see **Fig 1.2.4a**) Several of the known TNT2 mutations occur at the extreme N-terminal portion of the H1 helix and have been exclusively associated with Dilated Cardiomyopathy (DCM). The protein also includes the extended N-terminal, comprising the N-terminal "hypervariable" region and the largely α helical TNT1 and the extreme C-terminal (C-TnT) domains that were either not included in the cTn complexes that were crystallized or could not be resolved in the extant structures. These unresolved domains include more than 90% of the known disease-causing mutations in cTnT, and this lack of structural information limits our ability to understand the molecular pathogenesis of HCM. There is a flexible linker between TNT1 and TNT2 and little is known about its structure due to its hypervariability (Takeda et al 2003).

Approximally 65% of the cTnT mutation are found within or flanking **TNT1**, the N-terminal tropomyosin-binding domain of cTnT. TNT1 mutation trend to cluster at the N- and C- terminal ends of the domain, with two or several mutational hotspots occurring at residues 92 (i.e. R92Q. R92L, R92W) and 160-163(i.e Δ160E, E163R, E163K). R92Q and Δ160E are consistently associated with a particularly poor clinical prognosis (Alcalai et al, 2008). Interestingly these mutations show significant differences in their molecular phenotype despite being located within the same functional domain (Haim et al, 2007; Palm et al, 2001). The mutational hotspot at residues 160-163 is located within a conserved, highly charged region (158-RREEEENRR-166). It has been recently shown that this region may unwind to form a flexible hinge that is necessary for normal thin filament regulation. Thus, mutations in TNT1 may alter the flexibility of TNT1, which is inversely proportional to the cooperativity of calcium activation of the thin filament. The flexibility of this region may be important for the transduction of Ca^{2+} activated signal for activation of the thin filament (Manning et al, 2012).

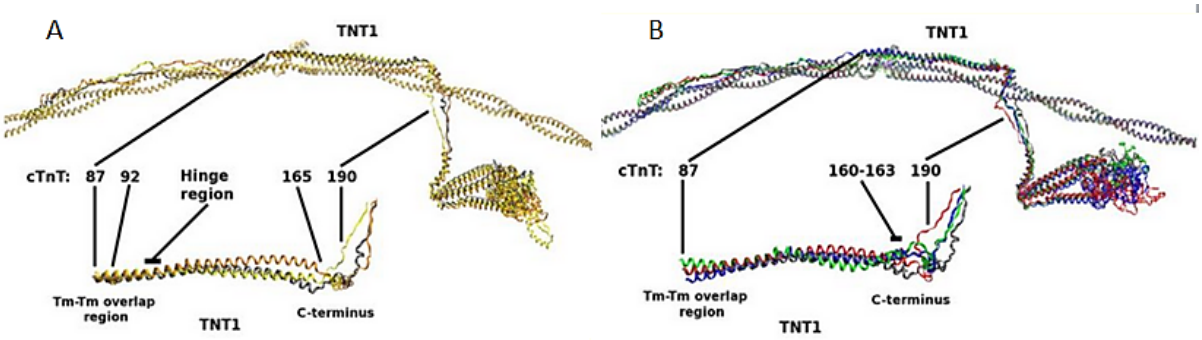

1.2.4b.Two sets of cTnT mutations at opposite ends of TNT1. Mutations in residue 92 in the Tm-Tm overlap region of TNT1 and mutations in residues 160 and 163 in the C-terminal portion of TNT1 adjacent to the cTnT H1-H2 linker.(A) cTnT R92L and R92W mutations compared with WT. Top: Average structures of cTn with overlapping Tm–Tm for WT (gray), R92L (yellow), and R92W (orange) aligned with respect to Tm. Bottom: TNT1 is enlarged and rotated to highlight a noticeable shift in the average position of TNT1 for mutants R92L and R92W that results from decreased interactions between TNT1 and Tm. (B) cTnT ΔE160, E163K, E163R mutations compared with WT. Top: Average structures of cTn with overlapping Tm–Tm for WT (gray), ΔE160 (red), E163K (blue), and E163R (green) aligned with respect to Tm. Bottom: TNT1 is enlarged and rotated to highlight a noticeable shift in the average position of TNT1 for mutants ΔE160, E163K, and E163R that results from decreased interactions between TNT1 and Tm.

1.3 Primary and secondary changes related to cardiomyopathy- associated cTnT mutations.

At present, there is no clear understanding as to why TnT mutations in particular pose a high risk for sudden death, as opposed to, for example, mutations in the myosin heavy chain, which usually cause a much greater degree of cardiac hypertrophy. Sudden cardiac death of HCM patients is often caused by ventricular tachyarrhythmias (Maron, 2000), but its cause remains unknown for patients with TnT mutations.

Disruption of cardiomyocyte Ca^{2+} homeostasis and excitation-contraction coupling has been shown to be an important early event in the pathogenesis of HCM (Semsarian et al, 2002). Increased [Ca^{2+}] in specific microdomains can also alter intracellular signalling pathways leading to adverse cardiac muscle remodeling.

How HCM-associated mutations in cTnT lead to different impaired cardiac function is not clear. In most cases, HCM is a disease that starts at the cardiac myofilament level triggering different remodeling of the heart. Each TnT mutation has somewhat different effects on myofilament properties though all mutations can be predicted to result in: (i) impaired relaxation, (ii) reduced diastolic compliance, (iii) reduced contractile reserve, (iiii) preserved systolic function under baseline conditions, and (iiiii) cardiac dysfunction under inotropic stimulation (Knollmann & Potter, 2001). A common feature shared by various HCM associated cTnT mutations is an increase in Ca^{2+} dependence of actomyosin interactions (Chandra et al, 2005). How such increase in **Ca^{2+} sensitivity** of force development leads to cardiac dysfunction is not understood. One possibility is that an enhanced Ca^{2+} sensitivity could provide a molecular basis for **hypercontractility**, which is a hallmark of these cTnT mutations. Consequently, this may lead to marked increase in **sarcomeric ATP consumption,** which could cause a mismatch between ATP synthesis and ATP usage by myocardial cells, exacerbated when stress is imposed on the heart. At present a question remains open: which alteration is a primary effect of the underlying mutation and what are the secondary consequences of cardiac remodeling?

1.3.1 Myofilament Ca^{2+} sensitivity.

Increased myofilament Ca^{2+}-sensitivity has been reported as a common dysfunction in experimental models of HCM and has been proposed as a trigger of disease pathogenesis (e.g.Marston, 2011). An augmented sensitivity to Ca^{2+} could affect cardiac myocyte relaxation and energetics and may contribute to electrical remodeling increasing the risk of arrhythmias (Baudenb+nacher et al, 2008). Recently, it has been reported that myofilament Ca^{2+} sensitization directly determines arrhythmogenic changes in cardiomyocyte Ca^{2+} homeostasis by increasing cytosolic Ca^{2+} buffering. This alteration in the intracellular Ca^{2+} handling could lead to proarrhythmic consequence such as pause-dependent potentiation of Ca^{2+} release, action potential prolongation, and triggered activity (Schober et al, 2012). The high myofilament Ca^{2+} sensitivity found in human HCM samples could partly reflects a hypo-phosphorylation of PKA-targets. PKA-mediated phosphorylation of myofilament proteins such as cTnI, cMyBP-C, and titin, in fact, is thought to exert a positive lusitropic effect also by decreasing myofilament Ca^{2+} sensitivity and enhancing cross-bridge cycling kinetics. Phosphorylation of cTnI at the PKA sites Ser^{23} and Ser^{24} leads to a decrease in myofilament Ca^{2+} sensitivity through a conformational change of the troponin complex. This structural change reduces the affinity of Ca^{2+} binding to cTnC (Solaro et al, 1976; Takimoto et al, 2004; Zhang et al, 1995). It has been shown that frameshift *MYBPC3* mutations, causing haploinsufficiency, enhanced Ca^{2+} sensitivity through hypophosphorylation of troponin I, secondary to mutation-induced dysfunction (van Dijk et al, 2009).

A recent study in human HCM with mutations in both thick- and thin-filament proteins showed higher myofilament Ca^{2+} sensitivity compared to donor samples. However, the higher Ca^{2+} sensitivity in sarcomere mutation positive HCM groups compared with non-failing donors coincided with lower phosphorylation levels of cMyBP-C and cTnI. Treatment of HCM samples with PKA increased

phosphorylation of the PKA target proteins and normalized myofilament Ca^{2+} sensitivity in *MYBPC3* mut, *TPM1* mut, and sarcomere mutation negative HCM to values observed in non-failing donors. In contrast, after PKA, higher myofilament Ca^{2+} sensitivity was still present in *MYH7* mut and *TNNT2* mut, suggesting that the Ca^{2+}-sensitizing effect is primary caused by these mutations (Sequeira et al, 2013).

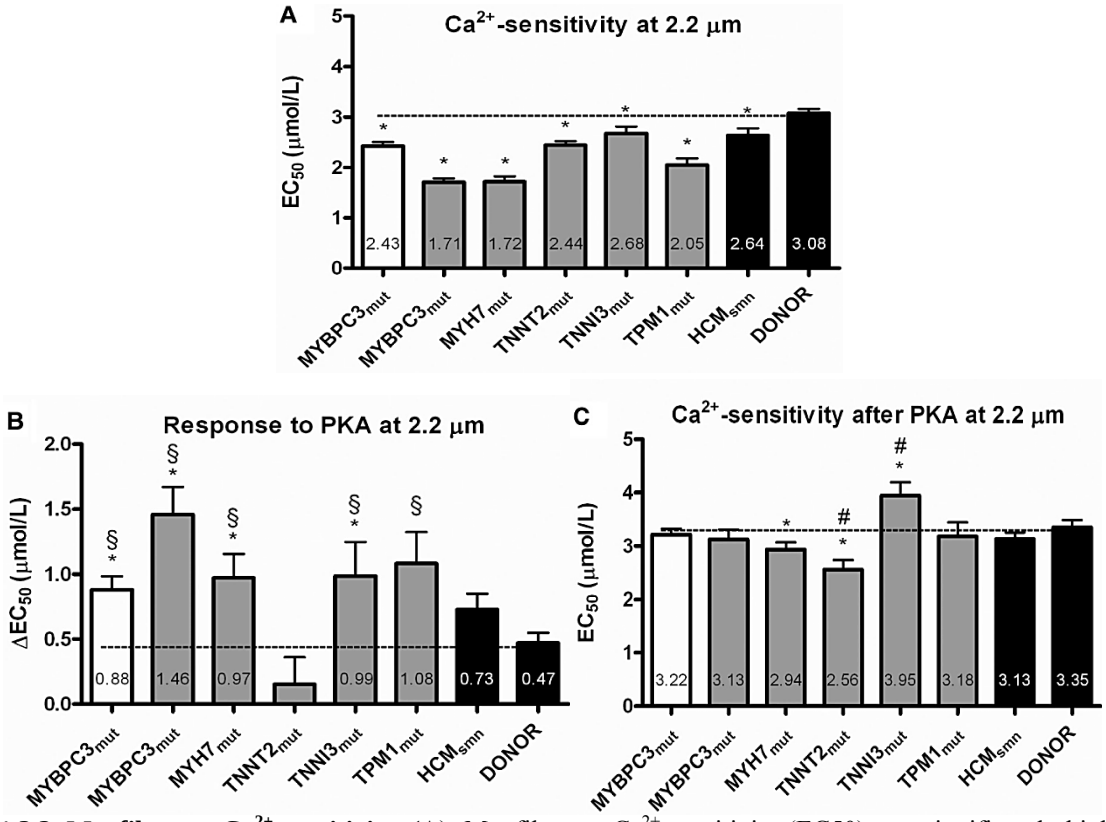

Fig 1.3.2. Myofilament Ca^{2+} sensitivity. (A) Myofilament Ca^{2+} sensitivity (EC50) was significantly higher in all HCM groups compared with donors. (B) The protein kinase A (PKA)–induced reduction (ΔEC50) in myofilament Ca^{2+} sensitivity was larger in HCM groups compared with donors, except in the *TNNT2*mut sample, in which PKA had no significant effect. (C) Myofilament Ca^{2+} sensitivity was similar in *MYBPC3*mut, *TPM1*mut, sarcomere mutation-negative HCM (HCMsmn), and donor after treatment with PKA, whereas it was higher than donor in *MYH7*mut and *TNNT2*mut. PKA-treated *TNNI3*mut cells showed a lower myofilament Ca^{2+} sensitivity compared with HCMsmn and donor. Open bar represents *MYBPC3* truncating mutation; solid gray bars represent missense mutations. **P*<0.05 vs donor; §*P*<0.05 vs *TNNT2*mut; #*P*<0.05 vs HCMsmn.

Many studies have shown that most HCM-TnT mutations alter the contractile properties of cardiac muscle, especially the Ca^{2+}sensitivity of force development and ATPase activity (see below) *in vitro* and *in vivo* (Gomes et al, 2004; Hernandez et al, 2001; Knollmann & Potter, 2001). HCM TnT mutants I79N, R92Q, F110I, E163K, and R278C increased Ca^{2+} sensitivity of force development when they were incorporated into porcine skinned cardiac fibers together with human cTnI and cTnC (Szczesna et al, 2000). A transgenic mouse model, expressing the I79N mutation, has demonstrated similar properties (*i.e.* increase in the Ca^{2+} sensitivity of force development and ATPase activity) as well as other phenotypic properties of HCM, such as impaired diastolic function. Similar results have been seen at both molecular and physiological levels, implying that altered Ca^{2+}regulation of muscle contraction by TnT mutations might be the primary mechanism for TnT-linked HCM. There are strong evidences that ΔE160 TnT mutation increases Ca^{2+} sensitivity of both myofibrillar ATPase activity and force development of skinned fibers by increasing Ca^{2+} affinity of TnC (Harada et al, 2000; Tobacman et al, 1999). Although the mechanisms by which single point mutation in TnT may cause a Ca^{2+} sensitizing are still not clear, an increased Ca^{2+} sensitivity of force development might be

explained by one of the following ways or a combination of them: i) increased Ca^{2+} affinity of TnC; ii) reduced inhibitory action of TnI, and iii) activation of the actomyosin interaction that indirectly leads to increased Ca^{2+} affinity of TnC (Harada & Potter, 2004).

1.3.2 Force generating capacity.

The precise impact of specific HCM mutations on the maximal force generating capacity of human cardiac sarcomeres remains controversial. A large number of studies have been published on the impact of HCM mutations on the force generating capacity of the sarcomere. The R403Q mutation in myosin heavy chain was the first mutation to be identified as responsible for familial hypertrophic cardiomyopathy (Geisterfer-Lowrance et al, 1990). On the basis of extensive work on systems containing the R403Q mutant myosin (Cuda et al, 1993; Fujita et al, 1997; Lankford et al, 1995; Roopnarine & Leinwand, 1998; Sata & Ikebe, 1996; Sweeney et al, 1994) which showed a loss of function, it was hypothesized that HCM was caused by altered acto-myosin interactions. Therefore, the resulting loss of sarcomere force would drive the hypertrophy of the left ventricle (Cuda et al, 1993; Marian, 2000). This apparent uniformity in the effects of HCM mutations led to a compensatory hypertrophic hypothesis for HCM. This hypothesis was then challenged by numerous findings. (Belus et al, 2008). A recent work in skinned cardiomyocytes and single myofibrils isolated from several HCM patients carrying mutations in different myofilament proteins, including mutation in thick (MYBPC3, MYH7) and thin (TPM1, TNNI3, TNNT2) filaments, has shown that the disease is usually associated with some impairment of the sarcomere maximal tension generating ability. However, low cardiomyocytes maximal force in HCM patients can be largely explained by reduced myofibril density and secondary hypertrophy remodeling rather than a primary defect of the mutation (Witjas-Paalberends et al, 2013). Evidence of enhanced motor activity has been reported for HCM mutations in cardiac myosin binding protein C and thin filament proteins (Homsher et al, 2000; Stelzer et al, 2006). In a study by Knollmann et al, the cardiac performance of isolated mouse hearts carrying the cTnT I79N mutation were examined and compared with transgenic mice expressing human wild-type TnT**.** Systolic function was significantly increased in Tg-I79N hearts at 0.5 and 1mmol/liter $[Ca^{2+}]_o$, with no difference in diastolic function; diastolic dysfunction became manifest at higher $[Ca^{2+}]_o$. *In vivo* measurements with echocardiography and Doppler confirmed that, at base-line, systolic function was significantly higher in Tg-I79N mice without evidence for diastolic dysfunction (Knollmann & Potter, 2001). It has been shown that single point mutations in the Tm binding site of TnT do not result in changes in maximal force-generating capability (Morimoto et al, 1998; Tardiff et al, 1999), but can enhance the isometric tension at submaximal Ca^{2+} concentrations, by increasing myofilament response to Ca^{2+}.

1.3.3 The energy cost of contraction.

A common feature of many studies on HCM disease mechanisms is the excessive energetic cost of tension generation by sarcomeric mutations (e.g. (Chandra et al, 2005; Ferrantini et al, 2009; Frey et al, 2006). Evidence that HCM sarcomere mutations may increase the energy cost of force production through inefficient or excessive ATP usage has led to the proposal of the "energy depletion hypothesis" for HCM. The energy cost of contraction has been evaluated through many different techniques. It has been shown, using nuclear magnetic resonance (^{31}P NMR) spectroscopy, that the cardiac phosphocreatine (PCr) to ATP ratio (PCr/ATP), a measure of energy status, is significantly reduced in HCM patient hearts and animal models for mutations in myosin heavy chain (MHC) (R403Q) and cTnT (R92Q) (Crilley et al, 2003; He et al, 2007; Javadpour et al, 2003; Jung et al, 1998; Luedde et al, 2009). In HCM patients the PCr/ATP ratio was reduced in mutation carriers both with

and without left ventricular hypertrophy, and it was even compromised in asymptomatic HCM. All these studies suggest that energy deficiency is a primary consequence of the underlying mutation rather than a secondary consequence of cardiac remodelling (either LV hypertrophy or heart failure). If myocardial wall tension and energy demand are not uniformly distributed in the left ventricle as suggested by theoretical models (DeAnda et al, 1998) and experimental studies, extra energy requirements could be more damaging in specific myocardial regions providing an explanation for the asymmetrical hypertrophy and degenerative changes observed in the interventricular septum of the patient (Belus et al, 2008).

Thin filament mutations exert their effects not only by altering Ca^{2+} sensitivity but also by increasing the energy cost of contraction (Chandra et al, 2005), similarly to HCM-related mutations in other genes (Ashrafian et al, 2003): the increased ATP consumption leads to energy depletion that alters the physiology of the whole heart (Javadpour et al, 2003). It was also observed in a mouse model expressing the cTnT R92Q mutation an increase in lipid deposition and smaller mitochondria. An intriguing possibility is that, with an increase in basal sarcomeric activation, chronic mismatch between ATP synthesis and ATP consumption by the overall cross-bridge activity may result in observed changes in lipid content and mitochondrial morphology.

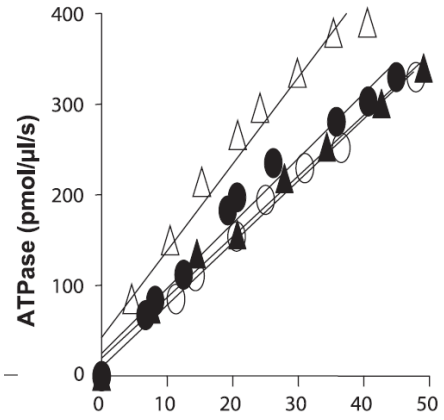

Fig 1.3.3 Relationship between steady-state isometric tension and ATPase activity in detergent-skinned muscle fiber bundles from TG mouse hearts. Simultaneous measurements of force and ATPase activity were carried out at different pCa values, and data were fitted using a linear regression analysis. ○, WTTG muscle fibers; ●, R92W TG muscle fibers ▲R92L TG muscle fibers; Δ, Delta-160 TG muscle fibers. resting SL was adjusted to 2.3 m. Slope values (tension cost) in $pmol*mN^{-1}*mm^{-1}* s^{-1}$ are WTTG, 6.8; R92W, 7.2 ;R92L, 6.7 and Delta-160, 9.6. For clarity, the linear fit shown in represent 1 set of data for WTTG, R92W, R92L, and Delta-160 TG muscle fibers. Modified from Chandra et al, 2005.

For instance, analyzing well-established mouse models carrying different cTnT mutations, it has been shown that the different effects of TnT mutations result in different disease phenotypes in transgenic mice. The tension-dependent ATP hydrolysis, in fact, increased only in Delta-160 TG muscle fibers but in R92L, R92W and R92Q was not altered compared to wild type mice (Tardiff et al, 1999) (see **Fig 1.3.3.** see also Introduction section 4)

.

1.3.4 E-C coupling alterations.

The mechanisms underlying HCM cardiomyocyte adverse remodeling in E-C coupling components are still under investigation. One of the predicted consequences of the energy depletion hypothesis for HCM is that reuptake of Ca^{2+} into the sarcoplasmic reticulum will be compromised because of the extreme energy requirements of the cardiac SERCA pump. In support of this notion, spectroscopy studies in transgenic mouse models of HCM have shown that ATP availability is reduced to a level at which SERCA function will be compromised (He et al, 2007; Javadpour et al, 2003; Spindler et al, 1998). Increased Ca^{2+} concentrations in specific micro-domains would activate hypertrophy-signalling pathways and mutation-induced abnormalities in myocyte Ca^{2+} handling could activate pathological hypertrophy signaling cascades. This idea is strongly supported by studies in HCM mice showing that treatment with Ca^{2+} channel antagonists partially blocks the development of pathological hypertrophy. Elevated diastolic intracellular [Ca^{2+}] and altered function of other ion transporters may also render the

myocardium vulnerable to the arrhythmias that underlie sudden cardiac death in HCM. The electromechanical profile of cardiomyocytes from HCM patients undergoing myectomy has been recently assessed and compared with that of cardiomyocytes from non-hypertrophic non-failing surgical patients by performing patch-clamp and intracellular Ca^{2+} studies (Coppini et al, 2013). Compared with controls, HCM cardiomyocytes showed prolonged action potential related to increased late Na^{+} (I_{NaL}) and Ca^{2+} (I_{CaL}) currents and decreased repolarizing K^{+} currents; increased occurrence of cellular arrhythmias; prolonged Ca^{2+}-transients and higher diastolic Ca^{2+}. Such changes were related to enhanced Ca^{2+}/calmodulin kinase II (CaMKII) activity and increased phosphorylation of its targets (see **Figure 1.3.4)**. Thus, an enhanced I_{NaL} seems to be a major contributor to the electrophysiological and Ca^{2+}dynamic abnormalities of ventricular myocytes and trabeculae from patients with HCM, suggesting potential therapeutic implications of I_{NaL} and CaMKII inhibition.

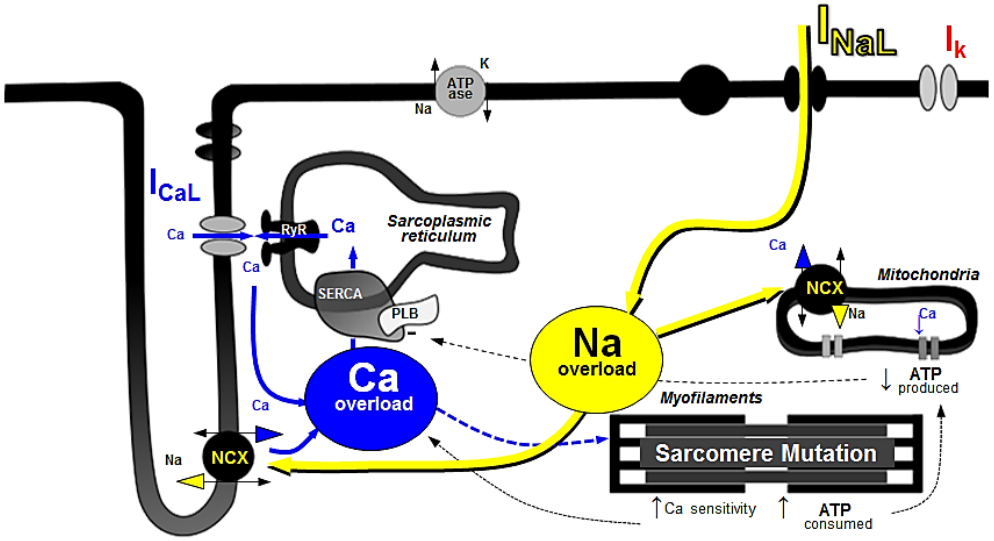

Figure 1.3.4: **Electro-mechanical remodeling in human HCM cardiomyocytes.** Sarcomeric mutations may cause a primary sustained increase of intracellular Ca^{2+} with multiple mechanisms: (i) increased sarcomeric ATP consumption that may lead to SERCA (and mithocondria) dysfunction and impaired Ca^{2+} removal; (ii) increased myofilament Ca^{2+} sensitivity that slows Ca^{2+} dissociation from the myofilaments and contributes to increased Ca^{2+} levels during diastole. Intracellular Ca^{2+} overload (in combination with increased production of reactive oxygen species) leads to sustained activation of CaMKII: increased phosphorylation of its downstream targets (Ca^{2+} channels, Ryanodine Receptors, phospholamban, Na+ channel) is responsible for the abnormalities observed in HCM cardiomyocytes, including increased I_{NaL}. Overall, these changes aggravate intracellular Ca^{2+} overload. The enhanced I_{NaL} is responsible for intracellular Na^{+} overload, which favors reverse over forward NCX mode. The latter contributes to cytosolic Ca^{2+} overload, further promoting CaMKII activation, thus setting up a vicious circle. Modified from Coppini et al, 2013.

Furthermore, a loss of t-tubules in the sarcolemmal membrane has been shown: in hypertrophied HCM cardiomyocytes, capacitance/volume ratio is reduced compared to control cardiomyocytes, reflecting a disproportion between surface vs. volume growth. (Coppini et al, 2013; Lyon et al, 2009). The reduction of t-tubular density, usually paralleled by increased cell dimensions, can be an additional pathogenic element contributing to alteration in Ca^{2+} handling and mechanical impairment. A decreased t-tubule density with loss of t-tubular currents can hinder a synchronous SR Ca^{2+}-release throughout the myocyte leading to a prolongation of $Ca^{2+}{}_{i}$ transient rise and decay (Ferrantini et al, under submission).

All these alteration have been also studied in animal models of HCM carrying sarcomeric mutations. These studies showed alterations of the kinetics of intracellular calcium transients (Szczesna-Cordary et al, 2007; Wang et al, 2006) and alterated properties of membrane electrical activity (Knollmann et al, 2003; Knollmann & Roden, 2008), such as changes in action potential duration (APD), APD

adaptation to heart rate and alterations of repolarizing potassium currents, even in the absence of hypertrophy.

The complexity of the potential role of altered Ca^{2+} fluxes is also exemplified by studies on animal models harboring specific mutations in TnT. For instance, measurement in Δ160E and R92L myocytes isolated from transgenic mouse hearts demonstrated (i) slower Ca^{2+} transient kinetics (ii) a significant reductions in SR Ca^{2+} load and uptake only Delta160E, and not R92L myocytes (iii) a significant Δ160E-specific reduction in the SERCA2a/PLB ratio, which may well underlie the observed alterations in Ca^{2+} homeostasis in Western blot analysis (Haim et al, 2007). Therefore, independent cTnT mutations result in significant mutation-specific effects in Ca^{2+} handling that may, in part, contribute to the observed clinical variability in cTnT-related FHC. Finally, all these functional changes observed in human HCM myocardium are likely a consequence of a complex remodelling process involving alterations of signaling pathways, rather than being a direct consequence of the causal sarcomeric mutations.

1.4 HCM murine models carrying troponin T mutation

Many animal models of HCM have been developed, including myosin heavy chain mutants (Geisterfer-Lowrance et al, 1990), myosin-binding protein C mutants and recently also tropomyosin and actin mutants. Here, the attention will be focused on the Troponin T mutants that are employed in the present study. As previously described, TNT1 mutations tend to cluster at the N- and C-terminal ends of the domain, with mutational hotspots occurring at residues 92–96 and 160–163. Despite their location in the same domain, these mutational hotspots exhibit significant differences in their molecular and clinical phenotypes.

A transgenic mouse model expressing a truncated mouse cTnT allele analogous to one found in HCM patients (Thierfelder et al, 1994) has been described (Tardiff et al, 1998). Heterozygous mice expressing the truncated cTnT at low levels (<5%) developed cardiomyopathy and had significantly smaller ventricles (18-27% decrease in heart mass in two independent lines of cTnT-Myc truncation mice at 4–5 months of age when compared to either non-transgenic siblings) and impaired cardiac contractility and relaxation. Interestingly, the same splice donor site mutation has also been generated in a transgenic rat model, which overexpresses the human truncated cTnT protein (Frey et al, 2000). These rats display features of FHC including diastolic dysfunction and increased susceptibility to ventricular arrhythmias, particularly during exertion or stress (Luedde et al, 2009).

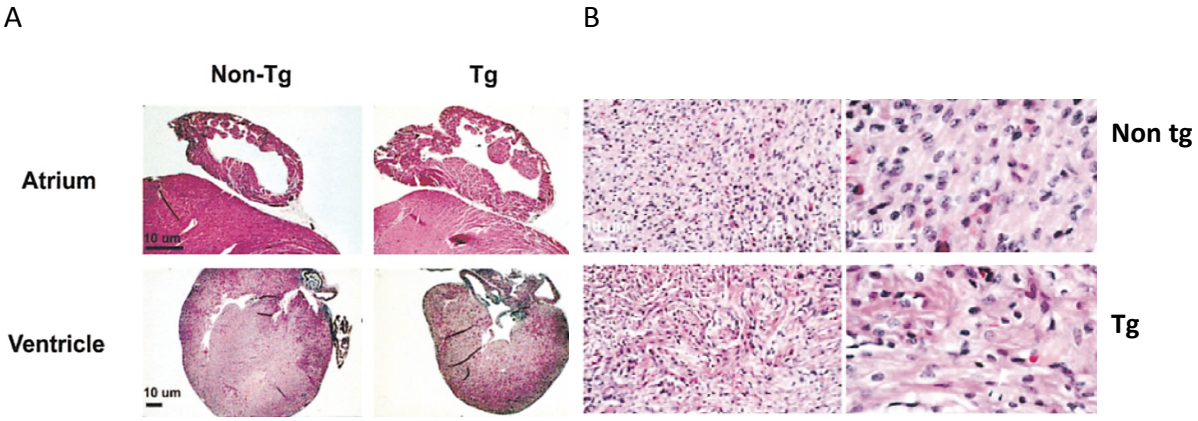

Figure 1.4a. A, Atrial and ventricular hypertrophy in 5-months-old heterozygous cTnT-Myc-truncation mice. Representative cross-sections from paraffin-embedded hearts stained with hematoxylin and eosin. B, Cardiac TnT-Myc-truncation neonatal mice display myocellular disarray and degeneration similar to that found in patients with FHC (modif. From Tardiff et al, 1998).

Histopathological analysis of mice cTnT-truncation mice hearts showed myocellular disarray and degeneration, but no fibrosis or myocyte hypertrophy (see **Fig 1.4a**). The cTnT-truncation mice bred to homozygosis expressed twice the amount of truncated protein (5–10%) than their heterozygous littermates and died within 24 h of birth. This demonstrates an important relationship between the quantity of mutant protein expression and severity of disease presentation.

Another mutation of cTnT, the Δ160E mutation, is caused by the in-frame deletion of three nucleotides encoding a glutamic acid at residue 160 (also reported as residue 163, as residues 160–163 are identical) and results in a severe form of HCM with several families exhibiting a high frequency of early sudden cardiac death (Pasquale et al, 2012; Watkins et al, 1995). Transgenic cTnT mouse line carrying 35% and 75% replacement of the endogenous cTnT with the Δ160E mutant form presented both mutation-driven changes in myofilament function: an increased ATPase activity and Ca^{2+} sensitivity (Chandra et al, 2005) and secondary Ca^{2+} handling alterations of cardiomyocytes. Both Δ160E-35% and Δ160E-70% exhibited dose-dependent shortened baseline sarcomere lengths and an impaired cardiomyocyte mechanics with significant decreases in resting intracellular calcium level, lower peak amplitude of the calcium transient and a decreased ability to remove calcium from the

cytoplasm. Transgenic myocytes exhibit a decrease in calcium load and an impaired SERCA2a activity (Haim et al, 2007). Moreover, Δ160E hearts had significantly smaller ventricles, impaired cardiac contractility and relaxation, myocyte disarray and degeneration without fibrosis or myocyte hypertrophy. Δ160E mouse hearts exhibited extensive remodeling over time when compared to Non-Transgenic siblings. These results suggest that this mutation causes a progressive ventricular remodeling in mice that increases in severity with transgene dose and well replicate disease expression in patients.

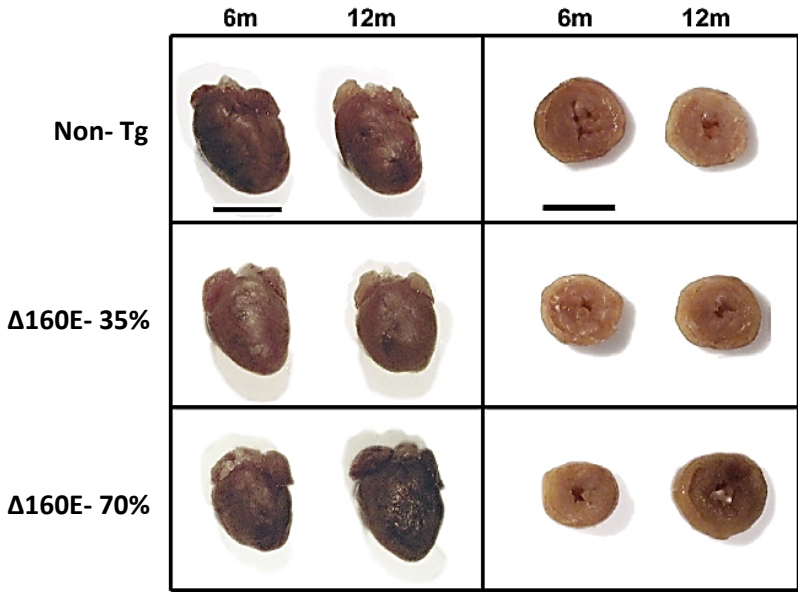

Figure 1.4b Gross morphology and size of transgenic hearts at 6 and 12 months. Representative whole hearts (left panel) and ventricular cross-sections (right panel) from each transgenic line at two time-points. Non-Tg control was sibling-matched. Bar represents 5 mm. Modified from Moore et al, 2013.

A cTnT transgenic mouse model carrying the missense mutation R92Q(Arg92Gln) within the TM-binding domain of cTnT, was also developed.(Javadpour et al, 2003; Tardiff et al, 1999). Similar to the truncated cTnT model, R92Q mice had small left ventricles, myocyte disarray, and lacked myocyte hypertrophy. In contrast, the R92Q hearts demonstrate significant interstitial fibrosis and up-regulation of hypertrophic markers. Studies with isolated cardiomyocytes from R92Q mice show increased basal sarcomere activation, impaired relaxation, and shorter sarcomere lengths. Measures of myocyte mechanics and Ca^{2+} kinetics in these mutants revealed a decreased rate of contraction, percent shortening, peak rate of relaxation, sarcoplasmic reticulum Ca^{2+} load, baseline Ca^{2+} levels, peak rate of Ca^{2+} rise and decline, Ca^{2+} peak amplitude, and SERCA/PLB ratios (Haim et al, 2007). Isolated working heart data are consistent, showing hypercontractility and diastolic dysfunction, both of which are common findings in patients with HCM. Moreover, both R92Q and Δ160E mice showed an increased frequency of arrhythmias (premature ventricular contractions) upon isoproterenol administration in the living animal as well as a slightly prolonged QRS and alterations in the atrio-ventricular conduction (Jimenez & Tardiff, 2011).

In contrast, patients who carry of the R92L (Arg-92-Leu) troponin T mutation often exhibit ventricular hypertrophy and eventually develop cardiac failure, while the frequency of sudden death is relatively low (Ertz-Berger et al, 2005).

Transgenic mouse expressing mutant R92L (Arg92Leu) and R92W (Arg92Trp) TnT were also generated and tested: accordingly, mice carrying R92L mutation showed a significant degree of hypertrophy with a later onset (7-10 months) and increased myocyte size, as well as slowed cardiac relaxation and residual diastolic tension. Light microscopic analysis of ventricular sections from both R92W and R92L adult mice revealed a broad range of histopathology consistent with that found in human mutant cTnT hearts, including myocyte disarray and degeneration, mild inflammatory cell

infiltration, occasional hypertrophied cells, and minimal fibrosis. In contrast to R92W, the R92L mice did not exhibit any significant induction of the hypertrophic gene program until late adulthood (10 months of age) (Guinto et al, 2009; Haim et al, 2007). Results from R92L and R92W myocytes showed mutation specific alterations in contraction and relaxation indexes at 2 months with improvements by 6 months. Alterations in Ca^{2+} kinetics remained consistent with mechanical data. R92L and R92W exhibited severe diastolic impairments at the early time point that improved with increasing age. Furthermore, mutant hearts demonstrate greater ATP utilization measured using ^{31}P NMR spectroscopy as decreases in [ATP] and [PCr] and $\Delta G_{\sim ATP}$ at all workloads and profound systolic and diastolic dysfunction at all energetic states. R92W hearts showed more severe energetic abnormalities and greater contractile dysfunction than R92L hearts (He et al, 2007).
Troponin T mutant mice, thus, seems to be able to replicate all the different clinical phenotypes of human HCM: an early onset disease with scarce hypertrophy and fibrosis but high risk of arrhythmias (Δ160E), a restrictive-like disease presentation with fibrosis and severe diastolic dysfunction (R92Q), a later-onset presentation with hypertrophy, impaired relaxation but only slight increase of arrhythmogenic risk (R92L). Available troponin T mutant mice are therefore an optimal model to study the pathophysiology of human HCM and test the efficacy of specific therapies on subjects with different disease phenotype. Here below a summary of what has been already examined in different cTnT mouse models carrying Δ160, R92Q, R92W and R92L mutation.

Gross heart morphology and histology

Parameters	Δ160E	R92W	R92Q	R92L
Heart hypertropy	35% line: progressing decrease in cardiac mass 70% line: less decrease due to an early onset of ventricular dilation [12]	Decrease cardiac mass[4]	Decreased cardiac mass[1]	Increase in cardiac mass[4]
Atria	Atrial dilation in the 70% line[12]		Progressive atrial hypertrophy over time and proportional increase with transgenic protein levels[1]	Atrial dilation[4]
Ventricle	35% line: smaller ventricular mass[12]	Decrease in ventricular mass[4]	Decrease in ventricular mass [1]	Small increase in ventricular mass[4]
Cell hypertropy	Absent in 35% line Some hypertrophied cells in 75% line[12]	Decrease in myocytes size[4]	Decrease in myocytes size[1]	Small increase in myocytes size[4]
Myofibrllar disarray	Moderate no fibrosis[12]	moderate to severe disarray and little fibrosis[4]	Moderate with perivascular fibrosis. Lipid deposition and increased numbers of mitochondria[1]	Mild to moderate no fibrosis no disruption of myofibrillar structure[4]

Pathogenic Signaling Pathways in the Heart

Biomarkers	Δ160E	R92W	R92Q	R92L
ANF		Early and progressive induction ANF αSK MCIP1[4]	92% line: eary and progressive induction. In 67% line: smaller degree with slow increase over the time. 30% line: low level [1]	No induction of ANF αSK MCIP1until adulthood[4]
BNF			decreased[1]	
MCIP1		Early activation[4]		
β-myosin			Progressive induction over time with late onset[1]	

In vivo and whole heart parameters

Parameters	Δ160E	R92W	R92Q	R92L
Whole heart Contractility +dP/dt	No changes compared to WT[12]	Impaired both at baseline and with inotropic challenge[7]	Hypercontractility. R92Q hearts failed to increase contractile performance in response to increases in $[Ca^{2+}]$[1 and 10]	Impaired both at baseline and with inotropic challenge[10]
Whole heart Contractility -dP/dt	70% line: significantly Impaired in response to an inotropic challenge[12].	Impaired with pronounced inability to increase their rate of relaxation in response to increased perfusate $[Ca^{2+}]$[7]	Impaired: no increase in contractile performance in response to inotropic challenge[1 and 10]	Impaired[10]
Aftercontractions	Increased after isoproterenol injection[13]		Increased after isoproterenol injection[13]	
Heart rate (Telemetry)	Impaired HR regulation[13]		Higher HR[13]	
Arrhythmias (Telemetry)	Heart block at baseline[13]		No at baseline[13]	
^{31}P NMR studies		Decreases in [ATP] and [PCr] and $\Delta G_{\sim ATP}$ at all workloads and profound systolic and diastolic dysfunction at all energetic states.[7]	Decreased [PCr] and increased [Pi] and [ADP] .$\Delta G_{\sim ATP}$ is lower. R92Q hearts have a lower driving force for ATPase reactions.[5]	Decreases in [ATP] and [PCr] and ΔG~ATP at all workloads and systolic and diastolic dysfunction at all energetic states.[7]

Skinned fiber bundles

Parameters	Δ160E	R92W	R92Q	R92L
Ca^{2+} sensitivy of force	1.3 fold increased[6]	2.5-fold increased[6]	nearly 2 fold increased[2 and 3]	2 fold increased[6]
Max force	no significant differences in Ca^{2+} activated max tension[6]	no significant differences in Ca^{2+} activated max tension[6]	no significant differences in Ca^{2+} activated max tension[2]	no significant differences in Ca^{2+} activated max tension[6]
Tension Cost	Increased[6]	No increased[6]	No increased[2]	No increased[6]
k_{tr}			2.2-fold increase in the Ca sensitivity of the k_{tr} No alteration at F max[2]	
V_{max} (IVM)*		Slight decrease and decreased Ca^{2+} sensitivity of thin filament sliding speed[11]		Slight decrease and decreased Ca^{2+} sensitivity of thin filament sliding speed[11]

*IVM= in vitro motility

Intracellular Ca^{2+} handling and SERCA function

Parameters	Δ160E	R92W	R92Q	R92L
Diastolic Ca^{2+}	Decreased[12]	Decreased at 6 months[9]	Decreased[10]	No changes/ Trend toward a decrease at 6 months[8 and 9]
Ca^{2+} Transient amplitude	Decreased[12]	Decreased at 2 months ameliorates at 6 months[9]	Decreased[10]	Normal at 2 months[9]
Ca^{2+} Transient Time to peak	Decreased[12]	Decreased at 2 months ameliorates at 6 months[9]	Decreased[10]	Trend towards a slower rate[9]
Ca^{2+} Transient Decay time	Decreased[12]	Decreased at 2 months ameliorates at 6 months[9]	Decreased[10]	Trend towards a slower rate[9]
SR content	Decreased[12]	Decreased[9]	Decreased[10]	Not diminished[9]
SERCA activity	Decreased (~50%)[12]	Decreased[9]	Decreased[10]	No changes[9]
Max velocity (nmol/ng/min)	Decreased[12]	Decreased but slight improvement at 6 months . EC_{50} decreased at 6 months[9]	Decreased (restored by elevated β-MyHC expression)[10]	No changes. EC_{50} decreased at 2 months. Comparable to WT at 6 months.[9]
SERCA /PLB	Trend toward a decrease in 35% line. Increased in 70% line[12]	Trend to an increased ratio[9]	Decrease[10]	No changes[8 and 9]

Intact ventricular cardiomyocytes

Parameters	Δ160E	R92W	R92Q	R92L
Baseline SL	Shortened[12 and 8]	Shortened[9]	Shortened[1]	No changes[8 and 9]
% of shortening	Diminished[12 and 8]	Diminished at 2 months, normal at 6 months[9]	Diminished[1]	No changes[8 and 9]
Peak rate of contraction	Decreased[12 and 8]	Diminished at 2 months, normal at 6 months[9]	Decreased[1]	No changes[8 and 9]
Peak rate of relaxation	Decreased[12 and 8]	Impaired at 2 months a trend of improvement at 6 months[9]	Decreased[1]	Impaired at 2 months a trend of improvement at 6 months[8 and 9]

Protein expression/Phosphorylation levels

Parameters	Δ160E	R92W	R92Q	R92L
SERCA2a expr	Diminished[8]	Trend towards decrease at 2 months worsening at 6months[9]	No alteration[1]	Normal / increased[9 and 10]
NCX	Augmented only in 70% line[8]	Augmented[9]		No altered[9 and 10]
P-PLB ser16/ thr 17	In 35% line: Trend toward an increase at 4 months.[12]	Trend toward an increase at 4 months. Significant increase at 6 months[9]	Increased protein level. Lower Ser16 P-PLB [10]	No changes[9 and 10]
P-TnI ser 22/23		Normal levels at 4 months. Decreased at 6 months[9]		Normal levels at 4 months. Decreased at 6 months[9 and 10]

Empty boxes: not determined values in literature. The references are shown below:

[1](Tardiff J et al, 1999)
[2](M. Chandra et al, 2001)
[3](Montgomery et al, 2001)
[4](Hertz Berger et al, 2005)
[5](Javadpour MM et al, 2003)
[6](M. Chandra et al, 2005)
[7](He H. et al, 2007)
[8](Haim HE et al, 2007)
[9](Guinto P. et al, 2009)
[10](Rice R et al. 2009)
[11](Manning EP et al, 2012)
[12](Moore R.K. et al, 2013)
[13](Jimenez et al, 2011)

Aim of the thesis.

Many of cTnT mutations linked to cardiomyopathies occur within the α-helical TM binding TNT1 domain, a highly charged region of unresolved high definition structure at the C-terminal end of TNT1. Mutations in this region result in a clinical subset of familial hypertrophic cardiomyopathy, phenotypically diverse and often severe.

Aim of this thesis is to determine the mechanistic links between thin-filament mutations and clinical phenotypes by studying the functional impact at sarcomeric and cellular level of different cTnT mutations in TG heterozygous mice.

First, we aimed to identify the primary sarcomeric alterations and the secondary electro-mechanical remodelling occurring in heterozygous transgenic mice carrying E163R cTnT mutation (an arginin substitution for the negative glycine at residue 163) so to understand how primary changes in myofilament efficiency could lead to secondary E-C coupling alterations. By comparing the abnormalities found in E163R to those identified in another mouse model carrying R92Q cTnT mutations, we investigate the mutation-specific primary (early) or secondary (late) components of the myocellular response.

To attain this goal, we combined varied expertise: cardiac mechanics, cellular electrophysiology, mechanical measurements on intact cardiac multicellular preparations, intracellular Ca^{2+} measurements from single cardiomyocytes, energetic and mechanical measurements on detergent skinned trabeculae, and analysis of mechanical and kinetic properties in single myofibrils with fast solution switching tecnique. Specific aims are clarified in the first part of each results section.

2: Methods

The experiments described in this thesis were aim to investigate : (i) the mechanical behavior of intact multicellular cardiac preparations; (ii) the mechanical and energetic behavior of detergent-skinned ventricular trabeculae; (iii) the mechanical and kinetic properties of single myofibrils; (iiii) epifluorescence measurements from single intact cardiomyocytes. All preparations were obtained from mouse hearts from WT and TG models. In the present chapter we provide a detailed overview of all experimental preparations and techniques used in the study.

2.1 Transgenic mouse model

2.1.1 Animal model, genotyping and assessment of gross heart morphology.

E163R transgenic constructs were generated in Jil Tardiff lab (Tucson, Arizona, USA) via pronuclear injection as previously described (Tardiff et al, 1998). In brief, a *c-myc* tag engineered onto the N-terminal end of the construct is used to identify the transgene via PCR (forward primer: TCCTCTTCAGAGATGAGCTTT; reverse primer: ACCTAGAGGGAAAGTGTCTT). E163R mutation was introduced via the Quiczk Change Site Directed Mutagenesis kit (Stratagene). Transgenic lines expressing a mid level of transgenic protein (50% E163R) were backcrossed into C57Bl/6 background for at least 7 generations and two male E163R progenitors were transferred in April 2011 from the Albert Einstein institute to our Animal facility (CeSaL) in Florence. The progenitors were inbreed with C57Bl/6 females and the colony was amplified for four generations. At four- to six-weeks of age mice were genotyped and at 24 to 28-weeks were used for the experiments. Sibling mice were used to provide Non-Transgenic controls (paired for each set of experiments). Experimental protocols and animal maintenance were performed according to local ethical committee for animal use.

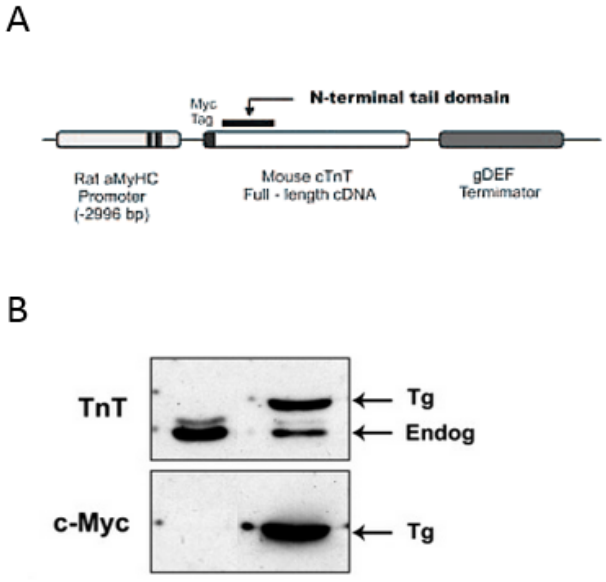

Fig 2.1.1 Characterization of mutant mice. (A) scheme of the transgenic gene (modified from Briar R. Ertz-Berger et al, 2005). (B) Western blot analysis of heart homogenates and Non-Tg mice probed with antibodies, as indicated. TnT upper band represents c-myc tagged transgenic protein and lower band represents endogenous cTnT (modified from Moore et al, 2013).

Gross heart morphology and chambers dimensions, were quantified as heart /body weight, ventricle/body weight and atria/body weight ratios. Mouse body weight was assessed right before the

sacrifice. Freshly isolated hearts from 6 month old mice were weighted right after perfusion in the KB buffer (see the protocol below). Atria were dissected from the heart, maintaining the atrio-ventricular ring attached to the ventricles. The left and right atrium were weighted together and separately. Heart masses calculated with this method and normalized on the animal body weight provide numbers that are comparable to those obtained from hearts that were treated with fixatives (Moore et al, 2013).

2.1.2 Markers of hypertrophy:

Quantitation of MHC-α/MHC-β in myocardial samples is widely recognized as a method for documenting progressive cardiac remodeling associated with cardiovascular disorders, including cardiomyopathies. In mice carrying R92Q cTnT mutation, for instance, an age-dependent α to β shift in myosin isoform was found (Tardiff et al, 1999). As already found in the R92Q model, the E163R cTnT model is also expected to show modifications of sarcolemmal and SR protein expression with disease progression. For this reason, some myocardial samples from E163R mice and WT siblings were used for proteomic and mRNA expression analysis.

- **Myosin Isoform expression**

Myofibril isolation and subsequent protein electrophoresis analysis of α and β MHC expression expression levels were performed as described previously by Belus et al, 2008; Reiser & Kline, 1998; Toniolo et al, 2005. Briefly, the MHC isoform composition of mouse cardiac samples was assessed using a minigel electrophoresis system and a nongradient gel by a procedure derived from Talmadge & Roy, 1993 (Talmadge & Roy, 1993). Electrophoresys was carried out at 4°C for 19h at 70 V. The augmented appropriate gel thickness (1 mm instead of 0.75 mm, in order to reduce resistance) low glycerol concentration in the separating gel, low voltage and prolonged running time allowed us to achieve the resolution required for the separation of the two adult cardiac MHC isoforms. Gels were stained with Coomassie Blue for quantitative analysis. The destained gels were digitalized and analyzed with a specific software (UN-SCAN-IT gel 6.0 software (Silk Scientific, Inc., UT, USA), allowing quantification of band intensity. Each band (MHC-α or MHC-β) was expressed as percent of the total MHC.

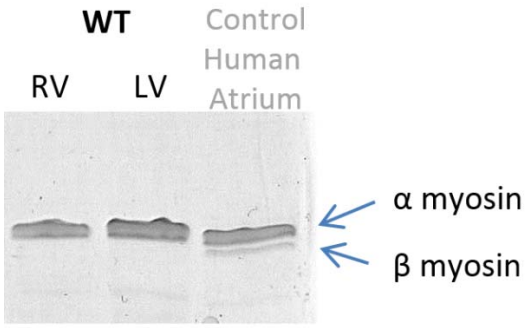

Fig 2.1.2 Gel analysis of mouse hearts. Representative 8% SDS-PAGE gel of a myofibril suspension from left and right ventricles of WT. Control human atrial myofibrils were used for comparison to identify the position of the β-myosin band; here, only α myosin is expressed in WT .

- **mRNA levels for sarcolemmal and SR proteins**

RT-PCR: mRNA isolated from septal specimens underwent reverse transcription and the resulting cDNA was employed for quantitative real time PCR using predesigned assays for the following genes: Kv4.3, KChIP, HERG2b, KCNQ1, CaCNA1.2, NaV1.5, NCX1, PLB, SERCA2a and RYR2. Total RNA from each frozen cardiac sample was isolated and DNase-treated with the RNeasy Fibrous Tissue Mini Kit (Qiagen) following manufacturer's instructions. Single-stranded cDNA was synthesized from 2 μg total RNA using the High Capacity cDNA Reverse Transcription Kit (Applied Biosystems) as described before. The genes selected for quantification were investigated using predesigned TaqMan® Gene Expression assays (Applied BioSystems, USA). All reactions were performed in triplicate and included a negative control. Relative quantification of the mRNA level for the different genes was determined by the 7500 system software (Applied BioSystems, USA), using the comparative method (ΔΔCt). In brief, the threshold cycle (Ct) difference of the index gene and the reference gene, calculated from each specimen, is subtracted from the average Ct of the control group; this value is used as the exponent of 2 to calculate ΔΔCt for each specimen. For all mRNA quantification assay, GAPDH was used as reference gene. In order to validate GAPDH as a reference gene, GAPDH mRNA was compared with ribosomal RNA 18S and expression level calculated as ΔΔCt.

2.2 Intact ventricular multicellular preparation and intact cardiomyocytes

2.2.1 Dissection of intact ventricular trabeculae

Right ventricular trabeculae, were selected because of their similarity with fascicles in the cardiac wall (Baudino et al, 2006; Hanley et al, 1999). They were dissected from mice as previously described (de Tombe & ter Keurs, 1990). Mice of both sex were heparinized (5000 UI/ml) and sacrificed with cervical dislocation. The heart was rapidly excised, perfused retrogradely via the proximal aorta with a modified Krebs-Henseleit solution (KH solution, see below) and placed in a dissection dish beneath a binocular microscope (**Figure 2.2.1a)**. During retroperfusion and dissection phases, the potassium concentration in the solution was raised to 15 mM to stop spontaneous beating of the heart. BDM 20 mM was also added to the solution to minimize contractures following cutting damages. Free running ventricular trabeculae were dissected from the right ventricle as shown in **Figure 2.2.1b**. Thin, unbranched, uniform trabeculae, running between the free wall of the right ventricle and the atrioventricular ring, were selected and carefully dissected by cutting through the atrioventricular ring on one end and removing a portion of the right ventricular wall on the other end (**Figure 2.2.1b**).

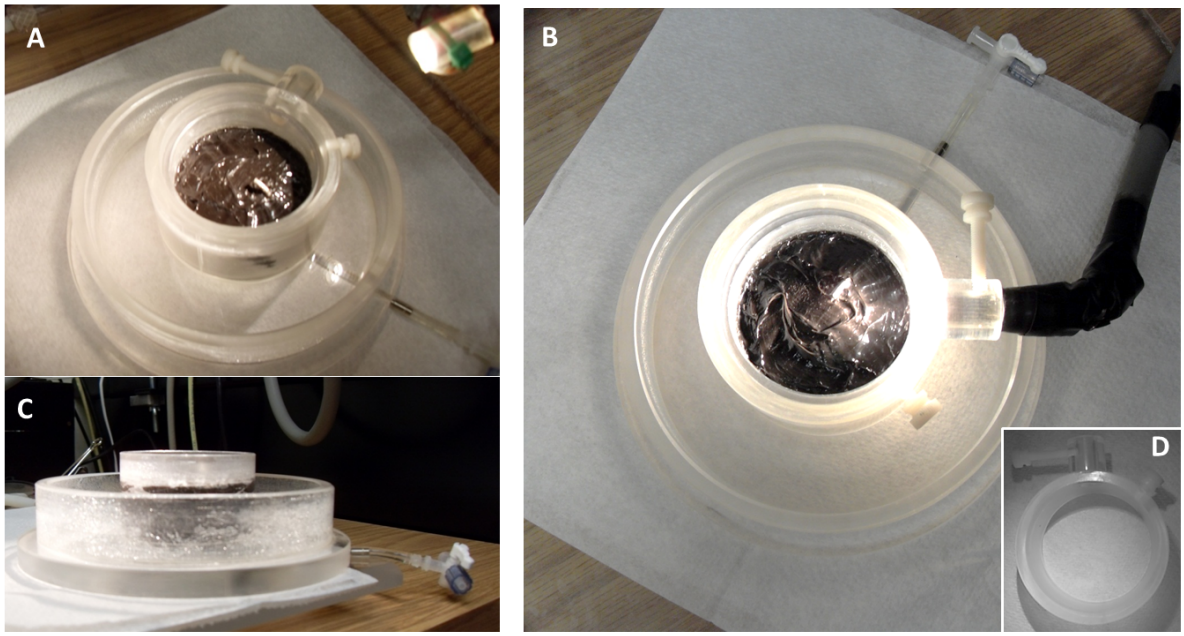

Figure 2.2.1a Dissection dish. Diagonal (A), top (B) and lateral (C) view of the dissection dish. It consists of i) an internal chamber, with an elevated bottom made of Sylgard (Sylgard® 170 Silicone Elastomer) to pin the tissue during dissection ; and ii) an external chamber (with lower bottom level) that works as a reservoir for solution overflow from the internal chamber. A metal cannula connected with the perfusion system and protruding t from the Sylgard bottom is designed to be gently inserted into the aorta for coronary retro-perfusion. An external ring mounted around the internal chamber works as light support allowing tissue trans-illumination during dissection for identification of small trabeculae under the atrio-ventricular ring. The dissection dish was designed by P.de Tombe, Lyola University of Chicago and H.D.J. ter Keurs University of Calgary)

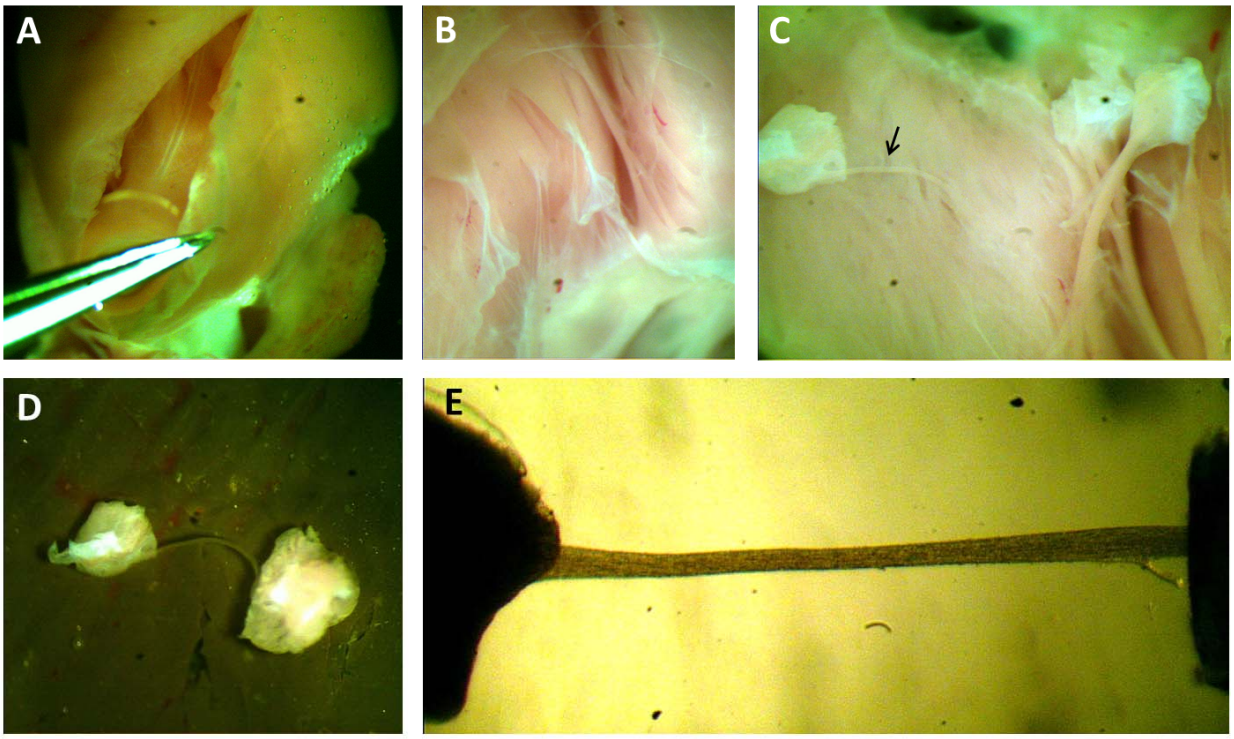

Figure 2.2.1b Dissection of right ventricular trabeculae. The free wall of the right ventricle is gently separated from the ventricular septum (A) and thin, unbranched, uniform trabeculae, running between the free wall of the right ventricle and the atrioventricular ring (B &C), are selected (e.g. trabecula indicated by the arrow) and carefully dissected by cutting through the atrioventricular ring on one end and removing a portion of the right ventricular wall on the other end. Dissected trabecula free in bath (D) and mounted in experimental apparatus (E).

The composition of modified Krebs-Henseleit solution was:

Table 1. *The composition of KH solution*

	Dissection solution	Experimental solution
	mM	mM
NaCl	**120**	**120**
KCl	**15**	**5**
$MgSO_4$	**2**	**2**
NaH_2PO_4	**1.2**	**1.2**
$NaHCO_3$	**20**	**20**
Glucose	**10**	**10**
$CaCl_2$	**1.5**	**2**
BDM	**20**	**-**
pH 7.4 with 95% O_2	**5% CO_2**	

2.2.2 Isolation of single cardiomyocytes from mouse hearts

Ventricular cardiomyocytes were isolated by enzymatic dissociation as previously described (Egorova et al, 2005). Briefly, the animal was heparinized (5,000 U/kg, i.p.) and scarified with cervical dislocation. The excised heart was immediately bathed in cell isolation solution and perfused retrogradely via the proximal aorta (**Figure 2.2.2 A)**. Cell isolation solution contained (in mM) 140 NaCl, 1.2 $MgCl_2$, 5 KCl, 2.8 sodium acetate, 10 glucose, 10 Hepes and 10 taurine, oxygenated with O_2; pH 7.4 (adjusted with NaOH). The coronary arteries were then perfused with this solution at 37°C for 3-4 min at a constant flow of 3 mL/min. The solution was then switched to a recirculating enzyme solution made of the same buffer added with 0.1 mg/mL Liberase (Liberase TM for mouse, Roche Applied Sciences). After 7-8 min, the ventricles were excised and cut into small pieces in buffer solution (**Figure 2.2.2** panel B**)**. Gentle stirring facilitated further dissociation of the myocytes. The cell suspension (**Figure 2.2.2** panel C**)** was let to settle and the cell pellet (~1 ml) was resuspended in Tyrode buffer (see **Table 2**) supplemented with 0.05 mM $CaCl_2$ and 1 mg/ml BSA. Calcium concentration was gradually raised to 1.0 mM

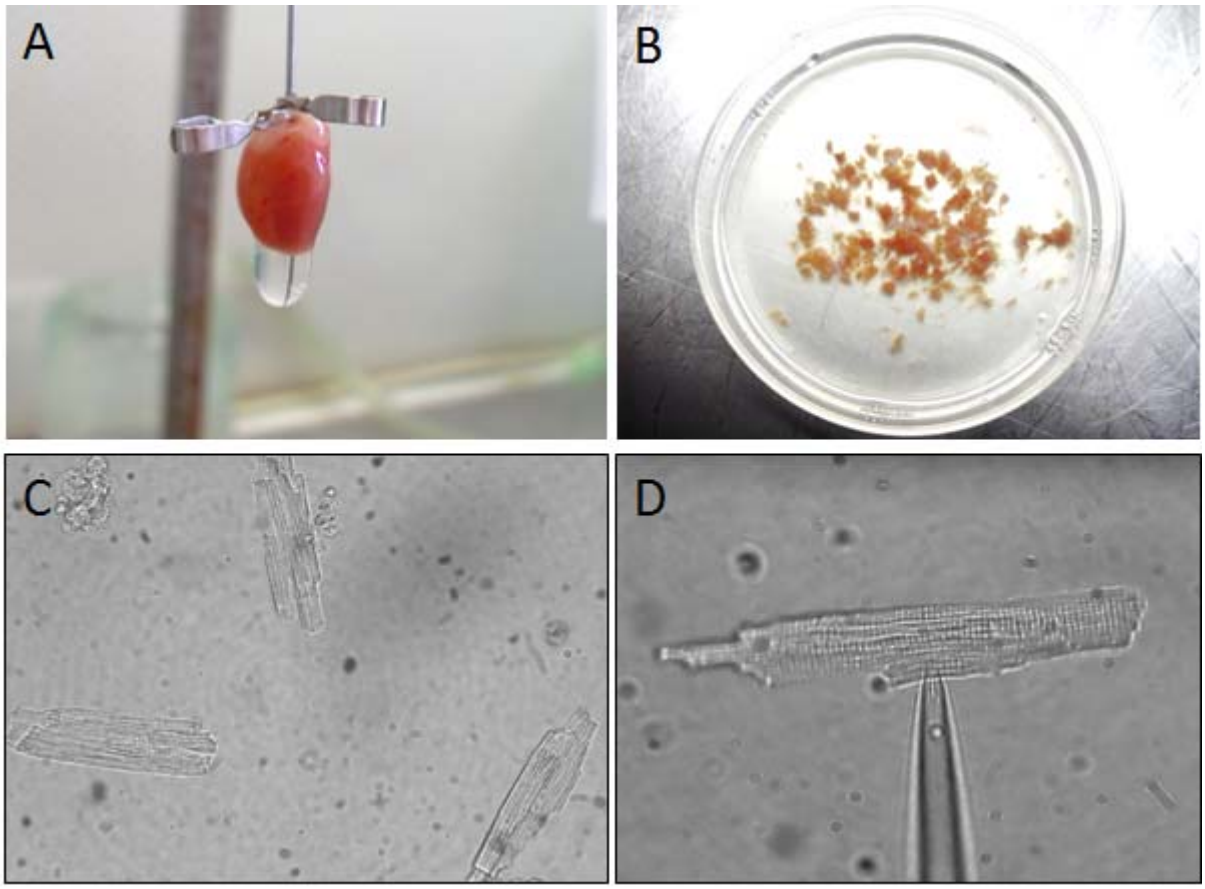

Figure 2.2.2 Enzymatic cell isolation. A) *Perfusion phase:* Cannulated heart retrogradely perfused at a constant flow of 3 mL/min at 37°C with the buffer for 3–4 min to wash out blood. B) *Cutting and stirring phase:* The ventricles were excised from the digested heart and cut into several pieces in buffer solution. Gentle stirring facilitated myocyte dissociation. C) Ca^{2+} *adaptation phase:* The cell suspension was let to settle and the cell pellet (~1 ml) was resuspended in Tyrode buffer (0.05 mM $CaCl_2$, 1 mg/ml BSA). Calcium concentration was gradually raised up to 1.0 mM, by addition of 0.05 mM of $CaCl_2$ every 10-15 minutes.

Table 2. *The composition of Tyrode buffer*

	mM
NaCl	**136**
KCl	**5.4**
Na_2PO_4	**0.33**
$MgCl_2$	**1**
Dextrose	**10**
pH 7.35 with NaOH	

2.2.3 Set up for mechanical measurements on intact cardiac trabeculae

Ventricular trabeculae were mounted between a basket-shaped platinum end of a force transducer (KG7A, Scientific Instruments Heidelberg, Germany or modified silicon strain gauge AE-801, SenSonor, Horten, Norway) and a motor (Aurora Scientific Inc., Aurora, Canada), both connected to micromanipulators. Muscles were initially perfused with the KH buffer without BDM at room temperature and stimulated at 0.5 Hz. Subsequently baseline conditions were set (30°C, 2mmol/L [$CaCl_2$], 1 Hz). Muscles were allowed to stabilize for at least 20-30 min before the experimental protocol was initiated.

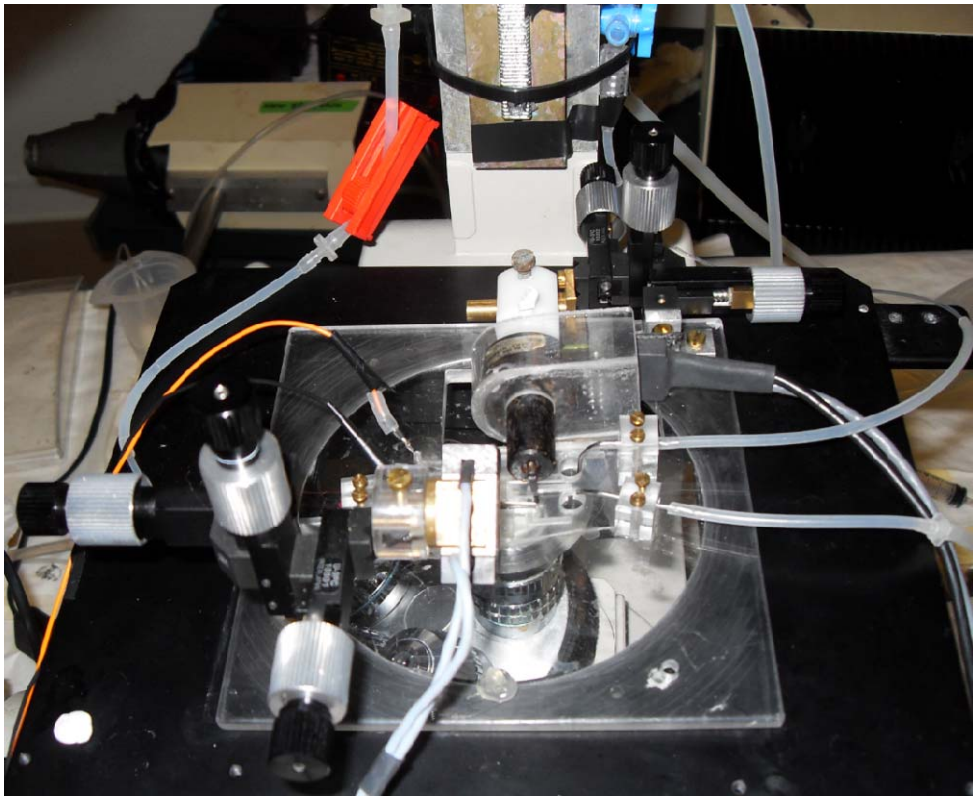

Figure 2.2.3a Set-up for mechanical measurements. The set-up was designed to perform mechanical measurements in small intact cardiac muscles. Bath dimensions were, in cm 0.5 wide x 0.4 depth x 2.5 length (volume~500µl); the bath has a thin glass bottom and is perfused with a flow of 1-10 ml/min. Temperature is controlled by heating or cooling the perfusion solution. Two parallel platinum wires deliver the electrical stimulation. Length controller and force transducer are mounted on two XYZ micrometer translation stages (Narishige U-3FC), attached to a basal plate that can be easily removed for cleaning or other purposes. The plate is mounted on an inverted microscope. Force, stimulation and motor position are respectively recorded or controlled through a Labview software developed in our laboratory.

Diastolic sarcomere length was assessed at the beginning of the experiment and readjusted, if needed, during the experimental protocol. 2D XY frames were acquired during diastole with a camera placed on one ocular of the microscope. Images were collected thought a 40x objective with bright field illumination. Trabecular diameter was measured in 2-3 points of the preparation (**Fig 2.2.3b**). Sarcomere length was assessed in two ways: (i) by selecting small regions of interests (ROIs) were the regular striation were clearly visible (approximately 2-4 µm xb10-20µm, corresponding to 5-10 sarcomeres of 1-2 myofibrils, see **Fig 2.2.3b** panel A) and analyzing the longitudinal intensity profile. Mean trabecular sarcomere length was calculated as an average of individual ROIs values (**Figure 2.2.3b** panel A&B); (ii) by selecting a large area (100 µm x 200 µm) and performing the FFT transform of the image. The spatial frequency corresponding to the first peak of the power spectrum was calculated and converted to the corresponding space distance (**Figure 2.2.3c**). Sarcomere length values obtained with the two methods were comparable. We used both methods, even if the second one reflects more accurately the mean sarcomere length of the entire population.

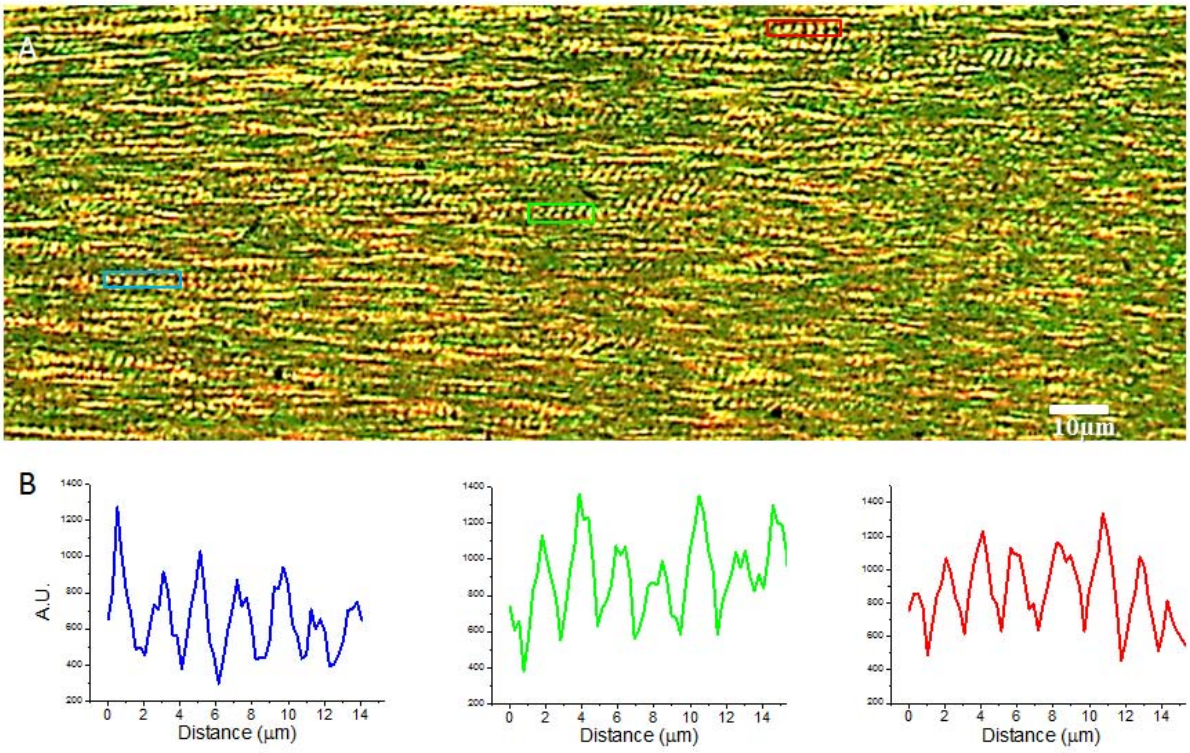

Figure 2.2.3b Assessment of diastolic sarcomere length: method 1 (A) 40x XY-frame of ventricular trabecula region. (Images are 1024x1024 pixels, 0.256 µm / pixel) For SL analysis three or more regions of interest (ROI) where sarcomeres are well-distinguishable and aligned were selected. ROI were specifically selected in distant areas of the image in order to be representative of the entire preparation, usually comprehending from 5 to 10 sarcomeres. (B) Mean longitudinal intensity profile calculated from each of the three ROI drown in panel A. Mean distance between individual picks corresponds to the SL of the selected ROI. Mean±SE value for trabecular SL was calculated by averaging the values obtained from all ROIs examined.

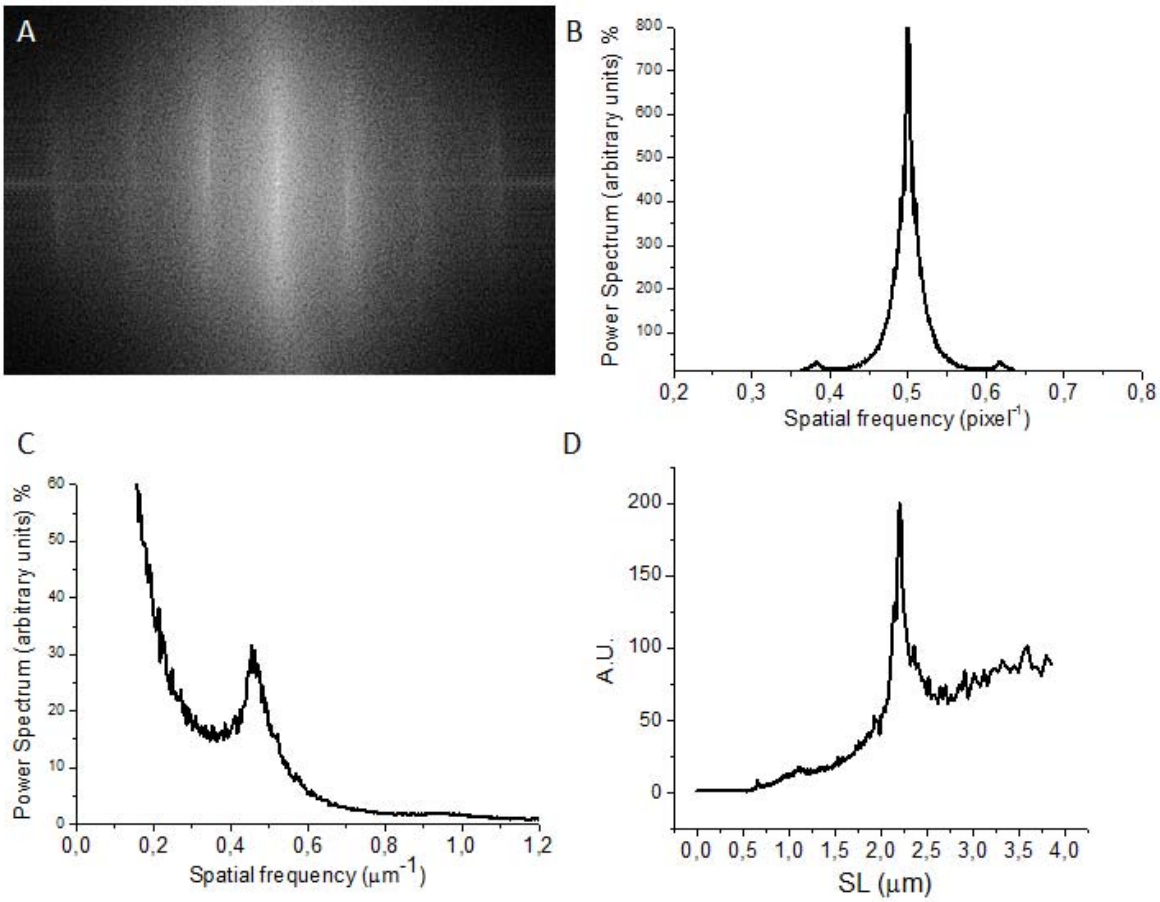

Fig2.2.3c. Assessment of diastolic sarcomere length: method 2. The sarcomere length (SL) was analyzed using a method based on the fast Fourier transform (FFT). We quantified the SL by measuring the position of the first peak of the power spectrum of the image. An open source imaging processing software (ImageJ 1.43u) was used to perform the analysis. (A-C) FFT transform (A) and corresponding row Power Spectrum (B) of the image reported in fig. **2.2.3b** panel A. The first peak corresponding to SL periodicity is shown magnified in (C and D). The intensity profile is reported in C as a function of the spatial frequency (μm^{-1}), in D as a function of the space distance (µm).

2.2.4 Experimental protocols and data analysis

Twitch force and kinetics were studied under control conditions and with the following protocols:

- Force frequency relationship

We assessed the effects of increasing stimulation frequencies (0.1-8 Hz) at 30°C. At each frequency, force was allowed to reach steady state before data were recorded (**Figure 2.2.4a A**). As previously described ,e.g. (Stuyvers et al, 2002), twitch force versus stimulation frequency forms a biphasic relation in rodents, with a descending limb (0.1 to 1Hz at 30 ºC) and an ascending limb (1 to 8 Hz at 30 ºC), **Figure 2.2.4a B&C**.

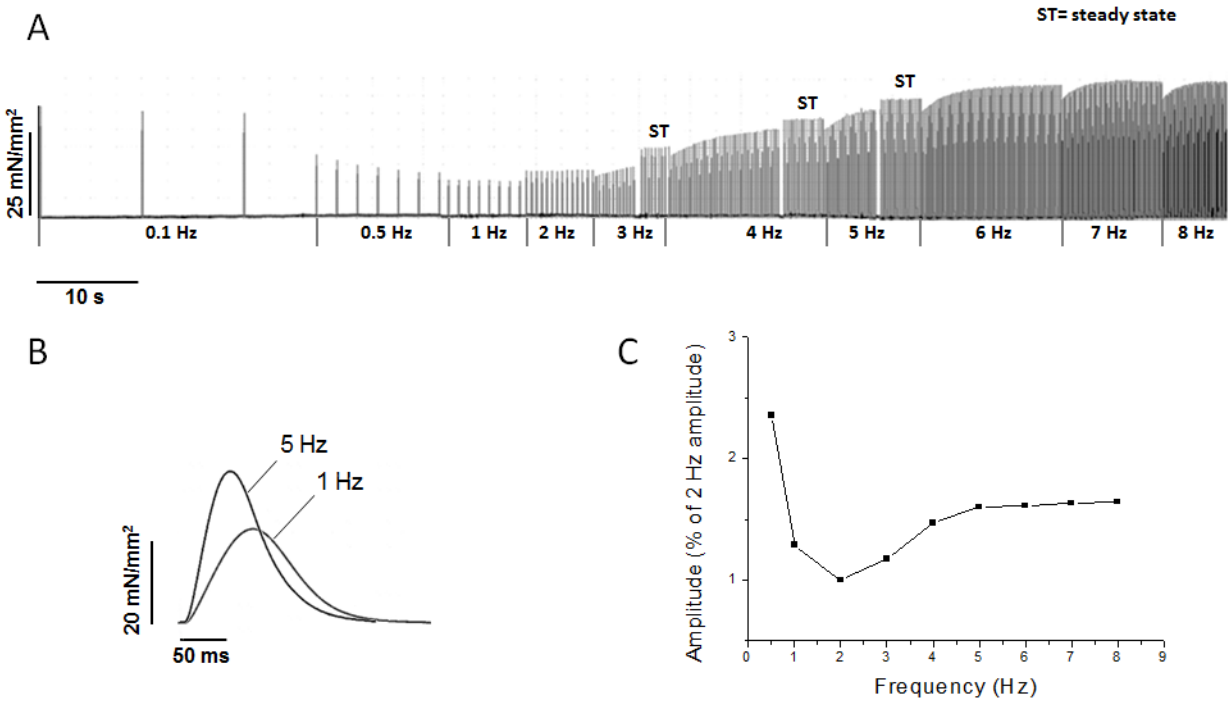

Figure 2.2.4a Force frequency relationship. Representative example of force response to increasing stimulation frequency in a mouse atrial trabecula. Traces (A&B) and force-frequency curve (C) show a positive response to high stimulation frequencies in atrial mouse myocardium (30°C, $[Ca^{2+}]_{out}$ 2 mM).

- Post rest potentiation

Post-rest potentiation was evaluated by inserting stimulation pauses after the last contraction of a steady series at 1 Hz and measuring the amplitude of the first beat after the pause . The effects of different intervals were evaluated, up to maximal pause duration of 60s. (**Figure 2.2.4b).**

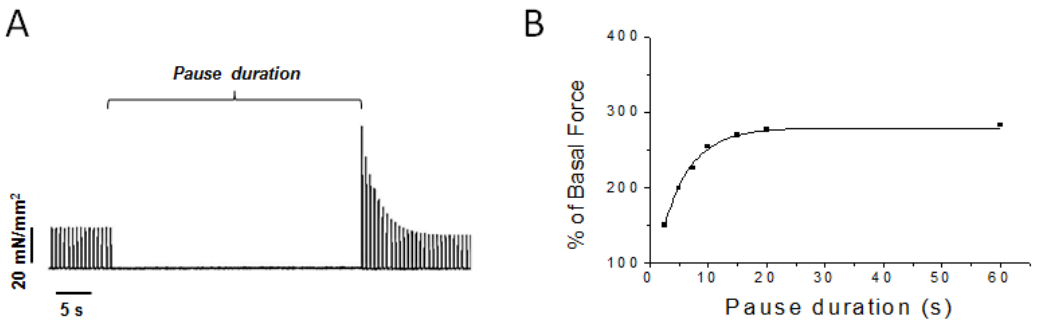

Figure 2.2.4b Post-rest potentiation Trace showing post-rest force in a mouse atrial trabecular. Curve in B show average percentage increase of force after different stimulation pauses at a basal frequency of 1Hz.

- Mechanical restitution and post extrasystolic potentiation

If a premature electrical stimulus is introduced into a regular stimulation sequence, the associated contraction (extrasystole) is reduced in amplitude and the following beat at regular interval is potentiated (post extrasystolic potentiation). After 30s of stimulation at 1Hz, a premature stimulus was given at increasing variable intervals (from 50ms to 900ms). Regularly paced stimulation is resumed 1s after the premature beat. Early premature beats (<150ms intervals) exhibited a high degree of fusion with the last regular beat: under this conditions the time course of steady state twitch force was

subtracted from the fused beat to estimate the force of the premature beat. Force of the first beat after the premature one was measured to evaluate post extrasystolic potentiation (**Figure 2.2.4c).**
Premature beat amplitudes normalized to the 1Hz steady state beat amplitude were plotted against the corresponding stimulus intervals. Restitution curves were fitted using a single exponential (Origin 8.0, Originlab); time constants and rates were calculated from the exponential fit.

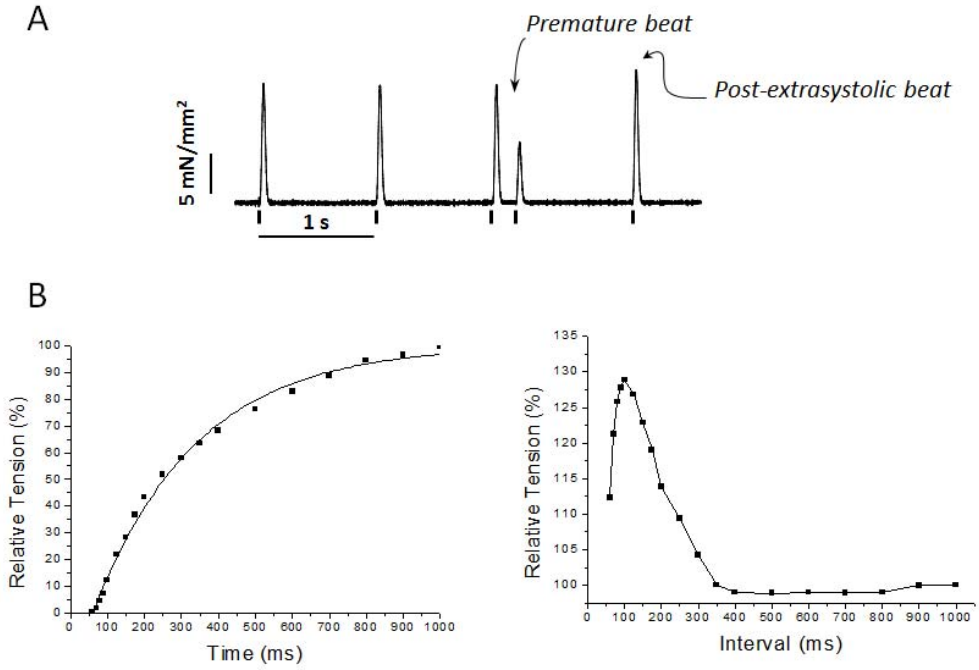

Figure 2.2.4c Mechanical restitution and post extrasystolic potentiation (A) Representative trace from a atrial mouse trabecula showing a premature beat at 250ms interval from 1Hz basal frequency and the following potentiated extra-beat. Restitution curve in B, left, shows the fractional recovery (%of 1Hz steady state) of force at the time of premature activation plotted against the interval time. Post rest potentiation curve in B, right, shows the fractional force of the extra-beat (%of 1Hz steady state) plotted against the interval time.

- Recirculation Fraction

The fraction of Ca^{2+} that recirculates in the cell during subsequent beats (Ca^{2+} recirculating fraction, RF) was estimated in isolated cardiac preparations based on the decay of the amplitude of subsequent contractions during dissipation of twitch potentiation. This because the amplitude of the contractions that follow a potentiated beat (during which Ca^{2+} release is larger) depends on the amount of released Ca^{2+} that is taken up by the SR during relaxation of the potentiated twitch, and is available for the next twitch (i.e., on the fraction of Ca^{2+} that circulates between cytoplasm and sarcoplasmic reticulum (SR) between two beats).
RF is represented by the slope of the linear relationship between the relative amplitude of subsequent contractions (Fn *vs*. Fn+1) during decay of twitch potentiation. In this study, we induced potentiation by rapid pacing (5 Hz), but similar results are expected if potentiation is induced by rest.
Measurements were taken at 0.5 Hz stimulation rate. Sample traces are shown in Chapter 4, Fig.4.5.

- Response to varied extracellular Calcium Concentrations.

Active stress development was tested at 1 Hz, with $[Ca^{2+}]_{out}$ varying between 1 and 10 mM. The trabecula was stimulated for at least 10 minutes after each solution change to achieve steady-state conditions. The different stimulation protocols described above were repeated at each $[Ca^{2+}]_{out}$ tested.

- Analysis of spontaneous activity

Spontaneous contractile activity (SP) in transgenic mice was elicited by trains of high frequency stimulation (3Hz at 30°C) followed by stimulation pauses of 15, 20, 30 and 60 s. Spontaneous contractions were identified as variations of force occurring during stimulation pauses and showing a minimum amplitude threefold higher then signal noise. First, the occurrence of total spontaneous activity was quantified plotting the occurrence of spontaneous contractions against pause duration. A second level of analysis was then performed. Several type of spontaneous activity were distinguished during stimulation pauses and classified into three groups: (i) single spontaneous contractions (S), (ii) multiple spontaneous contractions (M) (iii) regular spontaneous activity (R). R manifested as triggered activity and was distinguishable from M when the relative standard deviation (RSD) of the mean temporal distance between spontaneous beats was lower than 10%. Detailed properties of single types of spontaneous contractions were investigated. We evaluated the number and mean amplitude of spontaneous contractions for M, the mean frequency, duration (ms) and mean amplitude for R, the amplitude for S. In addition, spontaneous after-contractions were stochastically observed during steady state stimulation (0.2 to 8Hz at 30°C) and were also quantified in terms of amplitude and duration.

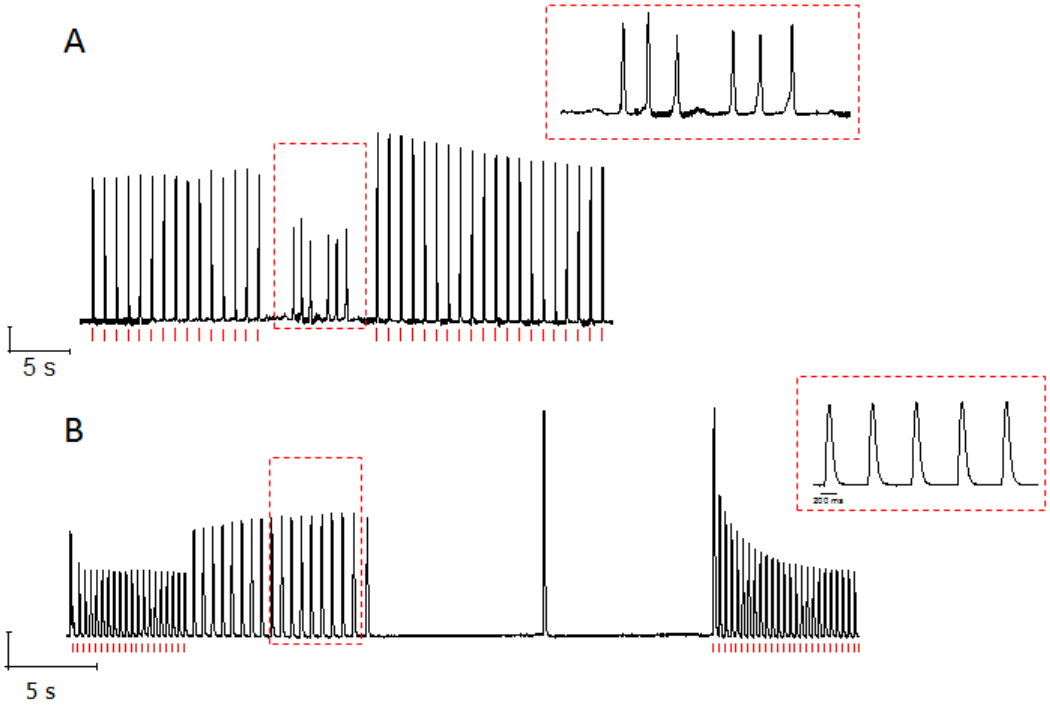

Figure 2.2.4d Spontaneous activity in TG trabecula. (A) representative trace showing multiple spontaneous contraction (M) during pauses, tracing details in the red box above. (B) triggered activity (R) and single spontaneous contraction (S) during pauses, tracing details in the red box above. Short red lines indicates the times of stimuli

2.2.5 Set up for intracellular Ca^{2+} measurements from single cardiomyocytes

Intracellular calcium measurements were simultaneously performed with membrane currents or potential recordings on patched cells. When electrophysiological measurements were not required, isolated myocytes were field stimulated with short (<5ms) pulses by platinum electrodes mounted on the sides of cell bath for field stimulation. Fluoforte fluorescence emitted at 513 nm was measured during fixed excitation at 492 nm wavelength. The emitted fluorescence was acquired by a photomultiplier (Hamamatsu photonics), to evaluate the global intracellular Ca^{2+} transient. Fluoforte (Enzo life Science) loaded by incubating cells for 30 minutes in bath solution containing 10 μM Fluoforte. After loading, cells were washed two times and were left 15-20 minutes in normal Tyrode solution. A small amount of the Cell-containing solution was transferred to a temperature-controlled recording chamber (experimental temperature= 35±0.5ºC), mounted on the stage of an inverted microscope.

2.3 Energetic and mechanical measurements in detergent-skinned cardiac multicellular preparations

2.3.1 Skinning procedure for detergent-skinned cardiac multicellular preparation

The experiments were performed using cardiac multicellular preparation (ventricular trabeculae) from which the sarcolemma and all the internal membrane system (e.g. sarcoplasmic reticulum, nuclear and mitochondrial membranes) were removed. These 'skinned' preparations can be activated by calcium in the presence of MgATP to produce isometric contractions. Thin, unbranched, and uniform trabeculae were carefully dissected from the right and the left ventricle. The preparations were 1.37±0.09 mm in length, 139±14 μm in width, and 147±17 μm in thickness (mean ± SEM, n=17). After dissection, the trabeculae were transferred to a dish containing cold (4°C) standard relaxing solution (see below) to which 0.1% (vol/vol) Triton X-100 was added in order to chemically permeabilize the preparation. The preparations were left overnight in this solution to allow solubilization of virtually all membranous structures. Next, a selected skinned trabecula was attached to aluminum T clips (Goldman & Simmons, 1984) and mounted in the experimental setup. Metal clips were made from aluminum kitchen foil by a printed-circuit etching technique. They had a T shape (**Fig 2.3.1**) similar to that described by Ford et al. (Ford et al, 1977). Of notice, block of tissue was left at both ends, in order to facilitate the procedure. A clip was bent tightly at each end of the skinned trabecula. The T-clips were pressed down on to the block of tissue only in the center of the arms of the T so that the foil edges would bend up away from the preparation and not damage the trabecula. Finally, the trabecula was transferred to the experimental apparatus on a little glass piece.

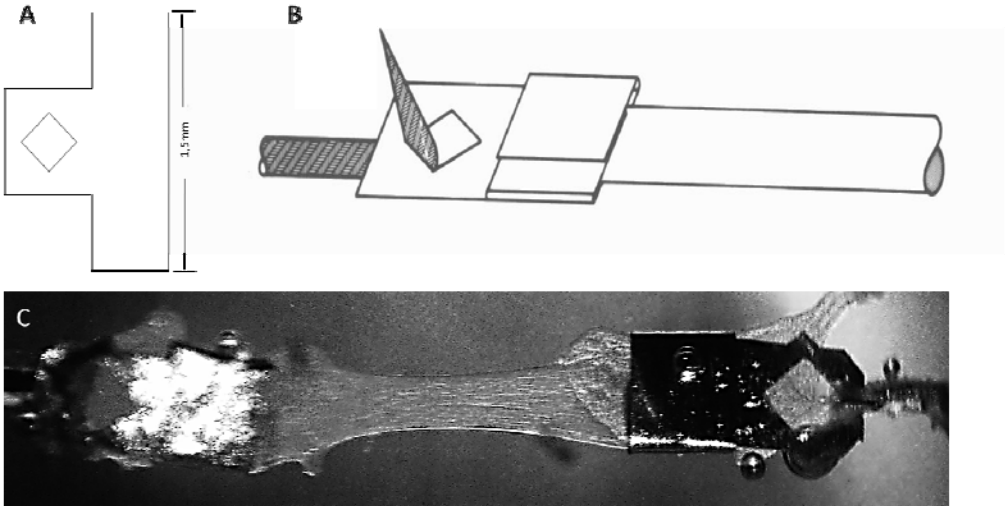

Fig 2.3.1. T-clips and mechanical attachments of the muscle preparation. (A) T-shaped aluminum foil clips for clamping to the skinned trabecula. **(**B**)** Method of attachment of the clip to the preparation (modified from Goldman & Simmons 1983). (C) Skinned trabecula attached to aluminum T clips and mounted in the experimental setup. The metal hook at the left indicates the position of the motor or tension transducer attachment.

2.3.2 Solution for ATPase measurements

The composition of the standard relaxing solution was as follows in **Tab 3**.

Table 3. *The composition of relaxing solution for skinning procedure and mounting*.

	Stock sol.	pCa9
MgProp	0.1M	6.078
NaEGTA	0.1M	10
KProp	1M	5.42
Na_2SO_4	0.1M	17.68
MOPS	1M	1
ATP		0.2996 g
Creatin Phosphate		0.3272 g
ml/ 100ml pH 7.0		

Three bathing solutions were used for the experimental protocol: a relaxing solution, a preactivating solution with low calcium-buffering capacity and an activating solution. The composition of these solutions is shown in **Table 4**. In addition, all solutions contained 0.9 mM NADH, 2.67 mg/mL pyruvate kinase (500 U/mg), 0.24 mg/mL LDH (870 U/mg), 10µM oligomycin B. Oligomycine together with sodium azide 5mM were added to suppress any residual mitochondrial ATPase or ATP synthase activity. The ionic strength of the solutions was maintained at 200 mM by adding the appropriate amount of potassium propionate (KProp). The pH was adjusted to 7.1 with KOH. Aliquots of these solutions (minus enzymes, NADH and oligomycin B) were stored frozen. On the day of the experiment, the solutions were thawed, enzymes and other chemicals were added, and the solutions were kept on ice until required. Solutions were applied in the sequence: relaxing, pre-activating, activating and relaxing.

Table 4. *The composition of experimental solution used*.

	Stock sol.	Activating	Pre-activating	Relaxing
Na_2ATP (mM)	-	5.73	5.83	5.83
CaEGTA (mM)	**100mM**	5.0	-	6.002
MgCl (mM)	**1M**	7.40	7.33	7.46
Kprop (mM)	**1M**	86.5	96.96	92.72
BES (mM)	**1M**	60.0	60.0	60.0
EGTA (mM)	-	-	0.5	5.0
HDTA (mM)	-	-	4.5	-
PEP (mM)	-	10.0	10.0	10.0
Na-azide (mM)	**50mM**	5.0	5.0	5.0
pH 7.10 Ionic strenght 200				

2.3.3 Apparatus for ATPase measurements

- **Apparatus**

The apparatus and the principle of the ATPase measurement were as described by Stienen, Roosemalen, Wilson & Elzinga (de Tombe & Stienen, 1995; Stienen et al, 1990). Briefly, the ends of the skinned trabecula were attached to a motor (Scientific Instruments Heidelberg, Germany) and to a force transducer harm (KG4, Scientific Instruments Heidelberg, Germany or modified silicon strain gauge AE-801, SenSonor, Horten, Norway), respectively (see **Fig 2.3.3a** panel A-B). The muscle preparation could be transferred manually between several baths to expose the trabecula to the various solutions that were used for the measurements (see **Table 4**). The bath system consisted of a series of wells of volume 80 µl. The bath that was used for the ATPase assay had quartz windows to allow transmission of near-UV light (340 nm) for the measurement of NADH absorbance. The volume of this bath was 30 µL and was continuously stirred by motor-driven vibration of a membrane (Potma et al, 1994) positioned at the bottom of the bath (see **Fig 2.3.3a** panel B&C). The baths were milled in aluminum blocks (anodized) and mounted on top of an aluminum base, through which water was circulated to allow temperature control of all solutions (21°C).

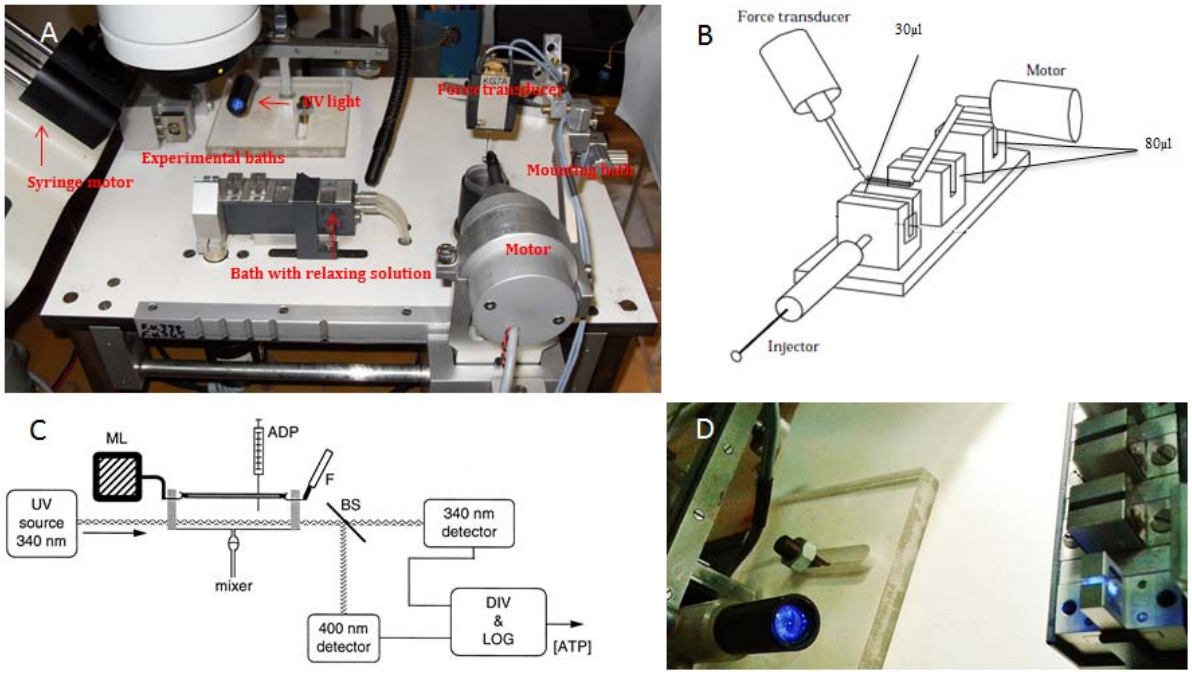

Fig 2.3.3a Apparatus for mechanical and ATPase measurements. (A) The set-up designed to perform mechanical and ATPase measurements from small skinned cardiac muscles. The preparation was mounted horizontally between the motor arm and the force transducer in the mounting bath, than transferred in the bath with standard relaxing solution to set trabecula length (B) Diagram of the experimental set up. The trabecula was than transferred between the basths which contained the relaxing and the preactivating solution (volume, 80µl), and the ATPase assay chamber (30 µl) which usually contained vigourously strirred activating solution. Modified from Potma et al,1994 (C) Photometric pathway. Near-UV light (340 nm) was projected through the bath just underneath the trabecula, split via a beam splitter (BS, 50/50), and detected at 340 nm (sensitive to [NADH]) and 400 nm (insensitive to [NADH]). An analog divider and logarithmic amplifier (DIV & LOG) produced a signal proportional to the amount of ATP consumed in the bath solution. The system was calibrated by injection of a known amount of ADP into ATPase assay chamber by means of a stepper motor-controlled syringe (ADP). Modified from de Tombe & Stienen, 1995. (D) Photograph of the near-UV light impacting the quartz windows of the assay bath. The laser spot is focalized in the chamber by a convergent lens and is less than 3mm in diameter when it impacts the preparation.

- **Measurement of ATPase activity**

The ATPase of the skinned trabecula was measured by a coupled enzyme assay (Glyn & Sleep, 1985; Kentish & Stienen, 1994; Potma et al, 1994; Stienen et al, 1993). The hydrolysis of ATP into ADP and inorganic phosphate (P_i) inside the preparation was coupled to the oxidation of NADH to NAD^+ (**Fig 2.3.3b**). Formation of ADP by the trabecula was stoichiometrically coupled first to the synthesis of pyruvate and ATP from phospho-(enol)-pyruvate (PEP), a reaction that is catalyzed by the enzyme pyruvate kinase, and subsequently to the synthesis of lactate, a reaction that is catalyzed by the enzyme lactate dehydrogenase (LDH) and during which NADH is oxidized to NAD^+. The breakdown of NADH was determined photometrically by measuring the absorbance of 340 nm near-UV light obtained from a 75-W xenon arc lamp (XBO75, Osram) that was projected through the bath just beneath the preparation. The arc lamp is a highly regulated source of current that maintains constant light output necessary for proper stable light output (see **Fig 2.3.3a** panel D). The transmitted light was passed through a beam splitter and then projected onto two photomultipliers. The ratio of light intensity at 340 nm, which is sensitive to the NADH concentration in the bath, and the light intensity at 400 nm, which serves as a reference signal, was obtained by means of an analog divider (see **Fig 2.3.3a** panel C). The output of the divider was applied to the input of a logarithmic amplifier to obtain a voltage that was linear proportional to the NADH concentration in the bath. The first time derivative of this signal, which is proportional to the rate of ATP consumption in the assay bath, was determined off-line by linear regression of the sampled data using custom-designed software. A small decline in the absorbance signal in the absence of the muscle fiber in the bath, caused by an ATPase contamination in the LDH enzyme preparation and by photo bleaching of NADH, was subtracted off-line from the absorbance data throughout the recording period. After each recording in the assay bath, the NADH absorbance signal was calibrated by multiple injections (Nanofil syringe, 10µL,WPI) of 300 nmol ADP (0.030 µL of 10 mM ADP solution) which were controlled by a stepper motor.

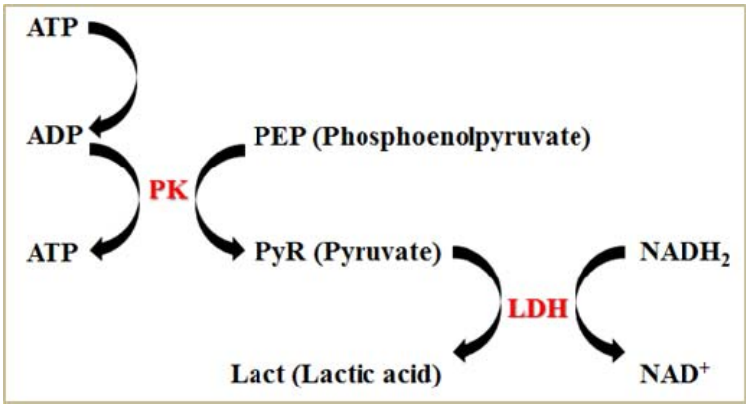

Fig 2.3.3b Coupled enzyme assay. Sequence of enzymatic reactions that occur in the assay bath during an activation. The reaction sequence is stoichiometric, i.e. the hydrolysis of 1 mol of ATP results in the oxidation of 1 mol of NADH.

2.3.4. Experimental protocol and data analysis

Three bathing solutions were used: a relaxing, a preactivating and an activating solution. The protocol consisted of one series of measurements under control conditions. Preparations were first incubated in relaxing solution for 5 min for a complete wash from the standard relaxing solution. Next, they were left in pre-activating solution with low calcium-buffering capacity for 3 min. Finally, they were transferred in the assay bath filled with activating solution, and from there they were returned to relaxing solution. During the first contracture the trabecula was kept isometric and activated maximally (pCa 4.5).Thereafter, if necessary, the length of the preparation was readjusted and usually remained stable throughout the experiment. Next, a second activation was performed at the saturating [Ca^{2+}], which served as a first force and ATP consumption rate reference. The next contractures were carried out at a range of intermediate [Ca^{2+}] that also included the relaxing solution (pCa9). These measurements were then followed by a final control contracture at saturating [Ca^{2+}] for run down correction. In each contracture, after active force had become stable and after sufficient data points were collected to allow reliable calculation of the rate of ATP consumption, the trabecula was quickly transferred in relaxing solution and a calibration of the system was performed (see **Fig 2.3.4a**). Activating solutions with different Ca^{2+} concentrations were made by appropriate mixture of relaxing and activating solutions:

- 95µl activating + 5 µl relaxing for a pCa 5.33 solution
- 90µl activating + 10 µl relaxing for a pCa 5.63 solution
- 85µl activating + 15 µl relaxing for a pCa 5.83 solution
- 80µl activating + 20 µl relaxing for a pCa 5.98 solution
- 75µl activating + 25 µl relaxing for a pCa 6.1 solution
- 70µl activating + 30 µl relaxing for a pCa 6.2 solution
- 65µl activating + 35 µl relaxing for a pCa 6.3 solution

At the end of the experiment, the length, width and depth of the trabecula mounted in the experimental setup was measured with an eyepiece equipped with a graticule (one small division corresponded to 0.02 µm).

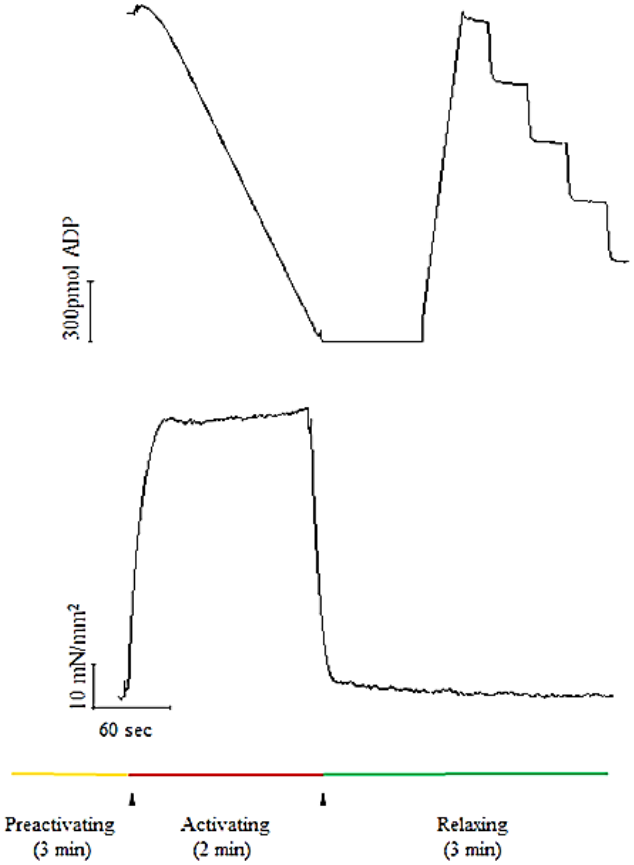

Fig 2.3.4a Recordings obtained during a typical contraction-relaxation cycle of a skinned mouse trabecula. Representative traces of NADH absorbance (top tracing) and force (bottom tracing) recorded simultaneously. A skinned trabecula was transferred to the ATP assay bath containing activating solution between the times indicated by the arrows: the force raised in response to maximal activation (pCa 4.5) and NADH absorbance started declining until steady-state was reached. After a couple of minutes of steady-state maximal force development, the skinned trabecula was transferred again in relaxing solution. Before calibration, the small decline in the absorbance signal in the absence of preparation caused by an ATPase contamination and by photo bleaching of NADH was recorded and then subtracted off-line from the absorbance data throughout the recording period. Absorbance signal was calibrated by multiple injections of 300 pmol ADP. Tension was expressed as force per cross-sectional area and NADH absorbance was normalized for the volume of the preparation.

Data Processing

Force and ATPase data were acquired through an analog to digital converter board (National Instruments) using custom-made software written in LabView 8.0. Data measurements were analyzed with a dedicated LabVIEW analysis program (made by P.P de Tombe, Lyola University, Chicago, USA) and with Origin 8.0. Steady state force was evaluated at each level of $[Ca^{2+}]$ activation, leaving the muscle stabilizing a couple of minutes in the activating solution. Force was normalized on the cross-sectional area, calculated by measuring both muscle width and thickness. Muscle thickness was evaluated thought a mirror placed at 45°. Similarly, steady state ATPase activity was the slope of the calibrated fluorescence signal, normalized on muscle volume. Muscle volume was calculated assuming the trabecula to be an elliptical cylinder.

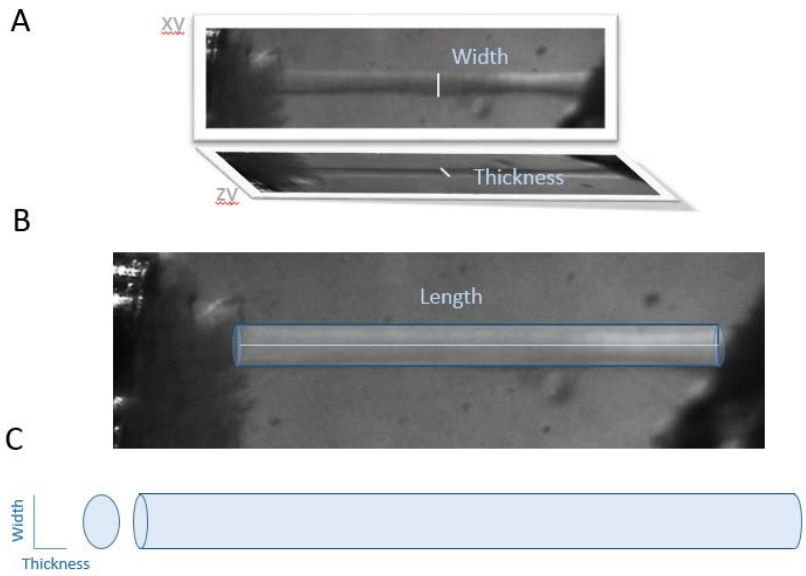

Fig 2.3.4b Evaluation of length, width and thickness of skinned trabeculae.(A) the width (XY axes) of the preparation was carefully measured using a stereoscope with a magnification of 5X through an eyepiece graticule where one small division corresponded to 0.02 µm. The same magnification was used to calculate thickness (ZY axes) thought the reflected image on a mirror placed at 45°(B) Trabecular length (L) was assessed with a magnification of 2X where 1 small division on the graticule corresponded to 0.05µm at the beginning and the end of the experimental protocols. (C) Geometrical model used to describe the entire trabecula, all preparations were assumed to be an elliptical cylinder where the cross sectional area was A= r*r*π and the volume was V= A* L.

- **F-[Ca^{2+}] and ATPase-[Ca^{2+}] relationships**

Sigmoidal force-[Ca^{2+}] and ATPase-[Ca^{2+}] relations were fit with a modified Hill equation:

$$F = \frac{F_{max}}{(1 + 10^{[(-EC_{50})/n]})}$$

$$ATPase = \frac{ATPase_{max}}{(1 + 10^{[(-EC_{50})/n]})}$$

where F and ATPase are steady state force and ATPase respectively, F_{max} is the maximum saturated value F can attain and ATP_{max} is the value of ATPase activity at F_{max}, EC_{50} is the concentration of Ca^{2+} at which F or ATPase activity are 50% of F_{max} or ATP_{max} and represents a compound affinity constant, and n represents the slope of the force-[Ca^{2+}] or ATPase-[Ca^{2+}] relations (the Hill coefficient).

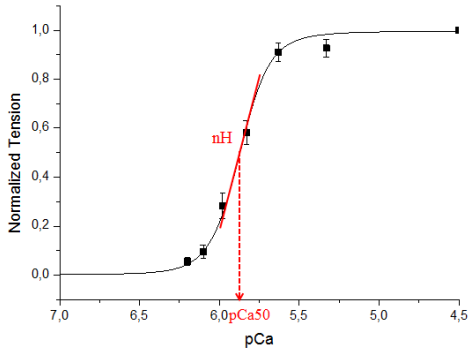

Fig 2.3.4c Average force–pCa relationships. Single points are the average value of force at specific [Ca^{2+}]; continuous line is the fit with a modified Hill equation. pCa is the log of the calcium concentration in the bath, nH is the Hill coefficient, and pCa_{50} is the log of the calcium concentration where the tension is half of F_{max}. The modified Hill equation was fit to the steady-state developed tension at each pCa from each experiment.

Steady state force and the rate of ATP consumption were corrected for the run down observed between the values measured in the second maximal activation and in the final control contracture and normalized to the predicted maximal values. The run down processes was assumed to be linearly progressive with the number of activations, without taking into account the sequence of specific pCa values nor the duration of each activation.

- **Evaluation of tension cost**

The tension cost (TC) is defined as the force-rate of ATP consumption relation. The force-ATPase relation is widely accepted as an index of rate of cross-bridge detachment (Brenner, 1988). Therefore, we simultaneously measured steady-state isometric force and ATPase activity at different [Ca^{2+}] and determined the relationship between the steady-state isometric tension and the rate of ATP hydrolysis. During isometric contractions at different [Ca^{2+}] an approximately linear relationship was found between ATPase activity and force (Potma et al, 1994). The rate of ATP consumption as a function of developed force (that is the TC) was analyzed on each individual muscle in two ways: (i) from the slope of the linear relationship between the values of ATPase activity and force at each pCa; (ii) as a ratio of maximal ATPase activity and maximal tension. With the first method, ATPase versus tension values was fitted by linear regression, without subtraction of the observed values of resting ATPase activity from the absolute values of ATPase at each pCa (**Fig 2.3.4d** panel A). The mean TC for a specific population of trabeculae is then calculated as an average of the individual slopes. With the second method, TC was assessed as maximal ATPase activity, with subtraction of the observed values of resting ATPase activity, and maximal tension ratio. In this case, the measure derived from an average of single ratios obtained at saturating [Ca^{2+}] from each trabecula. This last method seems to be less accurate than the method previously described although increasing the number of the ratios decreases the error in respect of the TC obtained from the slope of the linear relationship. To obtain the mean TC values among multiple preparations that belong to a specific population, e.g. WT trabeculae, TC could be also calculated by dividing the data in classes according to the level of tension developed, regardless of the values of pCa that was used to obtain each specific force level (de Tombe & Stienen, 1995). The slope was then calculated from the linear relationship between the mean values of force and corresponding mean ATPase activity once all the data have been grouped according to their amplitude. An example of the application of this method is reported in **Fig 2.3.4d** panel B.

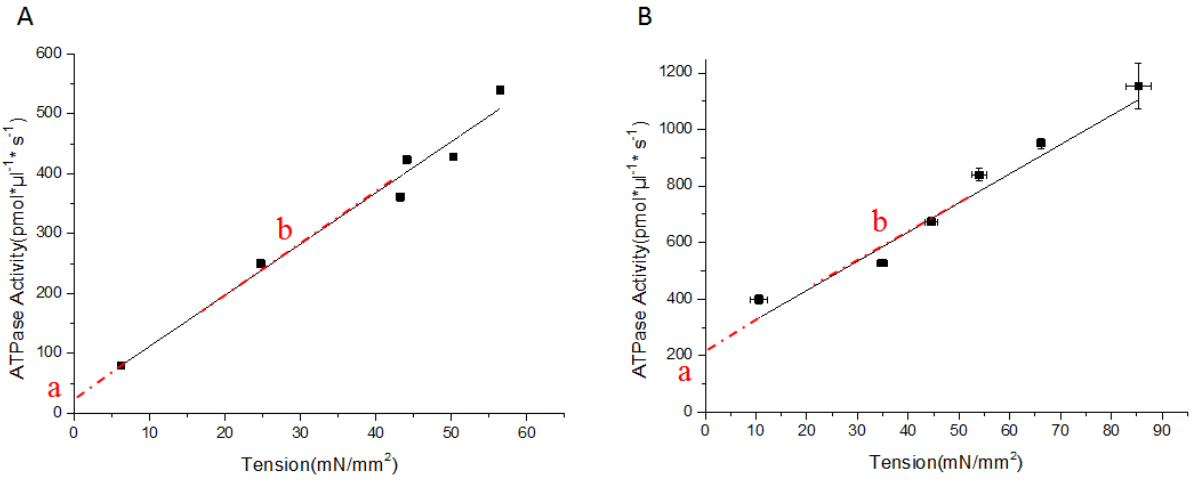

Fig 2.3.4d Tension-ATPase relationship (tension cost). (A)Linear **r**elationship between steady-state isometric tension and ATPase activity in one detergent-skinned trabecula from TG mouse heart; values of force and ATPase activity are plotted at each pCa. (B) Linear relationship between the mean values of force and corresponding mean ATPase activity values once the data from transgenic trabeculae have been grouped according to their amplitude. *b* is the slope of the of the linear relationship described by the equation y = *a* + *b**x and represents the tension cost; *a* is the intercept on the y axes which indicates the theoretical resting ATPase activity.

- **Other mechanical\energetic parameters**

Resting ATPase Activity

The resting ATPase activity is the rate of ATP hydrolysis that occur when the muscle is not developing active tension. This parameter was determined in resting conditions, in the absence of contractile activity (i.e. pCa = 9). This Ca^{2+}- independent ATPase activity could come from myosin and possibly other non-specific ATPase. Since mitochondrial activity was inhibited by sodium azide and oligomycine and since the Ca^{2+}-dependent ATPase activity of sarcoplasmic reticulum is supposed to be very low (Bottinelli et al, 1994) the ATP hydrolysis measured was almost completely attributable to myofibrillar ATPase activity.

Passive tension

When resting muscle is stretched beyond slack length, it develops passive tension. We determined passive tension of skinned trabeculae in relaxing solution by progressively stretching (54 µm step) the preparation at the beginning of the experiment. Trabeculae were completely slacked and steeped in relaxing solution then slow ramp, computer-controlled stretches of 54 µm were imposed to the preparations. Stretches were interrupted periodically by quite long rest periods during which length was kept constant to allow stress relaxation to occur. As expected from the muscle passive properties, passive tension was found to increase very slowly during the first steps and then much faster (**Fig 2.3.4e** panel A). In order to determine the transition between slow and fast passive tension rise we plotted the passive tension versus the stretching imposed to the trabecula using a single exponential fit (Origin 8.0, Originlab) **Fig 2.3.4e** panel B. Before the first contraction-relaxation cycle, trabecular length was set in the ascending limb of the passive tension- ΔL/L relationship, corresponding to sarcomere length around 2.2 µm (Left ventricular diastolic function, dysfunction and failure. Rusconi C., Hess O.M., Poggesi C.; ed. 2004)

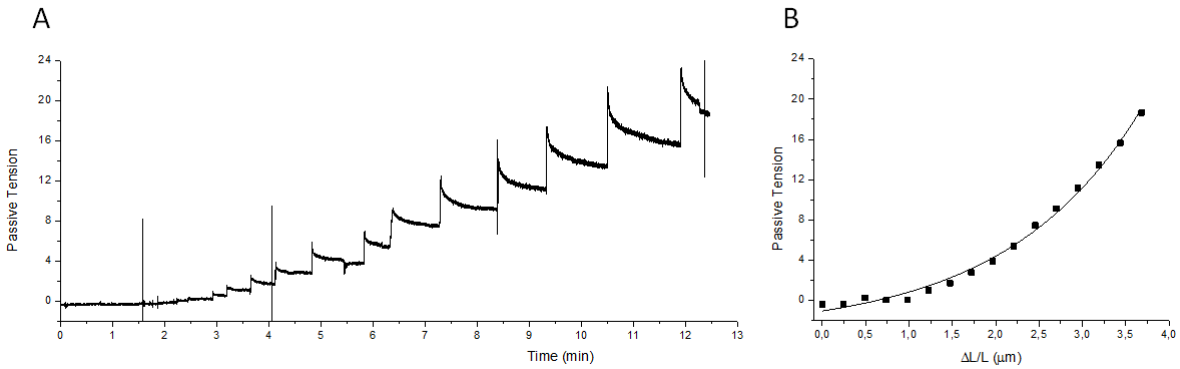

Fig 2.3.4e. Passive tension obtained from a skinned trabecula. (A) representative trace describing the trend of passive tension when stretches of 54 μm were imposed to the trabecula, here 15 streches were enforce for a total elongation of 8.1 μm . (B) Diagram representing passive tension plotted versus the stretching imposed expressed as the amount of stretching / final length ratio, the exponential fit showed a biphasic trend of the relationship.

Slack test

Passive tension was also determined in relaxing solution before the first activation-relaxation cycle and at the end of the experimental protocol by a slack-test protocol. A shortening step (ΔL) of 35% of the trabecular length was imposed, with a shortening and re-stretching step velocity of 500 ms. Slack duration was 2000 ms than the trabecula was re-stretched at the initial length. The tension tracings were collected for 10 seconds before and 10 seconds after the slack test was performed (see **Fig 2.3.4f**) Passive tension was estimated measuring the difference between the baseline and the transducer zero.

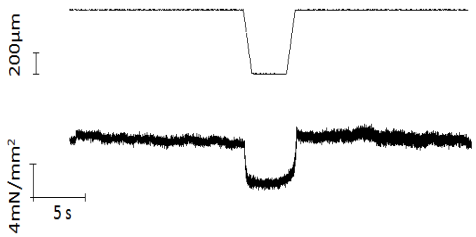

Fig2.3.4f. Slack test protocol. Tension (low tracing) and motor movement (upper tracing) recordings. In the example a shortening step of 35% of trabecula length was imposed after 10 sec, the trabecula remained slackened for 200 ms than re-stretched at the initial length.

2.4 Mechanical measurements on single myofibrils with fast solution switching technique

2.4.1 Myofibril preparation

Single myofibrils and small bundles of myofibrils were isolated either from fresh or frozen striated muscle samples. Muscle specimens were placed in small container bottom-covered with Sylgard, cut into thin strips and pinned down under a stereomicroscope in ice-cold rigor solution (see **Table 5**) (Linke et al, 1993). The strips were incubated for 3 h (4°C) in the same solution added with 1% Triton-X 100 or, alternatively, overnight with 0,5% Triton-X 100. After skinning the strips were rinsed to remove Triton with fresh ice-cold rigor solution (see **Table 6**) (Linke et al, 1993). All solutions to which the samples and myofibrils were exposed contained a cocktail of protease inhibitors including NaN3 (500 μM), pepstatin (5 μM), PMSF (200 μM), DTE (0.5 mM) and E64 + leupeptin (10 μM). The demembranated sample was then ready to be mechanically homogenized. Two or three pieces were transferred to a plastic centrifuge tube containing 1.5 ml ice-cold rigor solution added with a cocktail of protease inhibitors and homogenized using a tissue tearor (Biospec Products inc., USA, mod. 985-370) at medium speed for 15 seconds. A second homogenization was performed to refine the quality of suspension. All experimental solutions were made using double-distilled water (18 MΩ·cm) purified using the Milli Q system (Millipore Corporation, MA, USA). All experimental solutions were gauged with CRISON GLP 21 pH-meter (Crison, Barcellona, UE). The Linke's rigor solution can be replaced with Chamber relaxing solution (see below).

2.4.2 Experimental solutions

All experimental solutions, contained 5mM MgATP, an excess of magnesium over ATP so to give a free magnesium concentration of 1 mM and a re-phosphorilating system made of creatin kinase (200u/ml) and creatine phosphate (10 mM). Sodium sulphate and sodium propionate were added to adjust the ionic strength to 200 mM. All solutions had 10 mM MOPS and pH 7. EGTA concentration in the experimental chamber was 10mM, to keep the free Ca^{2+} low in between activation cycles. EGTA concentration was 1mM in relaxing and activating solutions used for the experiment. Measurements were performed at 15°C.

Table 5. *Linke-rigor solution (extracellular solution)*

	mM	**g/L**
NaCl	**132**	7.714
KCl	**5**	0.373
$MgCl_2$	**1**	0.203
Tris	**10**	1.211
EGTA	**5**	1.902
ml/ 100ml pH 7.1		

Table 6. *Rigor solution (intracellular solution)*

	mM	g/L
Tris	**50**	0.6055
KCl	**100**	0.7456
$MgCl_2$	**2**	0.0407
EGTA	**1**	0.0380
ml/ 100ml **pH 7.0** **with HCl**		

Table 7. *Chamber solution (pH 7).*
Solution used to fill the experimental chamber in which myofibrils were rinsed before the experiment

pCa	Stock sol.	9
MgProp	**0.1M**	6.078
NaEGTA	**0.1M**	10
KProp	**1M**	5.42
Na_2SO_4	**0.1M**	17.68
MOPS	**1M**	1
ATP		0.2996 g
Creatin Phosphate		0.3272 g
ml/ 100ml		

Table 8. *Relaxing and activating solutions (pH 7). Experimental solutions used during the fast solution switching protocol of myofibrilsactivation-relaxation.*

pCa	Stock sol.	4.5	8	9
$CaCl_2$	**0.1M**	1.084	0.0188	0
MgProp	**0.1M**	5.998	6.0028	6.002
NaEGTA	**0.1M**	1	1	1
KProp	**1M**	5.22	5.42	5.42
Na_2SO_4	**0.1M**	26.61	26.69	26.68
MOPS	**1M**	1	1	1
ATP		0.3036 g	0.2996 g	0.2996 g
Creatin Phosphate		0.3272 g	0.3272 g	0.3272 g
ml/ 100ml				

2.4.3 Experimental apparatus

The experimental apparatus (Piroddi et al, 2007) was centered around an inverted microscope (OLYMPUS IX70, Japan) placed on an air suspension table (Ealing System, Massachusetts, USA) and equipped with conventional bright-field and phase-contrast optics.
The microscope stand was equipped with a temperature controlled experimental chamber, where myofibrils were transferred and mounted, hydraulically controlled micromanipulators, tension transducer system, myofibril length-control motor and a rapid perfusion solution switching system

Experimental protocol

A small volume of myofibril suspension was transferred to a temperature controlled chamber filled with relaxing solution on the inverted microscope. Temperature control was achieved by means of a continuous flow of constant temperature water (SBF7, FALC INSTRUMNS, EU) inside a channel system dug in the chamber walls so that temperature could be stable at 15°C. The chamber bottom was made by a cover slip. Selected preparations (single myofibrils or bundles of few myofibrils, 25-80 μm long, 1-4 μm wide) were mounted horizontally between two glass microtools.
Firstly, one of myofibril ends was attached to the stretcher and raised vertically, leaving the other end still attached to the glass. This was then attached to the force probe, picking up the myofibril. Myofibrils were mounted taking advantage of the great spontaneous adhesiveness of myofibrils to glass, likely due to electrostatic attractions. The attachment of myofibrils to glass microtools was usually very strong and resisted maximal tension development during the contraction. As previously described (1.7), force was measured from the elastic deflection of the force probe, by projecting its image on a split photodiode. Average sarcomere length and myofibril diameter were measured from video images using Image J, a Java-based image processing program developed at the National Institutes of Health, USA. The initial sarcomere length l_0 of myofibrils was set around 2-2.2 μm. Myofibrils were activated and relaxed by rapid solution switching. A Selected myofibril was continuously perfused by one of two parallel streams of solutions (relaxing pCa 9.0 or activating pCa 4.5) delivered by the theta glass pipette positioned at right angle with the preparation. Myofibril was initially perfused by relaxing-low Ca^{2+} solution. Following rapid displacement of the injection pipette, myofibrils was then perfused by maximal activating solution allowing the development of isometric active tension. A second displacement of the pipette back to the initial position restored relaxing conditions: myofibrils were perfused again by fully relaxing low Ca^{2+} solution and tension relaxation transient could be recorded. The solution change took place with a time constant of 2-3 ms and was complete in less than 5ms.

Measured parameters

When a myofibril, mounted in the experimental apparatus and held in the solution stream of pCa9, was exposed to the activating solution (pCa4.5) by switching the position of the perfusion pipette, force rapidly raised to a maximum that was steadily maintained as long as the perfusion pipette is hold in the'activating' position. Maximal isometric tension (mN/mm^2) was calculated as maximum force developed (mN) normalized for the cross sectional area (mm^2) of the preparation. The cross-sectional area of myofibrils was calculated by assuming a circular shape and using as diameter the mean of the largest and the smallest width values along the preparation. The raise of isometric active tension to the plateau was approximately mono-exponential with rate constant k_{ACT}. As this rate constant could be influenced by the time course of solution change, we also measure the rate of tension generation under steady state Ca^{2+} activation using "Brenner maneuver" (Brenner, 1988) i.e. from the rate of tension redevelopment (k_{TR}) following a rapid mechanical perturbation. k_{TR} is known to reflect solely turnover kinetics of cross-bridges (CB).

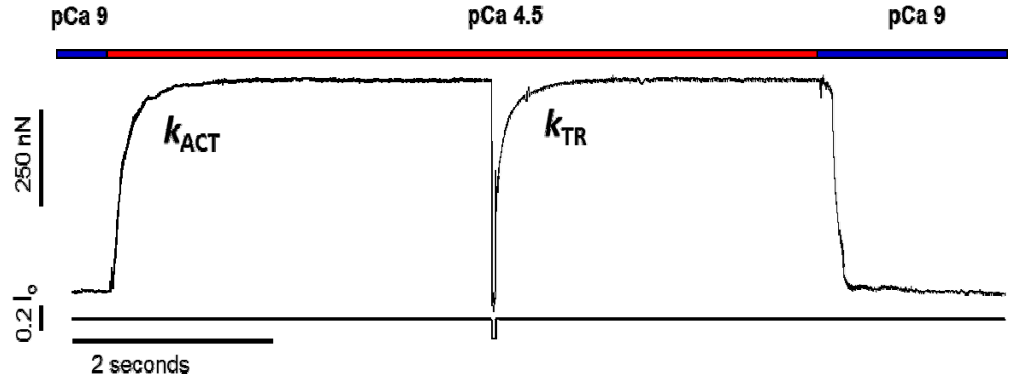

Figure 2.4.3a. Illustrative trace of force rise, characterized by constant rate k_{ACT}, in response to maximal activation (pCa 4.5), followed by release-restretch maneuver and redevelopement of tension, described by constant rate k_{TR}, and final relaxation phase after removal of Ca^{2+} (pCa9)

In our conditions, k_{ACT} is usually found equal to k_{TR} (Poggesi et al, 2005). Different values between k_{ACT} and k_{TR} could also suggest alteration in regulation and activation of thin filament.
Switching back the position of the perfusing pipette, myofibril was perfused again by fully relaxing low Ca^{2+} solution and tension relaxation was recorded.
In all types of striated muscles tested so far, the time course of force relaxation was biphasic (Tesi et al, 2002), starting with a slow linear force decay followed, after a 'shoulder', by a fast exponential relaxation phase. We measured the apparent rate constants of the slow linear and the fast exponential force decay (slow k_{REL} and fast k_{REL}; s^{-1}) and the duration of the slow phase of relaxation (ms). It has been shown that the slow linear force decay occurs under isometric conditions of sarcomeres and in the absence of Ca^{2+}. Slow k_{REL} is predominantly the apparent rate with which attached cross bridges leave force-generating states under isometric conditions. The fast exponential phase fast k_{REL} follows the 'give' of a few sarcomeres and is dominated by inter-sarcomere dynamics (Stehle et al, 2002).

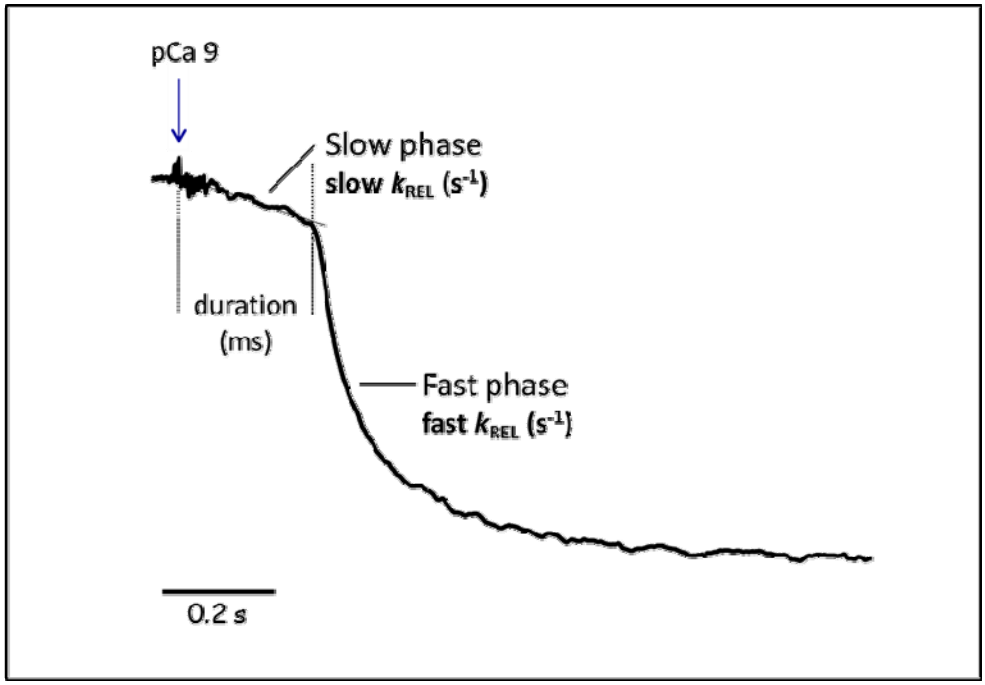

Figure 2.4.3b Relaxation following Ca^{2+} removal by fast solution switching was described by a slow linear phase that occurred under isometric conditions and a fast exponential phase reflecting inter sarcomere dynamics.

2.5 Statistical Analysis

Data from studies on skinned trabeculae, intact preparations, single myofibrils and isolated cardiomyocytes are expressed and plotted as means±SEM (Standard Error of Mean). Values were obtained from a number of independent determinations on different muscles: number of trabeculae (n) and number of hearts (N) are indicated in the figure legends for each set of measurements. Means were compared by paired or unpaired *t* test and, wherever appropriate, by two-way analysis of variance (paired measurements). Statistical significance was defined as $p < 0.05$ (N.S. = not significant). Absolute values of the variables and sample size for each experimental condition are provided in the figures and/or the respective legends.

3. Primary changes caused by E163R cTnT mutation: impact on cardiac mechanics and energetics.

The primary alterations of the contractile function and of tension cost caused by E163R cTnT-TNT1domain mutation have been investigated using skinned preparations or single myofibrils from non-transgenic (NTG) WT and transgenic (TG) mouse hearts.

3.1 Impact of E163R TnT mutation on Ca^{2+}-activated maximal tension, maximal ATP consumption and resting parameters.

Effect of E163R mutation in cTnT on Ca^{2+}-activated maximal tension and passive tension.
Simultaneous measurements of steady-state isometric force and of the rate of ATP consumption were performed at saturating [Ca^{2+}] in detergent-skinned trabeculae from E163R TG and NTG WT mouse hearts. Representative traces of maximal Ca^{2+}-activated tension and corresponding ATP consumption in WT and E163R trabeculae are shown in **Fig. 3.1.1.** No difference was found in maximal Ca^{2+}activated tension between the two groups of preparations (see **Fig 3.1.2**, panel A), indicating that E163R cTnT mutation had no significant impact on sarcomere maximal force generating capacity (average data given in **Table 3.1**). This is in agreement with previously reported data from different lines of TG mouse hearts expressing R92W cTnT, R92L cTnT, R92Q cTnT and Delta-160 cTnT (deletion of amino acid 160) showing that none of the mutant had any significant impact on Ca^{2+}activated maximal tension (Chandra et al, 2001; Chandra et al, 2005). Passive tension was determined in relaxing solution by a slack-test protocol, imposing a shortening step of 35% of the trabecula length followed by a shortening and re-stretching step. At sarcomere lengths around 2.2 μm, there was a remarkable trend towards an increase in passive tension in E163R trabeculae although the difference was not statistically significant (see **Fig. 3.1.2** panel B and Table 3.1).

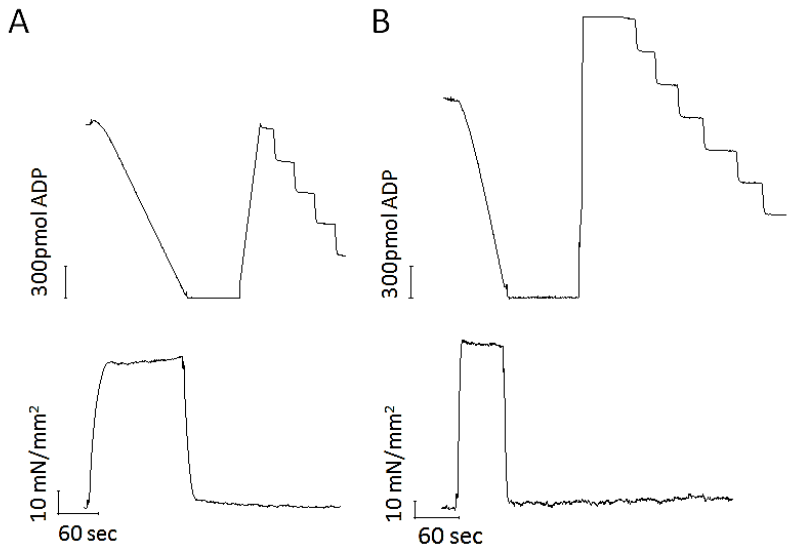

Fig 3.1.1 Original recording of NADH breakdown signal (*top*) and force (*bottom*) during maximal Ca^{2+} activation. ATPase activity was determined during steady state activation. Background, non-muscle ATPase activity was measured upon removal of the muscle from the measurement chamber, followed by calibration of the NADH signal via repeated injections of 300 pmol of ADP into the measurement chamber. Data were obtained from skinned mouse right ventricular trabeculae of WT (panel A) and E163R (panel B) hearts.

Effect of E163R mutation in cTnT on Ca^{2+}-activated maximal and resting ATPase activity.
Maximal ATPase activity was determined during steady-state maximal activation from the NADH breakdown since consumption of NADH was stoichiometrically coupled to ADP production (see Methods). The slope of [NADH] decline vs time was normalized by trabecula volume to obtain ATP consumption rates (pmol $\mu l^{-1}s^{-1}$). Interestingly, while maximal active tension was comparable to

controls, the average isometric ATPase activity at full activation of E163R TG was significantly higher than in WT (see **Fig. 3.1.2** panel C; Mean data in **Table 3.1**).

Table 3.1 *Mechanical and energetic parameters obtained in skinned cardiac trabeculae from WT and E163R TnT mutant mouse heart.*

Parameter	WT	E163R	*p*
$\mathbf{F_{max}}$ (mN mm^{-2})	**60±6.64**	**56±7.17**	N.S.
$\mathbf{ATPase_{max}}$ (pmol µl^{-1}s^{-1})	**680.68±55.52**	**931.27±115.54***	0.04
$\mathbf{T_{pass}}$ (mN mm^{-2})	**5.73±1.75**	**8.82±2.35**	N.S
$\mathbf{ATPase_{rest}}$ (pmol µl^{-1}s^{-1})	**155.05±17,11**	**322.91±73.32***	0.01

Values are means ± SE. Ca^{2+} maximal tension and ATPase activity were measured in activating solution. Passive tension and resting ATPase activity were assessed in relaxing solution. *$p<0.05$.

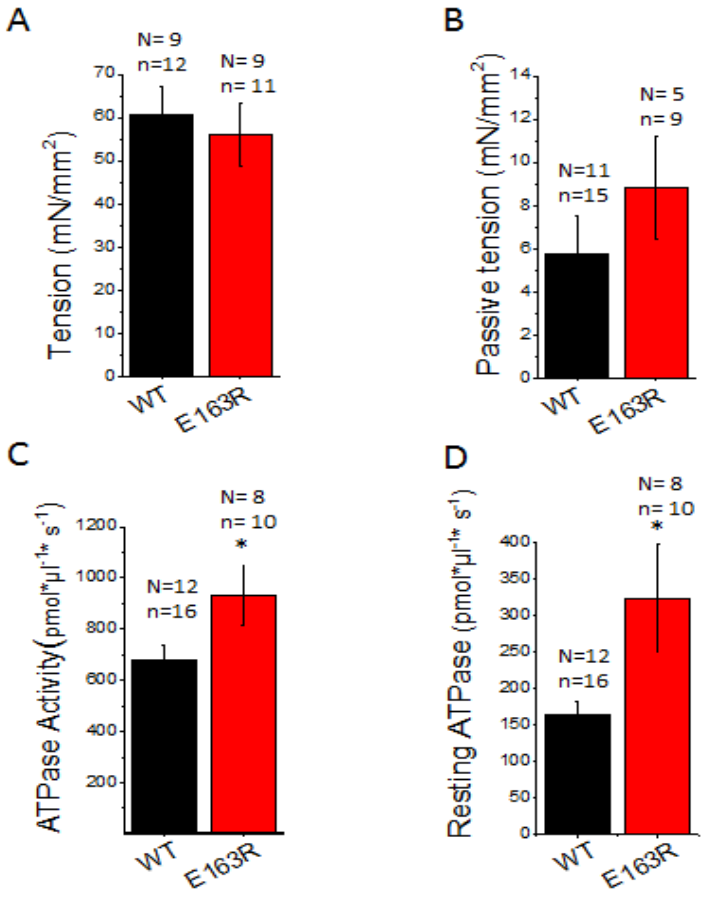

Figure 3.1.2 E163R TnT mutation increases maximal and resting ATP consumption without affecting active and passive tension. (A) Maximal isometric active tension measurements of WT (black) and E163R TnT mutant (red) trabeculae were made at saturating (maximal) [Ca^{2+}]. No singnificant difference was found in F_{max} between the two groups. (B) Passive tension obtained from WT (black) and E163R TnT mutant (red) trabeculae measured with a slack test protocol. (C) Ca^{2+}activated maximal ATPase activity of WT (black) and E163R TnT mutant (red) trabeculae was measured at saturating [Ca^{2+}]. Student's *t* test analysis revealed a significantly higher $ATPase_{max}$ of E163R trabeculae compared to WT. (D) Resting ATPase activity of WT (black) and E163R TnT mutant (red) trabeculae was measured in the absence of contractile activity (i.e. pCa = 9). Student's t test analysis revealed significantly higher $ATPase_{rest}$ of E163R trabeculae compared to WT. Temperature 21°C. Experimental conditions are given in METHODS. Bars above columns are S.E.M. N=number of mouse and n=number of trabeculae

This result is similar to what has been previously observed in TG mouse hearts expressing cTnT Delta-160 mutation while other mutations in codon 92 (i.e. R92W, R92L and R92Q), showed no significant differences in in Ca^{2+}-activated maximal ATPase activity (Chandra et al, 2001; Chandra et al, 2005; Montgomery et al, 2001). This would suggest that the position of the mutation can be crucial to determine a primary effect on tension dependent ATP consumption. Similarly, resting ATPase activity of E163R treabecule was significantly higher when compared to WT (see **Fig. 3.1.2** panel D). Resting ATPase activity was determined in the absence of contractile activity (i.e. pCa = 9). The increase in ATP consumption even in resting condition suggests an overall higher rate of ATP hydrolysis in E163R sarcomeres.

3.2 Enhancement of myofilament Ca^{2+} sensitivity in E163R detergent-skinned trabeculae.

Modifications of Ca^{2+}sensitivity are common features in many HCM mutations studied so far. Although there was no significant difference in Ca^{2+}-activated maximal tension of trabeculae from E163R and WT mouse hearts, at all submaximal activating [Ca^{2+}] there was a significant increase in the tension development in E163R when compared to WT**.** As shown in **Fig 3.2.1,** the pCa-tension relationships of E163R trabeculae were shifted leftward, so that pCa_{50} value, which represents the midpoints of pCa-ATPase relations, was significantly higher compared to WT. Mean values are shown in **Table 3.2**.

An increased Ca^{2+}sensitivity of tension development caused by E163R cTnT mutation is expected from the effects observed in presence of other mutation in the same site (e.g. Δ163R or E163K) (Harada & Potter, 2004) and in other mutational hot spots in cTnT (e.g. missense mutation on codon 92 such as R92W, R92L, R92Q) (Chandra et al, 2001; Chandra et al, 2005). The Hill coefficient values for E163R TG trabeculae were also significantly decreased compared to WT trabeculae (see table 3.2).

Table 3.2. *Normalized pCa-tension and pCa- ATPase relationships in detergent-skinned mouse cardiac trabeculae.*

Parameter	WT	E163R	*p*
pCa-tension relationship			
pCa_{50} values	**5.80±0.035**	**5.99±0.039****	0.003
Hill coefficient (n_H)	**5.33±0.245**	**3.99±0.45***	0.012
pCa-ATPase relationship			
pCa_{50} values	**5.87±0.045**	**6.02±0.029***	0.019
Hill coefficient (n_H)	**3.67±0.33**	**2.64±0.22***	0.025

Values are means ± SE. Data from the normalized pCa-force and pCa- ATPase measurements were fitted to a modified Hill equation to derive the pCa_{50} and Hill coefficient (n) values. E163R mutation in cardiac troponin T (cTnT) increases Ca^{2+} sensitivity of force and ATPase activity in ventricular cardiac trabeculae**p<0.05**p<0.01*

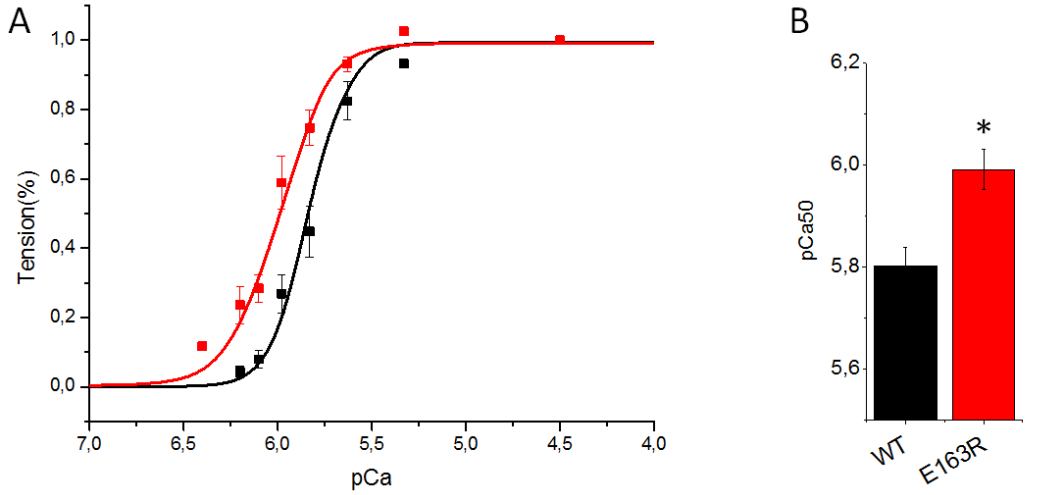

Figure 3.2.1 Normalized pCa-tension relation in detergent skinned trabeculae. (A) pCa-Ca^{2+} activating tension relation of wild type (black tracing) and E163R transgenic trabeculae (red tracing,).Tension values are normalized to those measured at pCa4.5. Data points are means and error bar represents SE. Data are fit to a modified Hill equation (see methods) pCa50 and Hill coefficient (*n*) values derived from the non linear fits are listed in Table 2.2. (B) pCa_{50} values expressed in means ± S.E.M. of 10 determinations from 8 different WT hearts (black) and 8 determinations from 6 different E163R TG hearts (red). (see also Table 3.2).

We also tested whether an increase in tension at submaximal [Ca^{2+}] of E163R trabeculae was followed by a parallel change in ATPase activity by measuring ATPase activity at different Ca^{2+}activation levels. The data shown in **Fig 3.2.2** demonstrate that, although the amplitude of the pCa_{50} shift was slightly smaller compared to the increase in Ca^{2+} activated tension, there was also a significant increase in Ca^{2+} sensitivity of ATPase activity in TG skinned preparations. Therefore, in agreement with pCa-tension relations, pCa-ATPase relations of E163R trabeculae were shifted leftward when compared to WT. The average fit parameters obtained in all trabeculae are given in **Table 3.2**. A similar effect was observed also for the Hill coefficient of the normalized pCa- ATPase relationship was also significantly decreased in E163R trabeculae compared to WT

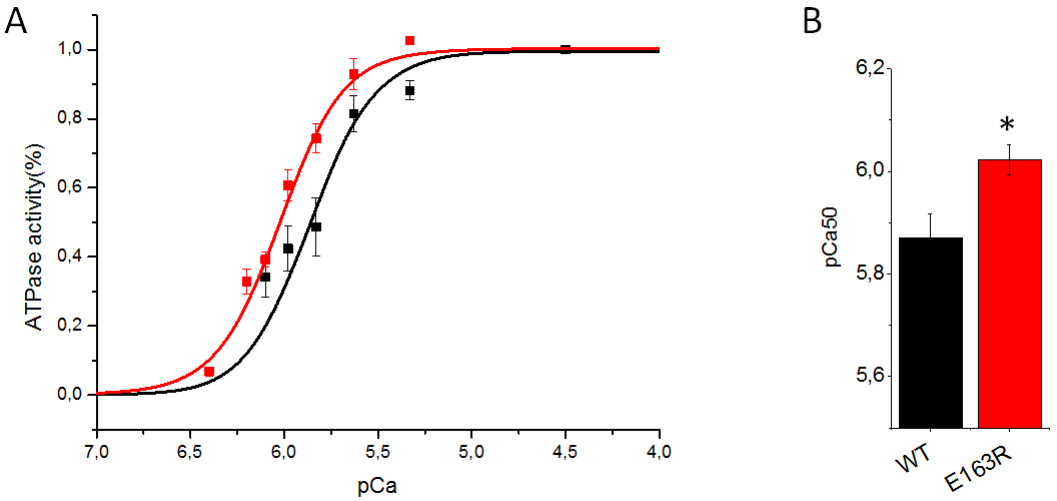

Figure 3.2.2. Normalized pCa-ATPase relation in detergent skinned trabeculae. (A) pCa-ATPase relation of wild type (black tracing) and E163R transgenic trabeculae (red tracing). ATPase values are normalized to those measured at pCa4.5. Data points are means and error bar represents SE. Data are fit to a modified Hill equation (see methods) and pCa50 and Hill coefficient (*n*) values derived from the non linear fits are listed in Table 2.2. (B) pCa50 values expressed in means ± S.E.M. of 10 determinations from 8 different WT hearts (black) and 8 determinations from 6 different E163R TG hearts (red). (see also Table 2.2).

3.3 Impact of E163R mutation in cTnT on tension-dependent ATP consumption.

Fig 3.3 shows the relation between the rate of ATP consumption and the level of steady state force for the TG and NTG skinned muscle preparation. The force-ATPase relation, i.e. Tension Cost (TC) is widely accepted as an index of rate of cross-bridge detachment rate (Brenner, 1988). Therefore, we simultaneously measured steady-state isometric force and ATPase activity at different [Ca^{2+}]. To better analyze the rate of ATP consumption as a function of developed force we used different approaches, see table 3.3. In the first istance, TC was assessed as maximal ATPase activity, with subtraction of the observed values of resting ATPase, and maximal tension ratio. In this case, the TC measures derived from the average of single ratios obtained at saturating [Ca^{2+}] from each trabecula (mean values are given in **Table 3.3**). This first approach indicated that the TC was significantly higher in E163R trabeculae compared to the mean ratio calculated from WT (see **Fig 3.5**, panel C). This significant alteration in the economy of force maintenance in E163R trabeculae was also observed from the slope of the linear relation between steady state force and rate of ATP consumption at each pCa (see **Fig 3.5**, panel A&B). In this case the TC was calculated as the average slope of the single slopes obtained from each trabecula. Finally, we evaluated the TC as the slope from the linear relationship between all single values of ATPase activity and active tension and as the slope from the linear relationship between the mean values of force and corresponding mean ATPase activity once all the data were grouped in tension amplitude classes (see **Fig 3.5** panel D&E). In all cases, E163R cTnT mutation significantly affected the mean tension-ATPase relations. The change in tension cost was significant and averaged a 37% increase. The intercept values of the TC linear regression fits represent the extrapolated resting ATPase activity. The intercept values were determined both from the slope of the individual linear relationships and from the pooled data obtained in all trabecuale and collected in bins. Mean intercept value obtained in the E163R group was significantly higer when compared to WT group. Of note, absolute values of the intercepts (data shown in **Table 3.3**) were similar to those that were directly measured as resting ATPase Activity. (Intercepts were: 213.70±27.32 and 344.37±61.79 and resting ATPase Activity was: 155.05±17.11 and 322.91±73.32, for WT and E163R, respectively)

Table 3.3*. Tension Cost (ATPase Force^{-1})*

Parameter	WT	E163R	*p*
$ATPase_{max}$/ F_{max}	**11.48±0.59**	**17.95±2.59****	0.009
TC_1			
Slope	**7.91±0.36**	**12,57±2,02****	0.004
TC_2			
Slope	**9,91±0,67**	**13,46±1,49***	0.0253
Intercept	**213.70±27,32**	**344.37±61,79***	0.0453
TC_3			
Slope	**9,46±0,39**	**13,03±0,06****	0.0015
Intercept	**221.49±14.18**	**355.92±24.59****	0.0015

Values are means ± SE. TC calculated as mean $ATPase_{max}$/ F_{max} ratios from all trabeculae. The TC was determined from the slope of the relationship between ATPase activity and active tension measured at each pCa (TC_1). TC was also assessed from the slope of the linear relationship between all single values of ATPase activity and active tension (TC_2), finally data were pooled in 20% wide steady state force bins to obtain an average pooled force- rate of ATP consumption relation (TC_3). *$*p<0.05$** $p<0.01$*

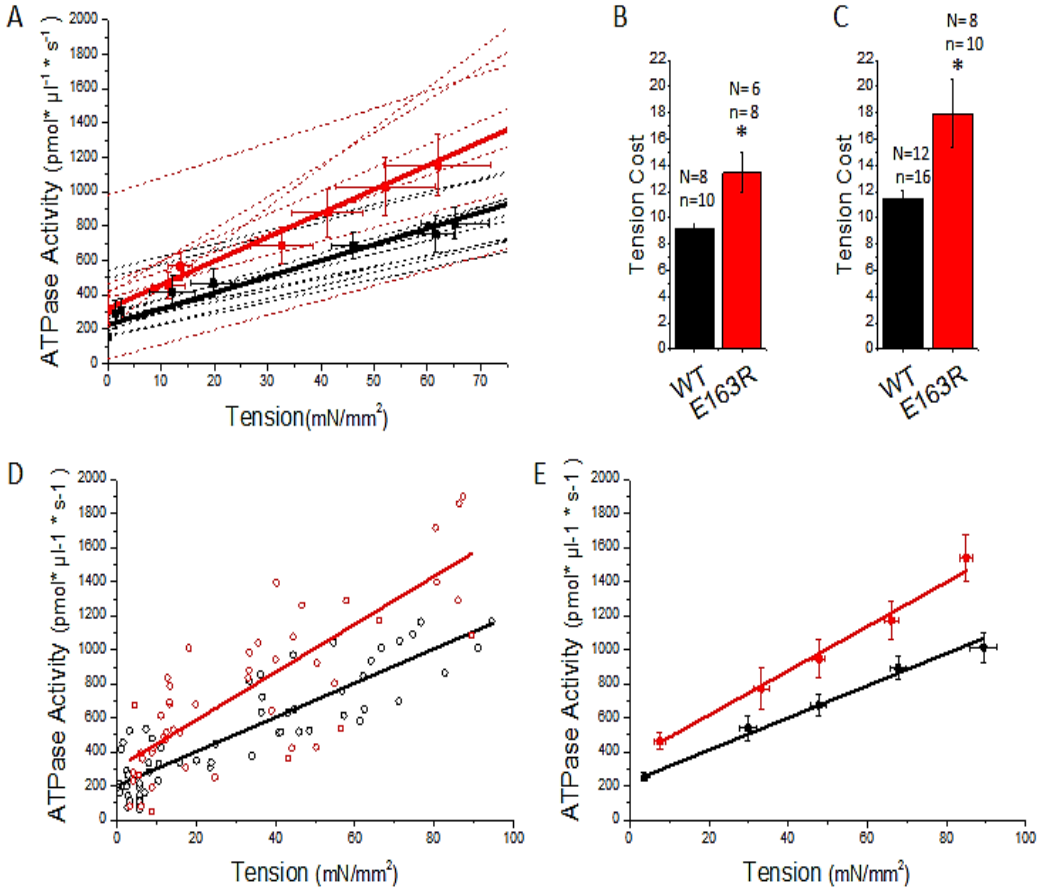

Fig 3.3.Tension Cost. (A) TC was determined from the slope of the relationship between ATPase activity and active tension measured at each pCa. ATPase versus active tension values obtained from 10 WT and 8 E163R trabeculae were fitted by linear regression (black dash lines for WT and red dash lines for E163R) without subtraction of the observed values of resting ATPase activity from the absolute values of ATPase. Bold lines represent the mean of single fits. Data at each pCa are presented in means (black points for WT and red points for E163R) ± S.E.M (black bars for WT and red bars for E163R) of 10 determinations from 8 different WT hearts (black) and 8 determinations from 6 different E163R TG hearts (red). (B) Istogram showing the mean TC determined as an average of the individual slopes of the linear relationship between ATPase activity and active tension at each pCa. (C) TC as a ratio of $ATPase_{max}$ and F_{max} of the individual trabeculae. Bars above columns are S.E.M, N=number of mouse and n= number of trabeculae. (D) Mean TC was determined from the slope of the linear relationship between all single values of ATPase activity and active tension (black circles for WT, n=59 and red circles for E163R, n= 51). ATPase versus tension values were fitted by linear regression (black line for WT and red line for E163R), without subtraction of the observed values of resting ATPase activity from the absolute values of ATPase. (E) Average pooled force- rate of ATP consumption relation in10 determinations from 8 different WT hearts (black) and 8 determinations from 6 different E163R TG hearts (red). Data were pooled in 20% wide steady state force bins. Data are presented in means ± S.E.M, see also table 3.3.

3.4 Tension development and relaxation in single myofibrils isolated from E163R and WT hearts

Single myofibrils isolated from WT and E163R mouse hearts were mounted for force recording as described in methods**.** Representative traces of tension responses to maximal Ca^{2+} activation by fast solution switching are shown in **Fig 3.4. (**panel A). Average data of sarcomere length (SL), maximal isometric tension (P_0), activating rate constants k_{ACT} and k_{TR} and resting tension (RT) for both myofibril groups are shown in Table 3.4.1. Values obtained in WT mice myofibrils were comparable to what was previously observed (Kreutziger et al, 2011; Piroddi et al, 2006).
In the E163R myofibrils, maximal isometric tension (P_0) as well as kinetics of tension development and redevelopment (k_{ACT}, and k_{TR}) were comparable to WT (see **Table 3.4.1** and **Fig 3.4.** panel A&B). In both myofibril populations, the time course of Ca^{2+}- activated tension development was mono-exponential. The activating rate constants k_{ACT} and k_{TR} were not significantly different in the two groups, indicating that k_{ACT} is not limited by the rate with which thin filaments are switched on by Ca^{2+}. In both myofibril groups, there was a slight reduction of k_{TR} compared to k_{ACT} but this effect was negligible and likely caused by mechanical run down of preparations.
In the E163R myofibrils, resting tension in pCa9 (i.e. in absence of Ca^{2+}), expressed as a percentage of $\mathbf{P_0}$, was significantly increased compared to WT. This is in agreement with the trend toward an increase in passive tension observed in E163R trabeculae.

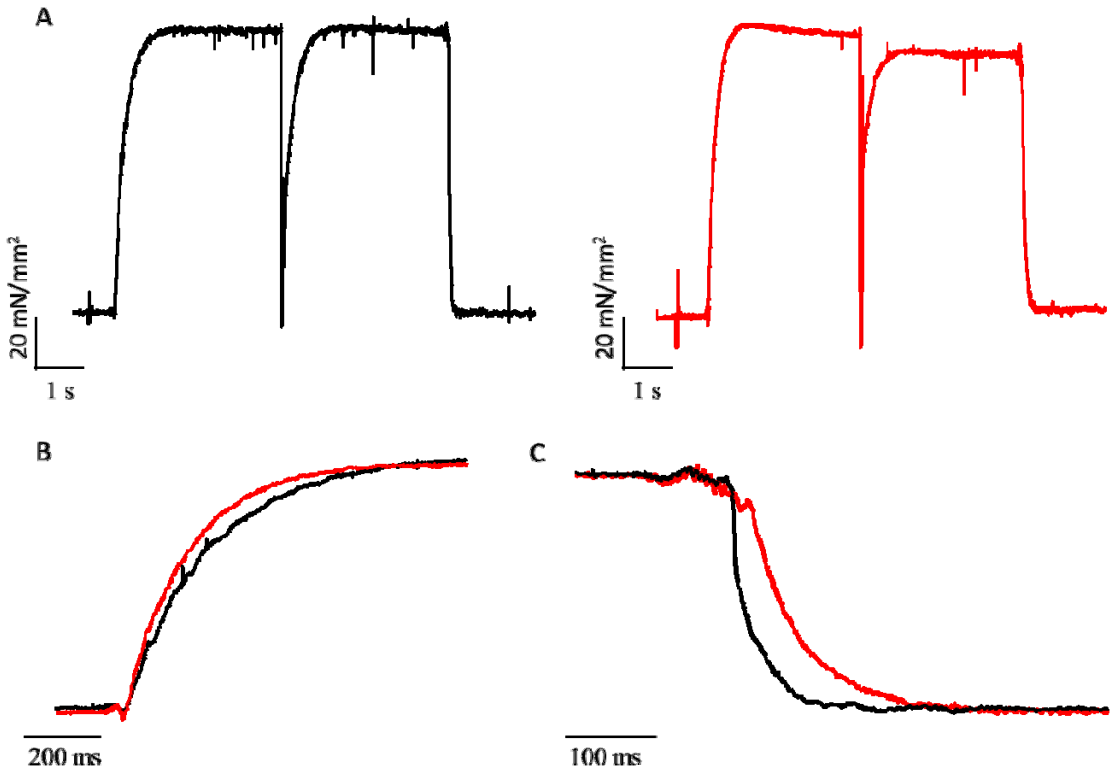

Fig 3.4. Representative traces of E163R and WT myofibrils activation and relaxation. (A) representative tension responses of E163R TnT mutant (red) and WT (black) myofibrils maximally activated (pCa 4.5)and fully relaxed (pCa 8) by fast solution switching technique. Temperature 15°C. (B) Kinetics of force generation in E163R TnT mutant (red) and WT(black). The time course of tension activation following sudden Ca^{2+} increase of E163R TnT myofibril and WT myofibril after normalization for maximal tension. (C) Kinetics of force relaxation in E163R (red) and WT (black). The time course of tension relaxation following sudden Ca^{2+} removal of E163R TnT myofibril and WT myofibril after normalization for maximal tension.

Table 3.4.1 *Active tension generation parameters.*

	SL (µm)	P_0 (mN mm^{-2})	k_{ACT} (s^{-1})	k_{TR} (s^{-1})	Rtens/ P_0
WT	**2.15 ± 0.02**	**204±15**	**5.50± 0.32**	**4.64 ± 0.17**	**0.08 ± 0.008**
	n= 42	n= 41	n= 24	n= 23	n= 23
E163R	**2.16 ± 0.01**	**198 ± 18**	**5.71 ± 0.30**	**4.43 ± 0.13**	**0.12 ± 0.01***
	n= 34	n= 32	n= 20	n= 18	n= 19

Values are means (± S.E.M.) of P_0, k_{ACT}, k_{TR} in E163R TnT mut. *versus* WT. *p<0.05 and **p<0.01 estimated by Student t test; n= number of myofibrils). Experimental conditions: 15°C, pCa relaxing and activating solutions, 9.0 and 4.5 respectively; [MgATP] 5 mM; [P_i] < 5µM

Force relaxation occurs when myofibrils are subjected to a step reduction of [Ca^{2+}] below the contraction threshold. Tension relaxation phases of WT and E163R myofibrils are shown on a faster time scale in **Fig 3.4**.panel C. The time course of force relaxation was biphasic, starting with a slow, almost linear, force decay, followed after a shoulder by a faster exponential relaxation phase, (Piroddi et al, 2007; Stehle et al, 2002; Tesi et al, 2002). The slow phase is described by two different parameters, duration of slow phase (ms) and its rate or slow k_{REL} (s^{-1}). The second fast exponential relaxation phase, is described by its rate fast k_{REL} (s^{-1}). In E163R myofibrils compared to WT we observed a prolonged duration of the slow phase of relaxation. Interestingly, although the duration of the slow phase was prolonged, its kinetics slow k_{REL} tended to be accelerated by approximately ~ 40%. This is consistent with the increase in TC described above. In fact, it has been shown (Poggesi et al, 2005; Stehle et al, 2009) that the slow linear force decay occurs while sarcomeres are isometric and its rate constant (slow k_{REL}) is predominantly the apparent rate with which attached crossbridges leave force-generating states or apparent detachment rate (g_{app}). The prolonged slow phase duration of E163R myofibrils may be related to an increase in Ca^{2+}sensitivity that we found in E163R. This is in agreement with previous observations in myofibrils reporting that a reduced Ca^{2+} k_{off}, associated with an increase of calcium sensitivity, causes a prolongation of the slow relaxation phase (Kreutziger et al, 2011).

Table 3.4.2 *Tension relaxation parameters*

Myofibrils batches	Tension Relaxation		
	Slow phase		Fast phase
	Duration (ms)	k_{REL} (s^{-1})	k_{REL} (s^{-1})
WT	**81.12 ± 3.60**	**0.87± 0.13**	**27.67± 2.36**
	n= 24	n= 24	n= 24
E163R	**109.50± 5.35****	**1.22 ± 0.20**	**19.31 ± 1.17****
	n= 20	n= 20	n= 20

Values are means (± S.E.M.) of relaxation in E163R TnT mut. *versus* WT. *p<0.05 and **p<0.01 estimated by Student t test; n= number of myofibrils). Experimental conditions: 15°C, pCa relaxing and activating solutions, 9.0 and 4.5 respectively; [MgATP] 5 mM; [P_i] < 5µM

The fast exponential phase which follows the "give" of a few sarcomeres is dominated by inter-sarcomere dynamics (Stehle et al, 2002). The kinetics of the exponential phase of relaxation was

slower in E163R myofibrils compared to WT and in some cases relaxation was incomplete. Of note, the prolongation of the slow relaxation phase combined with a reduction of the fast k_{REL} results in a prolongation of the overall relaxation in E163R compared to WT myofibrils which may significantly affect the twitch kinetics of the intact E163R myocardium (see below, Results **Fig 4.2**). The slower kinetics of the exponential phase of relaxation in E163R myofibrils compared to WT could be related to the increased RT observed in the mutant: in fact, the relaxation behavior of E163R myofibrils resembles the relaxation of control myofibrils following sudden decrease in $[Ca^{2+}]$ to levels just above contraction threshold, e.g. pCa 6 instead of pCa 8 (Tesi et al, 2002). This would indicate that residual thin filament activation after Ca^{2+} removal allows recruitment of some new cross-bridges and is responsible for slowing down myofibril force decay and for the increase in RT. This observation is in agreement with our measures of ATPase activity in resting conditions in E163R and WT trabeculae (see above) showing a clear increase of resting ATPase in the mutant. Both findings, then, consistently report the presence of residual crossbridge interactions in the absence of Ca^{2+} in E163R myofibrils and suggest an impairment of the switch off mechanism of the thin filament in the presence of E163R cTnT mutation.

4. RESULTS. Secondary remodeling related to E163R cTnT mutation: E-C coupling abnormalities, spontaneous activity and propensity towards arrhythmias.

Ca^{2+} handling abnormalities are an early-onset pathogenic element in HCM (see introduction).
Here we aim:

- **i)** to characterize the E-C coupling and pro-arrhythmogenic changes occurring in heterozygous transgenic mice carrying E163R cTnT and understand how they concur with the primary effects of the mutation to determine the contractile performance of intact E163R miocardium;
- **ii)** to compare these Ca^{2+} handling abnormalities to those identified in widely described cTnT mouse model carrying R92Q mutation, and
- **iii)** to test the effects of specific pharmacological interventions, which may be effective to acutely reverse some of the E-C coupling and mechanical alterations observed.

Intact trabeculae and single cardiomyocytes were used to measure force, intracellular Ca^{2+} and sarcolemmal currents or action potentials.

4.1. Mechanics of intact E163R cTnT trabeculae: E-C coupling alterations and pro-arrhythmogenic changes.

Heterozygous mice carrying the E163R mutation did not present any significant alteration of the gross heart morphology compared to WT littermates (Figure 4.1). Additionally, they did not present any α to β shift in myosin isoforms, denying this as a potential mechanism for the mechanical changes we observed.

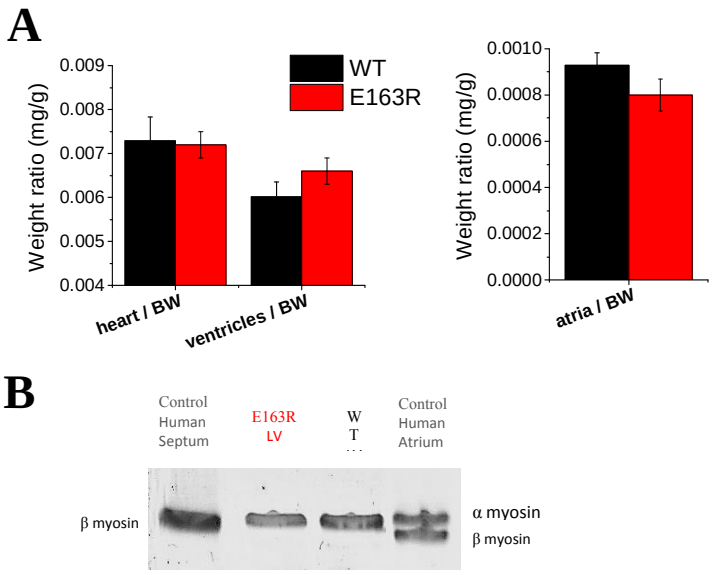

Figure 4.1. Gross heart morphology and markers of hypertropy. (**A**) mean data of Heart/Body Weight, Atria/Body Weight, Ventricles/Body Weight Ratios in 10 Wild type (WT) mice and 10 E163R HE mice. Mice age was 6 months. (**B**) 8% SDS-PAGE gel of a myofibril suspension from left and right ventricles of WT and E163R mice. Control human atrial myofibrils were used for comparison to identify the position of the β-myosin band; only α myosin is expressed in both WT and E163R mice.

We assessed the mechanical properties of intact trabeculae dissected from the hearts of E163R mice, as compared with trabeculae from WT littermates. Force was recorded during stimulation at different frequencies (from 0.2 to 6 Hz). Temperature was 30°C. Mean sarcomere length was 2.14±0.03 μm. Twitch amplitude and kinetics were analyzed and results are summarized in **Fig. 4.2.**

Figure 4.2 (panel A) shows the biphasic (Stuyvers et al, 2002) steady-state FFR in control and E163R mice ventricular trabeculae with a descending limb (0.2 to 1Hz) and an ascending limb (1 to 8 Hz). The relationship between isometric twitch tension and stimulation frequency was maintained in E163R muscles (Figure 4.2.A), in both limbs of the relationship. Instead, the kinetics of force development and relaxation were markedly affected by E163R mutation. Time to peak contraction and time from peak to 50% relaxation were both prolonged in E163R with respect to WT trabeculae (Figure 4.2B, C).

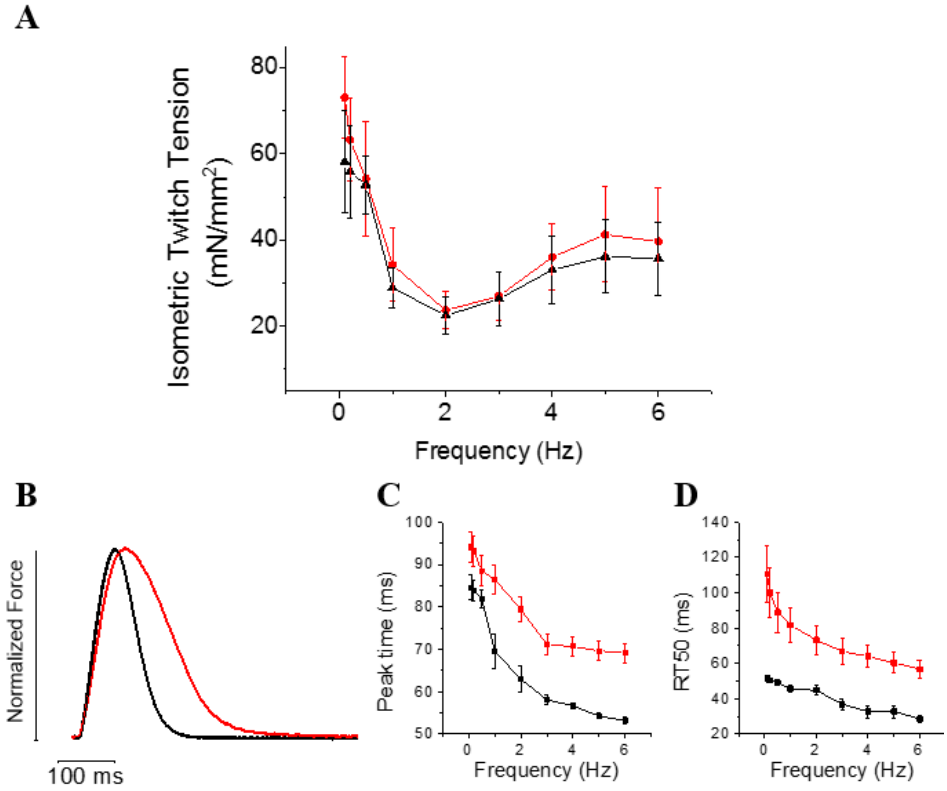

Figure 4.2. Isometric twitch tension in E163R and WT TnT mutant mice. (A) Relationship between twitch amplitude and pacing frequency at steady state in WT (N=10, n=14) and E163R (N=10, n=12) trabeculae. **(B)** Normalized representative twitch traces from a WT and a E163R. **(C-D)** Mean±SEM data for time from stimulus to peak (C), time from peak to 50% relaxation (D) in WT (N=10, n=14) and E163R (N=10, n=12).

As shown in **figure 4.2**. panel A, maximal isometric twitch tension measured during rested-state contraction (i.e. contractions at 0.1or 0.2 Hz) or at high pacing rates (above 6 Hz) were unchanged in E163R trabeculae compared to WT.

To further assess whether maximal isometric twitch tension was affected by the mutation, in a subset of trabeculae we measured force during acute administration of the β-adrenergic agonist Isoproterenol, applied at a concentration of 10^{-7} mM. The effects of the Isoproterenol 10^{-7} mM (Iso) on contraction parameters of E163R and WT trabeculae are reported in **Figure 4.3**. In both WT and E163R trabeculae mean isometric twitch tension increased more than 3 times upon administration of Iso, with no significant differences between the two groups (**Figure 4.3** B). Iso accelerated peak time and 50% relaxation time in WT trabeculae, and, to a larger extent, in E163R trabeculae. However in E163R trabeculae under Iso, while peak time was normalized to WT level, relaxation was still prolonged (**Figure 4.3** C). Adrenergic receptor density measurements has been previously shown to be the same in R92Q mice versus non transgenic mice (Jimenez & Tardiff, 2011).

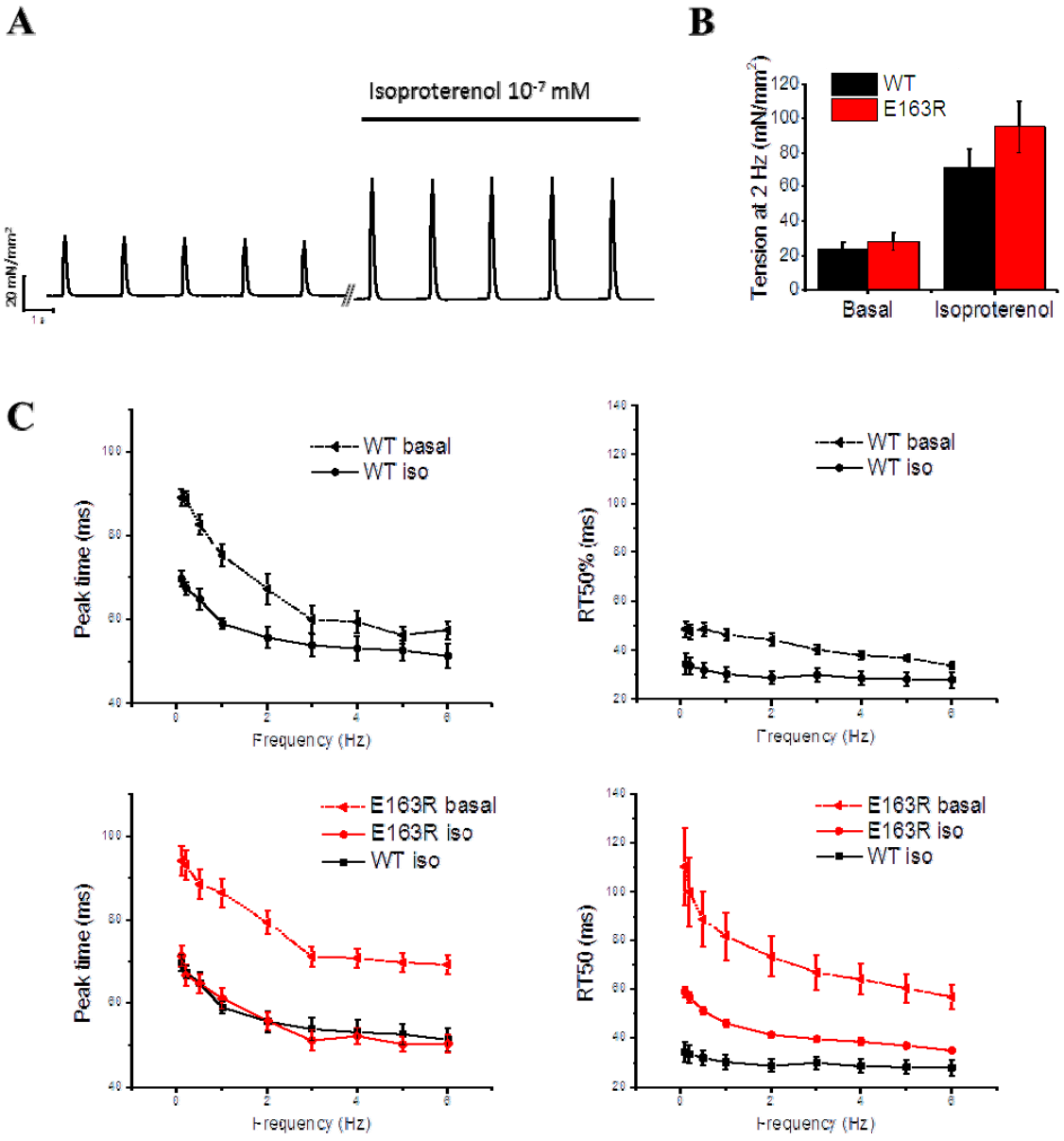

Figure 4.3. Effects of Isoproterenol 10^{-7} mM on isometric twitch tension in E163R and WT TnT mutant mice. (A) Representative force traces, showing the effect of acute administration of Isoproterenol 10^{-7} mM on contractions **(B)** Mean±SEM data for peak isometric twitch tension in WT (N=10 n=12) and E163R (N=10 n=10) trabeculae. **(C)** Mean±SEM data for time to peak (left panels) and time from peak to 50% relaxation (right panels) in WT (N=10, n=12) and E163R (N=10, n=10).

Short term interval-force relationship.

When a premature stimulus is introduced into a regular stimulus sequence, the associated contraction (extrasystole) is reduced in amplitude. The force of the extrasystolic beat increases with increase in the interval preceding the premature stimulus until the steady-state force is again established (Mechanical Restitution) (Hasenfuss et al, 1999) (**Figure 4.4**, panel A). At molecular level, the rate of mechanical restitution is determined by SR refilling and SR refractoriness, established by the balance between SERCA and RyR2 activity (Banijamali et al, 1991). In E163R mice, mechanical restitution was faster compared to WT. Mean restitution rates (τ), calculated as the average of individual τ of the restitution curves, were 0.452±0.046 s for WT and 0.254±0.036 s for E163R trabeculae ($p<0.05$, unpaired). As expected, mechanical restitution was accelerated by the application of Iso, when the rate of SERCA

activity (i.e. SR refilling) and the recovery of RyR from inactivation/adaptation is increased. However, also in the presence of the drug, the difference between the two groups is maintained, and mean τ is higher in E163R then in WT trabeculae (0.186±0.018 s vs 0.132±0.018 s, p<0.05, unpaired).

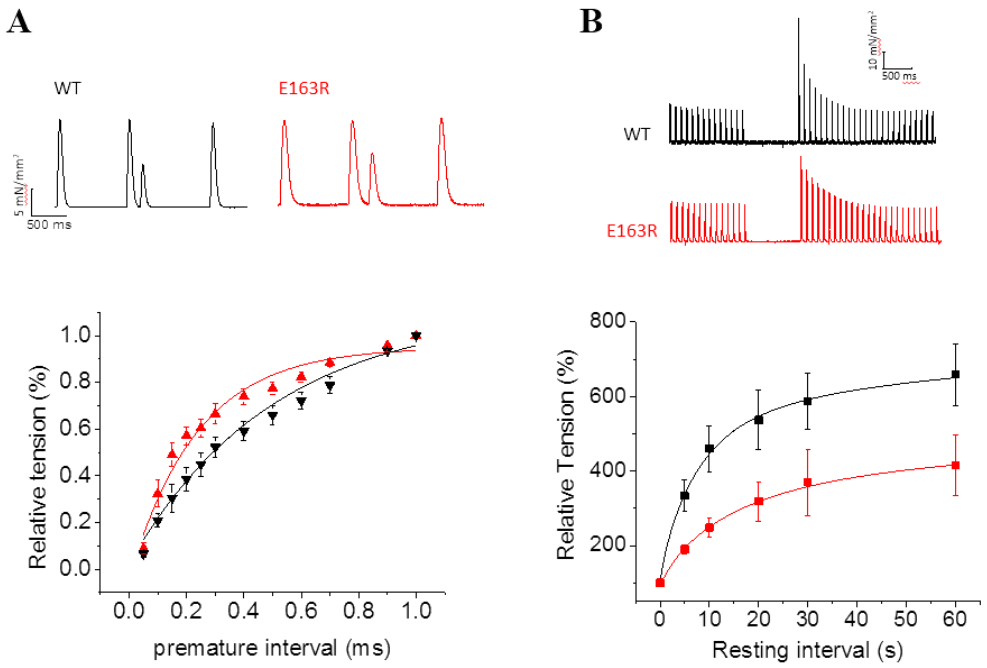

Figure 4.4. Short term interval-force relationship in E163R and WT cTnT mutant trabeculae. (A) Top, WT and E163R representative force traces, showing a premature beat at 250 ms. Bottom, Mean±SEM values of relative tension (normalized on contraction amplitude at 1 Hz steady state stimulation) plotted against the premature interval to obtain the restitution curves in WT (N=10 n=12) and E163R (N=10 n=10) trabeculae. **(B)** Top, WT and E163R representative force traces, showing a stimulation pause of 10s. Mean±SEM values of relative tension (normalized on contraction amplitude at 1 Hz stady state stimulation) plotted against the resting interval to obtain the post-rest potentiation curves in WT (N=10 n=12) and E163R (N=10 n=10) trabeculae.

Maximum post-rest potentiation was also measured in WT and E163R trabeculae (**Figure 4.4.** panel B). Stimulation pauses of variable duration were inserted into a steady 1 Hz series. Active tension developed after 60s pause (interval inducing maximum twitch potentiation) were 6.58±0.82 times of steady state contractions in WT and is reduced to 4.16±0.81 in E163R mice (p<0.05 E163R vs WT). Both, changes in SERCA activity or RyR2 refractoriness could be responsible for these alterations of the short-term interval force relationship.

The decline of potentiated beats following a period of high stimulation rate was analysed to estimate the so-called Ca^{2+}-recirculation fraction (**Figure 4.5**) (Bassani et al, 2001). RF is a parameter estimating the cellular recirculation of Ca^{2+} which depends on the balance between Ca^{2+} re-uptake by the SR Ca-pump (SERCA) and Ca^{2+} extrusion through the cell membrane, mainly accomplished by the Na^{+}/Ca^{2+}-exchanger (NCX). (Obayashi et al, 2006). At basal conditions, RF was similar in WT and E163R trabeculae. Likewise under Iso, RF augmented as expected by an increased SERCA activity in both WT and E163R (by approximately 7% and 6%, respectively), with no significant differences between the two groups. This suggests that SERCA function, and its response to PKA, was substantially maintained in E163R mice and identifies RyR2 as the potential responsible for the alterations of mechanical restitution and post rest potentiation observed above. The indication of substantially maintained SERCA vs NCX activity in this mouse line also suggests that prolonged twitch relaxation is more likely related to primary E163R cTnT- related changes at sarcomere level, as confirmed by the comparison of the mechanical behaviour of single myofibrils E163R and WT (see Result section 3.4). As discussed below, this could be a characteristic element for this mutation that

contradistinguishes the E163R from other cTnT mutation which are associated with a markedly reduced SERCA activity (Rice et al, 2010) (see **Fig. 4.11** below).

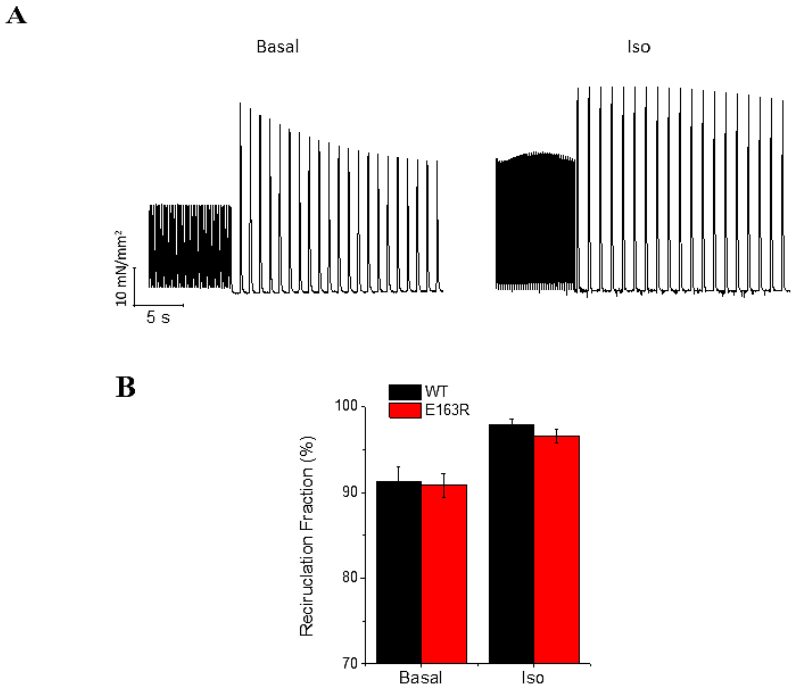

Figure 4.5. Ca^{2+} Recirculation Fraction (RF) in E163R and WT cTnT mutant trabeculae. **(A)** Stimulation protocol to estimate RF. The muscles were stimulated at 5 Hz for 20 s, then stimulation rate was reduced to 1 Hz. RF was estimated in isolated cardiac preparations based on the decay of the amplitude of subsequent contractions during dissipation of twitch potentiation. RF was evaluated at baseline and under Isoproterenol 10^{-7} mM. (B) Mean±SE values of RF in WT (N=10 n=12) and E163R (N=10 n=10) trabeculae in the two conditions.

Intracellular Ca^{2+} measurement in single cardiomyocytes

In a subset of experiment we measured the intracellular calcium transient in single cardiomyocytes isolated from WT and E163R cTnT mutant hearts, as described in Methods paragraph 2.2.5. Similarly to intact multicellular preparations, single cardiomyocytes underwent various stimulation protocols including (e.g. different pacing rates and stimulation pauses) and pharmacological tests. Ca^{2+} transients (CaT) were assessed at 30 °C and at $[Ca^{2+}]_o$ of 2 mM.

As shown in **Table 4.1**, no significant difference was found in E163R CaT amplitude compared to WT at various stimulation frequencies (1, 3 and 5 Hz). Interestingly, CaT kinetics such as time to peak, decay time to 50% and decay time to 90% were significantly faster in E163R compared to WT. This preserved decay phase of CaT is in agreement with the maintained SERCA function suggested by Ca^{2+} recirculation fraction assessment in WT and E163R trabeculae. In addition, preserved decay phase of CaT suggests that the observed prolongation of twitch kinetics in the intact E163R is entirely due to changes at myofilament level, i.e. to the overall prolongation of myofibrils relaxation (see Result section 3.4). Furthermore, the Ca^{2+}sensitizing effect of E163R mutation (see Result section 3.2 **Fig 3.2.1**) , by enhancing the static intracellular Ca^{2+} buffering capacity, can account for the accelerated CaT kinetics, both time to peak and decay time (Bers et al, 2003).

Since CaT rise was not prolonged and myofibrils activation kinetics was unchanged in E163R versus WT, the prolongation of the twitch time to peak in E163R is hard to be explained. Recent findings by J. Tardiff group (personal communications) described a severe degree of structural remodeling in E163R myocardium including myofibril disarray within the cells and myocytes misalignment within the tissue. This structural disarray, by increasing non homogeneity of muscle contraction, could slow down the kinetics of force development in E163R trabeculae (Ter Keurs et al, 2008).

Table 4.1 *Calcium Transient amplitudes and kinetics in WT and E163R*

WT	Stimulation Frequency (Hz)	**AMPLITUDE (fluorescence a.u)**	**TIME TO PEAK (ms)**	**DACAY TIME TO 50% (ms)**	**DACAY TIME TO 90% (ms)**
	1	**2.808±0.316**	**29.8±1.6**	**164.6±7.5**	**346.9±17.9**
	3	**2.068±0.261**	**28.5±1.2**	**120.9±3.4**	**223.5±6.6**
	5	**1.863±0.315**	**25.8±1.7**	**96.9±2.1**	**155.8±2.7**
E163R					
	1	**3.215±0.474**	**26.0±0.9***	**126.2±4.8****	**277.1±15.7****
	3	**2.369±0.339**	**25.5±0.8***	**99.5±2.1****	**188.2±4.0****
	5	**1.903±0.289**	**24.6±0.8***	**84.1±1.2****	**141.1±1.5****

Values are means ± SE. N =8 n= 4 and N=7 n=40 for WT and E163R respectively, where N=number of mouse and n=number of cardiomyocytes. **p<0.05; **p<0.01*

4.2. Comparison of Ca^{2+} handling abnormalities with those identified in cTnT mouse model carrying R92Q mutation

In the previous chapter we assessed the Ca^{2+} handling and twitch contraction abnormalities in E163R compared to WT. In order to better investigate the E-C coupling changes occurring in E163R mice and to evaluate if these alterations could be specific of this mutation, we compared E163R mice with another widely described cTnT mouse model carrying R92Q mutation.

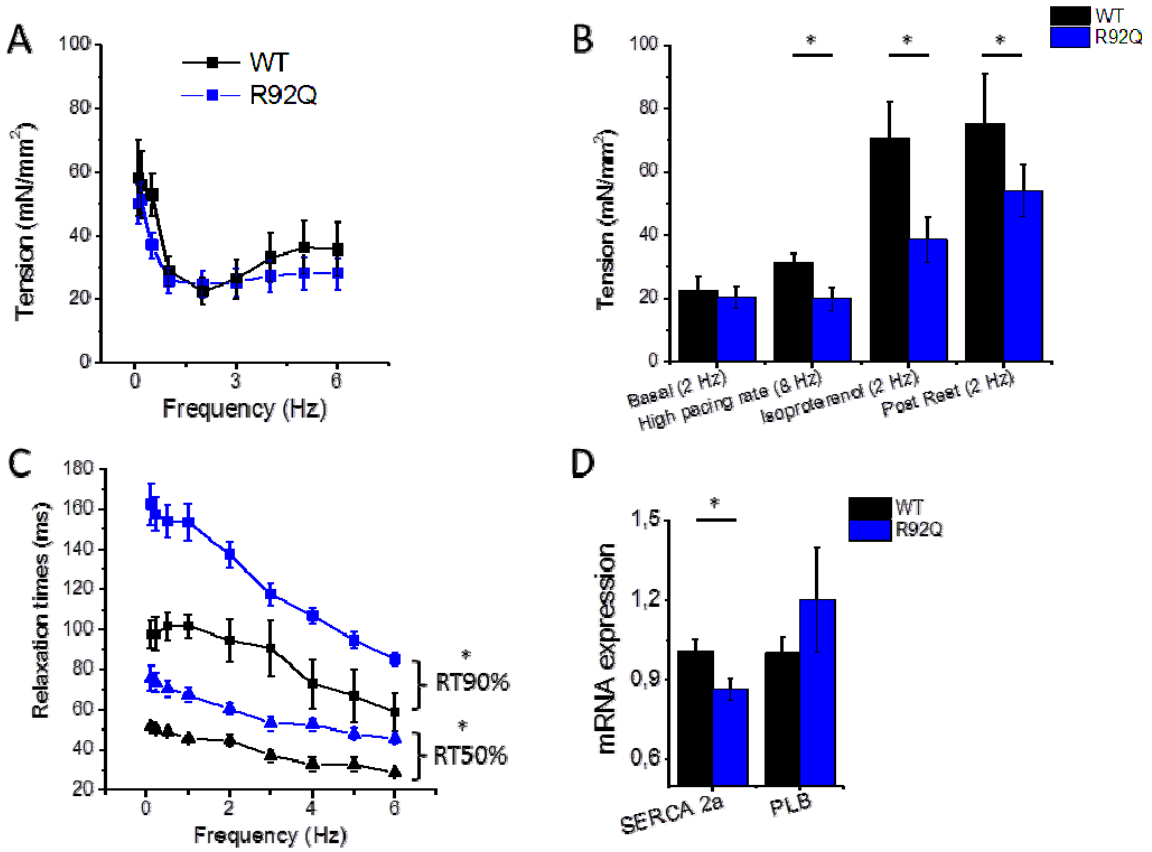

Figure 4.6. Isometric twitch tension and relaxation properties in R92Q and WT TnT mutant mice. (A) Relationship between twitch amplitude and pacing frequency at steady state in WT (N=6, n=9) and R92Q (N=7, n=12) trabeculae. (B) Mean±SEM data of twitch tension under various inotropic stimuli: high pacing rates, Isoproternel 10^{-7} and resting pauses (C) Mean±SEM data for time from peak to 50% and 90% relaxation in WT (N= 6, n=9) and R92Q (N=7 , n=12). (D) RNA expression of SERCA2a and PLB genes, relative to GAPDH in WT (N=6) and R92Q (N=5) left ventricular samples.

In **Fig 4.6,** panel A shows the relationship between isometric twitch tension and stimulation frequency in R92Q and WT trabeculae. In R92Q, a depression of the ascending limb of the FFR was observed with significantly reduced twitch amplitude at 8 Hz pacing rate (**Fig 4.6,** panel B). To further assess whether maximal isometric twitch tension was affected by the mutation, we measured force during acute administration of Isoproterenol, applied at a concentration of 10^{-7} mM (Iso) and maximum post-rest potentiation (**Fig 4.6,** panel B) In both WT and R92Q trabeculae mean isometric twitch tension increased upon administration of Iso; but, the twitch tension increase in R92Q group was significantly lower when compared to WT (~ 70% and ~200% in R92Q and WT, respectively). The maximum post-rest potentiation was also measured as well as mechanical restitution which is described below (paragraph 4.3). Active tension developed after 60s pause was reduced in R92Q (panel B).

Furthermore, the kinetics of force relaxation was markedly affected by R92Q mutation. Time from peak to 50% and time from peak to 90% relaxation were both prolonged in R92Q with respect to WT trabeculae (**Fig4.6** panel C), while time to peak was not affected.
We further assessed the features of the intracellular CaT of R92Q cardiomyocytes compared to WT (**Fig 4.7** and Table 4.2). As shown in **Table 4.2**, R92Q CaT amplitude was significantly lower when compared to WT at all stimulation frequencies (1, 3 and 5 Hz), in line with the reduced twitch amplitude at high pacing rates. Decay time to 50% and decay time to 90% of the CaT were significantly slower in R92Q myocytes compared to WT, while time to peak was not affected.

Table 4.2 *Calcium Transient amplitudes and kinetics in R92Q*

R92Q	Stimulation Frequency (Hz)	**AMPLITUDE (fluorescence a.u)**	**TIME TO PEAK (ms)**	**DACAY TIME TO 50% (ms)**	**DACAY TIME TO 90% (ms)**
	1	**1.865±0.249***	**28.5± 1.7**	**206.3±7.1****	**497.9±20.5****
	3	**1.412±0.190***	**26.8±1.2**	**133.5±2.7****	**246.3±4.1****
	5	**1.164±0.160***	**26.1±0.9**	**102.0±1.5****	**162.7±1.5****

Values are means ± SE. N =12 n= 68, where N=number of mouse and n=number of cardiomyocytes. **p<0.05;* ***p<0.01*compared to WT values in table 4.2.

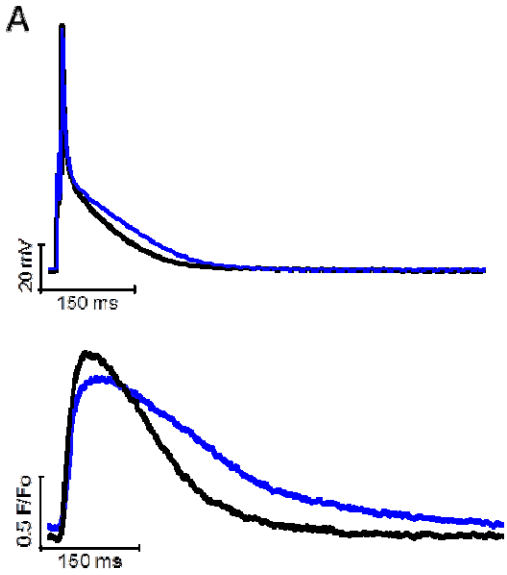

Figure 4.7. Electro-mechanical remodelling in R92Q cardiomyocytes. (A) *top* Representative traces of action potential (AP) measured from WT (black tracing) and R92Q (blu tracing) cardiomyocytes. R92Q AP duration is prolonged compared to WT. *Bottom* representative traces of Ca^{2+}transients from WT (black tracing) and R92Q (blu tracing). Decay time to 50% and 90% were significantly slower in R92Q compared to WT.

The prolongation of relaxation in R92Q trabeculae and the slower rate of CaT decay are likely related to a reduced SERCA activity as indicated by the following results: (i) in R92Q myocardium SERCA2a expression was significantly lower when compared to WT while PLB levels were maintained (**Fig 4.6** panel D), (ii) Ca^{2+} recirculation fraction was markedly reduced, indicating a reduction of SERCA versus NCX activity (see **Fig4.10**).

4.3 Spontaneous activity in E163R and R92Q myocardium and effect of Ranolazine.

Here, we investigated the occurrence of spontaneous beats in E163R and R92Q trabeculae (**Figure 4.8**). Spontaneous activity was elicited by a run of stimulation (e.g. 1 Hz in Figure 4.8 A, 3 Hz in Figure 4.8 B) followed by a resting period. The same protocol was repeated in the presence of Iso. Both groups compared to WT showed increased spontaneous activity during pauses, in the form of either irregular premature contractions (**Figure 4.8 A**) or run of regular spontaneous beating (**Figure 4.8 B**). Additionally, in both mutants we observed after-contractions and premature beats not only during stimulation pauses but even during the regular stimulation (**Figure 4.8 C**). This was never observed in WT.

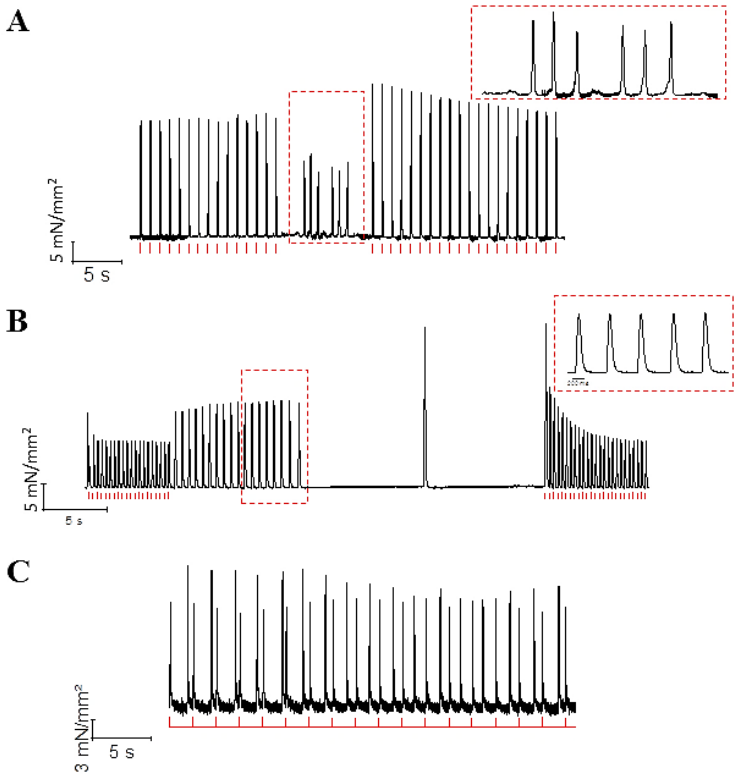

Figure 4.8. Spontaneous activity in E163R and R92Q cTnT mutant trabeculae. (A) Representative traces from an E163R trabecula showing an example of spontaneous activity during pauses. Short red lines indicate the times of stimuli. In this case the spontaneous activity is present in the form of multiple irregular premature contractions. (B) A second example of spontaneous activity during stimulation pauses in a E163R trabecula. In this case we observed a 10 s run of regular spontaneous contractions (with cycle-length of 580 ms, frequency 1.72 Hz), followed by a single spontaneous contraction that occurred after other 10 s. (C) A third example of spontaneous activity in a E163R trabecula, which occur in the form of after-contractions and premature contractions during regular activity.

The occurrence of spontaneous contractile activity was quantified as shown in **Figure 4.9**. Both at baseline and under Iso the occurrence of spontaneous contraction during pauses (total number of spontaneous events per resting period) was significantly increased in E163R and R92Q trabeculae with respect to WT (see **Fig 4.9** panel D). In the R92Q group was observed an increase in the occurrence of spontaneous beats with an increment of pause duration under ISO, but this behavior was not observed in the in E163R group where the occurrence did not depend on pause duration (**Fig. 4.9**, panel C). Ranolazine 10 μM (Ran) applied on top of Iso significantly reduced the occurrence of aftercontractions and premature beats below basal levels in both E163R and R92Q.

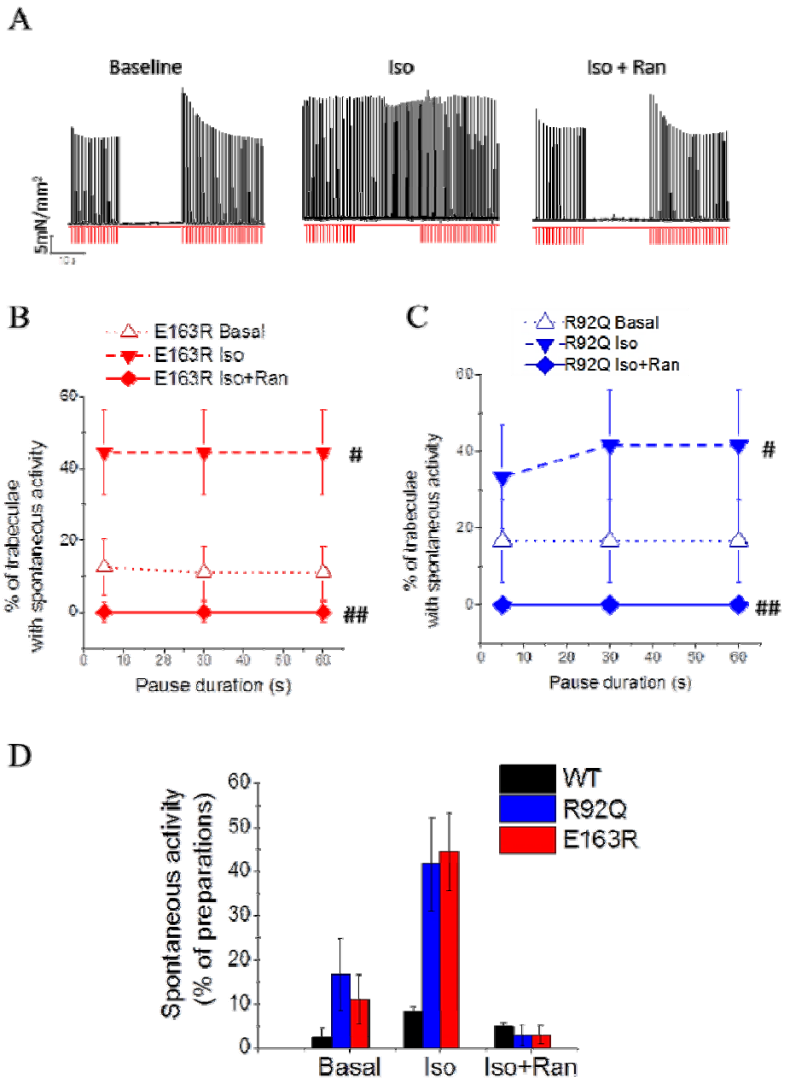

Figure 4.9. Increase in Spontaneous activity in E163R and R92Q in the presence of Iso and its reversal by Ranolazine. (A) Representative traces of spontaneous activity during pauses induced by Iso and reversed upon addition of Ranolazine 10 μM (Iso+Ran). (B) Mean±SE values of the global occurrence of spontaneous activity during pauses in E163R (N=10 n=10) and (C) in R92Q (N=7 , n=12) plotted against the duration of the resting interval. # $p<0.05$ paired T test vs. basal and ## $p<0.01$ paired T test vs. Iso.

Next, we evaluated whether spontaneous aftercontractions and beats observed in muticellular preparations were paralled by spontaneous Ca^{2+} fluxes in sigle cardiomyocytes. The occurrence of Ca^{2+} waves and spontaneous Ca^{2+} transients (CaT) during stimulation pauses was evaluated in WT, E163R and R92Q cardiomyocytes. As shown in **Fig 4.10** in basal condition, the occurrence of spontaneous Ca^{2+} waves was significantly higher in both E163R and R92Q mutants when compared to WT and, comparing the two mutants, the occurrence of spontaneous Ca^{2+} waves was much higher (approximately double) in E163R cardiomyocytes. Upon administration of Iso, as expected, the number of spontaneous Ca^{2+} waves augmented significantly in both WT and mutants. However, also in Iso, both E163R and R92Q showed a significantly higher occurrence of these spontaneous events compared to WT. The effect of Iso was more pronouced in R92Q so that the number of spontaneous Ca^{2+} waves under β-adrenergic stimulation was comparable in E163R and R92Q. The enhancement of spontaneous Ca^{2+} waves induced by Iso was reversed to basal levels in both R92Q and E163R mutant upon addition of Ran, with a negligible effect in WT.

Summarizing, the administration of Ran during β-adrenergic stimulations had a quantitatively larger effect in R92Q (-54%), milder effect in E163R (-17%) and negligeble effect in WT.
We also quantified the occurrence of spontaneous Ca^{2+} transients in basal condition, under Iso and under Iso+Ran. As shown in **Fig 4.10 panel D** in basal condition, the occurrence of spontaneous CaT was significantly higher in both E163R and in R92Q when compared to WT and significantly augmented under administration of Iso in the three groups, though the increase measured in the two mutant was significantly higher when compare to WT. Administration of Ran on top of Iso reversed almost completely the effect of Iso in both mutants with a negligible effect on WT. Of note, while the occurrence of Ca^{2+}waves was higher in E163R compared to R92Q, the occurrence of spontaneous CaT was similar in the two mutants.

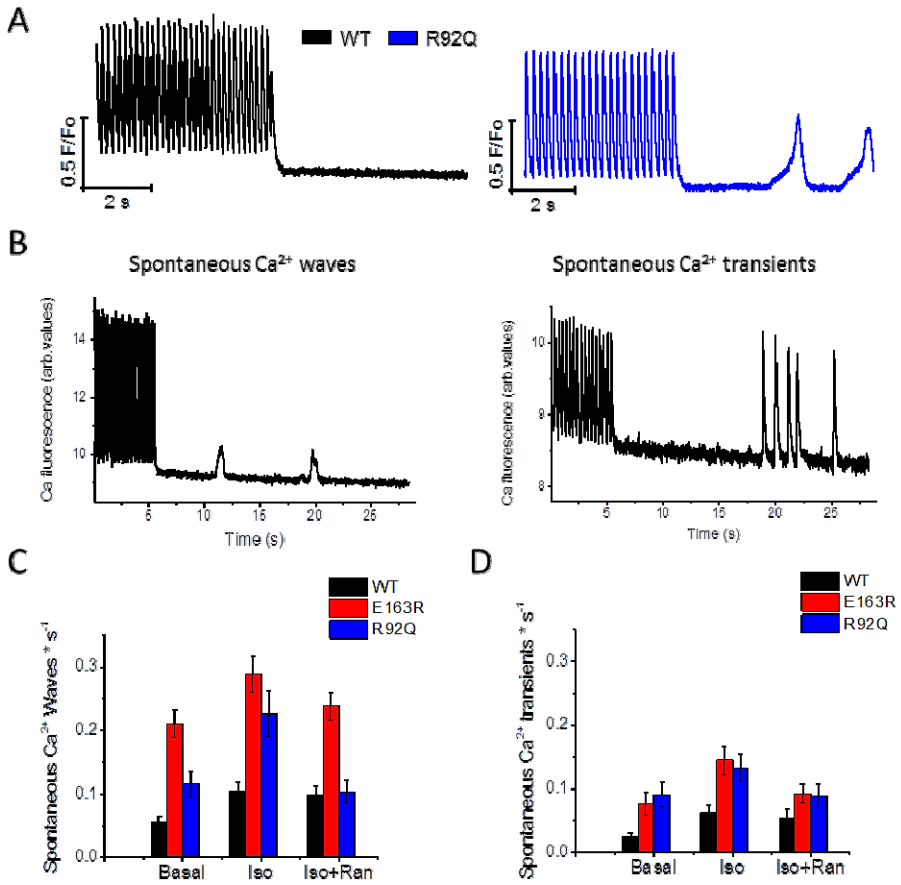

Figure 4.10. Spontaneous Ca^{2+} waves and spontaneous Ca^{2+} transients in E163R and R92Q cardiomyocytes. (A) Representative intracellular Ca^{2+} recordings from a WT and a R92Q cardiomyocyte, showing a run of stimulation at high frequency (5 Hz) followed by stimulation pauses of various duration (2-20s).The R92Q cardiomyocyte shows two spontaneous Ca^{2+} transients occurring during the resting period. (B) Example traces showing spontaneous Ca^{2+} waves (left) and spontaneous Ca^{2+} transients (right). Spontaneous Ca^{2+} waves were defined as fluorescence variation ≤ 20% of the corresponding Ca^{2+} transient at steady state stimulation. The occurrence of spontaneous Ca^{2+} waves and Ca^{2+} transients is quantified in (C) and (D), respectively. The number of events was normalized per time unit (s).

To better understand the mechanism underling these pro arrhythmogenic spontaneous events we employed Ca^{2+} recirculation fraction (RF) and mechanical restitution protocols to investigate NCX and RyR2 function, respectively.
As mentioned above, RF was similar in WT and E163R trabeculae but markedly reduced in R92Q indicating an increased role of NCX versus SERCA for cytosolc Ca^{2+} removal in R92Q. As shown in **Fig 4.11,** under Iso, RF increases in all groups. Administration of Ran completely reversed the RF enhancement to baseline values in R92Q and partially in E163R but not in WT. The more pronounced

effect of Ran on R92Q group is likely related to an increase role of NCX in this mouse line compared to E163R. In fact, Ran by reducing intracellular [Na^+] and [Ca^{2+}] indirectly promote forward NCX function.

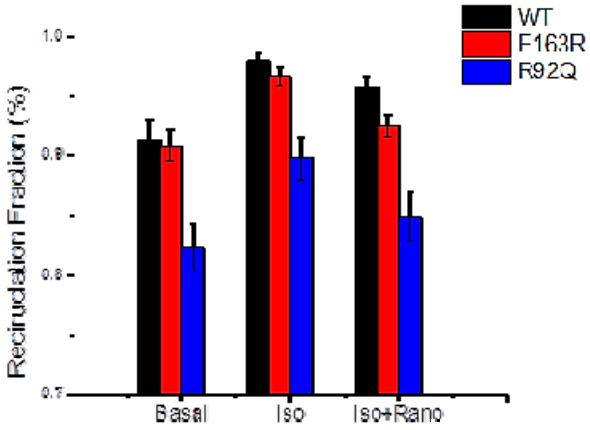

Fig 4.11 Ca^{2+} Ricirculation Fraction in WT, E163R and R92Q mutant trabeculae in Iso and Iso+ran.
RF was estimated in isolated cardiac preparations based on the decay of the amplitude of subsequent contractions during dissipation of twitch potentiation at baseline, under Iso 10^{-7} mM and under Iso + Ran. Mean±SE values of RF in WT (N=10 n=12, balck) E163R (N=10 n=10, red) and R92Q (N=7, n=12, blue) trabeculae in the three conditions.

Preliminary measurements of intracellular diastolic Ca^{2+} levels showed that Ran reduces diastolic Ca^{2+} in R92Q with mild or no effect in E163R and WT.
Mechanical restitution was also assessed in Iso and Iso + Ran, as shown in **Fig 4.12**. At baseline, mechanical restitution was faster in both mutants, including R92Q where SERCA activity is reduced. Acceleration of mechanical restitution induced by Iso was reversed in both mutants upon addition of Ran **(Fig 4.12** panel A**)** while this effect was negligible in WT (**Fig 4.12** panel B**)**. This would indicate that shorter RyR2 refractoriness which could contribute to generate spontaneous Ca^{2+} waves and CaT, may be a mechanism underlying spontaneous activity in both R92Q and E163R. The beneficial effect of Ran on mechanical restitution may support an additional effect of Ran on RyR2 function other than its notorious effects as I_{NaL} blocker, which have been previously described (Parikh et al, 2012).

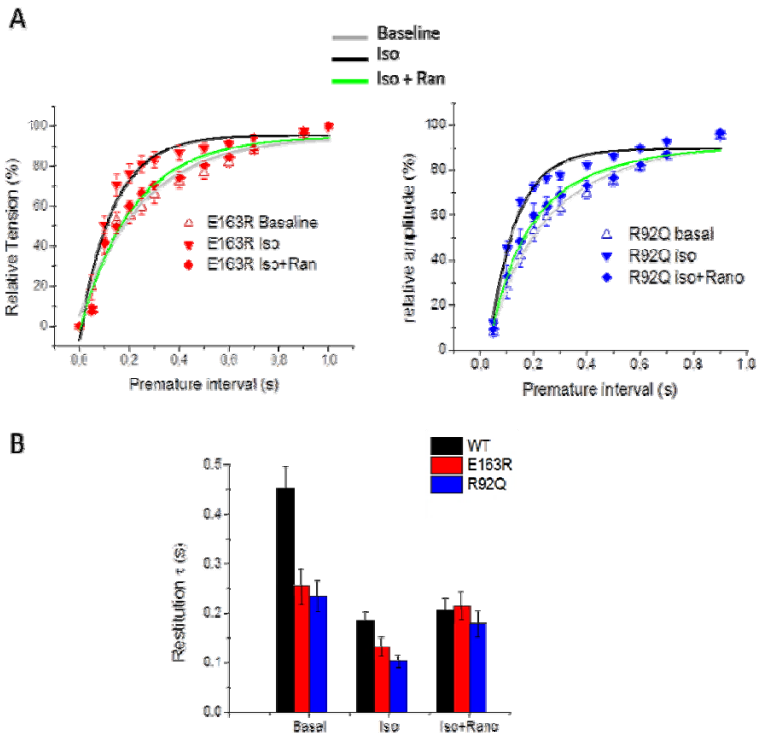

Fig 4.12 Mechanical restitution in WT, E163R and R92Q trabeculae in Iso and Iso+ran. (A) Mean±SEM values of relative tension (normalized on contraction amplitude at 1 Hz steady state stimulation) plotted against the premature interval to obtain the restitution curves in basal conditions (gray line) under Iso (black line) and under Iso+ Ran (green line) in E163R trabeculae (N=10 n=10) on the left and in R92Q traculae (N=7, n=12) on the right. (B) Restitution τ at baseline, under Iso 10^{-7} mM and under Iso + Ran. Mean±SE values of τ in WT (N=10 n=12, balck) E163R (N=10 n=10, red) and R92Q (N=7, n=12, blue) trabeculae in the three conditions.

5. Summary and discussion

In HCM, primary functional alterations at sarcomere level (Belus et al, 2009) are associated with secondary modifications in Ca^{2+} handling and E-C coupling, leading to alterations of myocardial contractility and to a pro-arrhythmogenic phenotype (e.g. Coppini et al, 2013). The relative contribution of primary vs secondary alterations is still unknown and the molecular bases of this adaptive/ maladaptive remodeling are still poorly understood.

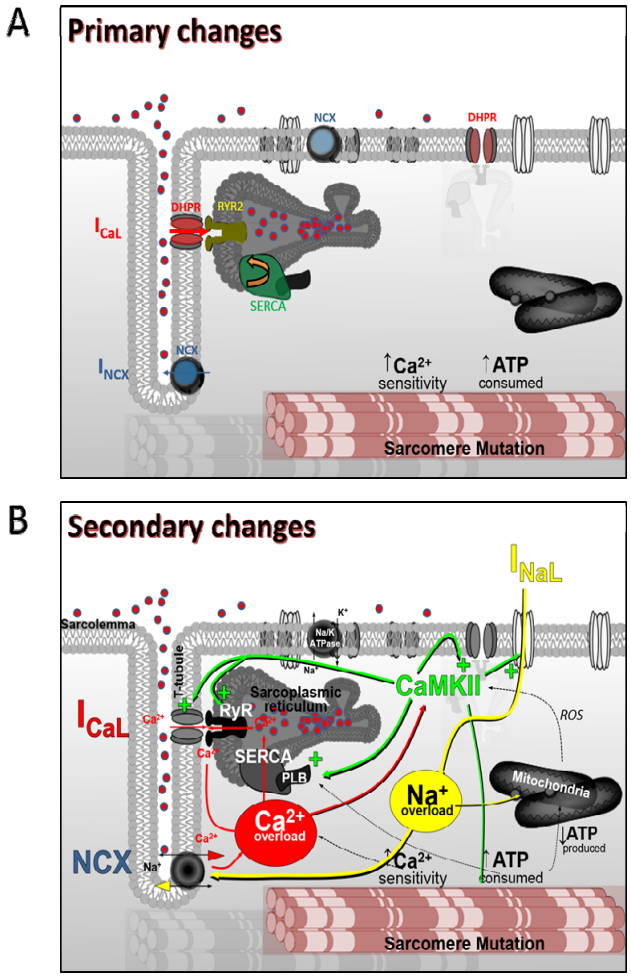

Fig 5.1 Primary and secondary changes in HCM myocardium. (A) Sarcomeric mutations may cause direct alterations in sarcomeric function: increased sarcomeric ATP consumption and enhanced myofilament Ca^{2+} sensitivity could together trigger a secondary adaptative/ maladaptative cellular remodeling. (B) The energy depletion at sarcomeres levels may lead to SERCA (and mithocondria) dysfunction and impaired Ca^{2+} removal, an enhanced myofilament Ca^{2+} sensitivity slows Ca^{2+} dissociation from the myofilaments and contributes to increased Ca^{2+} levels during diastole. Intracellular Ca^{2+} overload (in combination with increased production of reactive oxygen species) could be responsible for triggering the secondary remodeling in cardiomyocytes.

The aim of this work was the study these changes in skinned trabeculae and single myofibrils as well as intact trabeculae and cardiomyocytes from the ventricles of transgenic mouse models aged 6 months carrying HCM-related mutations of cTnT E163R and R92Q.

In E163R myocardium vs WT:
(1) no significant difference was found in maximal Ca^{2+} activated tension between E163R and WT skinned trabeculae and myofibrils. Twitch tension and maximal contractile reserve were also the same in E163R and WT intact preparations.

(2) The force-ATPase ratio, i.e. the Tension Cost, of skinned trabeculae was about 40% higher in E163R than in WT trabeculae. The results support the idea that impaired sarcomeric energetics may be central to HCM disease process. The change in tension cost is in agreement with the observed trend toward a 40% faster isometric relaxation rate of E163R myofibrils (slow k_{REL}). Both parameters reflect cross-bridge detachment rate under isometric conditions that may be accelerated in the presence of the mutant TnT.
(3) Passive tension of E163R skinned trabeculae and myofibrils tended to be increased compared to WT preparations and was associated to an increase in the resting ATPase activity of E163R trabeculae. These features suggest that the E163R mutation in cTnT may impair thin filament switch off mechanisms contributing to the prolongation of the overall relaxation duration observed in E163R myofibrils (Tesi et al 2002).
(4) E163R skinned trabeculae exhibited an enhanced Ca^{2+} sensitivity of tension and ATPase compared to WT trabecuale. This may also contribute to the prolonged slow relaxation phase duration observed in E163R myofibrils (Kreutziger KL et al 2011).
(5) Impaired relaxation of E163R myofibrils can be responsible for the prolonged twitch duration of E163R intact preparations in the absence of decelerated Ca^{2+} transient kinetics and myosin isoform shifts

In R92Q myocardium vs WT we observed:
(1) Preserved peak isometric twitch tension at low inotropic level but reduced contractile reserve under inotropic challenge (Isoproterenol, high pacing rates and long pauses), paralleled with a reduction in Ca^{2+}transient amplitude.
(2) Prolonged relaxation kinetics in intact ventricular trabeculae associated with reduced SERCA function and slower decay rate of Ca^{2+}transients.
(3) A reduction of Ca^{2+}recirculation fraction, indicating an enhanced NCX activity.
(4) Prolonged action potentials due to ionic current remodeling.
Primary changes of myofilaments function (increased Ca^{2+} sensitivity but unchanged myofibril ATP consumption) (Chandra et al, 2000; Chandra e al, 2005), have been previously described in R92Q hearts.
Both E163R and R92Q cTnT mutants showed:
(1) Frequent after-contractions or spontaneous beats during pauses, which increased in response to isoproterenol.
(2) Higher occurrence of spontaneous Ca^{2+} waves and Ca^{2+}transients under isoproterenol.
(3) Faster mechanical restitution, indicating shorter RyR2 refractoriness.

The relative low degree of E163R mutation-related secondary remodeling render this model a valid prototype to dissect primary mechanisms from secondary HCM- related pathophysiological alterations.
Most of the studies aimed at understanding primary changes in muscle function have shown that increased myofilament Ca^{2+} sensitivity and enhanced sarcomeric ATP consumption are common (although not inescapable and highly specific) in HCM, independently from the genetic defect involved (Crilley et al, 2003; Marston, 2011).
A specific mutation could directly affect individual proteins conformation and thus their function, such as protein- protein interaction or the affinity for specific substrates (e.g. Ca^{2+} and ATP). It is quite intuitive to assume that mutations occurring in specific sarcomeric protein binding sites could directly alter the specific affinity of the protein for its substrate. It is much tougher, instead, to comprehend how mutations located elsewhere could affect a specific protein function.
For instance, a mutation occurring in cTnI can cause a protein conformational change varying its affinity for cTnC and leading to changes in myofilament Ca^{2+} sensitivity. Alternatively, modifications in myofilament Ca^{2+} sensitivity introduced by the mutation can directly be related to variation of cTnC

binding affinity for Ca^{2+} (Kobayashi and Solaro, 2006). Similarly, in term of ATP utilization, a mutation occurring in Myosin head can directly affect the ATPase domain thus varying the affinity for the substrate. Alternatively, when mutations are located elsewhere in myosin or in other myofilament proteins such as cTnT, changes in ATP consumption could derive from more indirect mechanisms. Thus, the E163R mutation on cTnT, altering both Ca^{2+} sensitivity and tension cost according to our results, could be an interesting model to gain better insight in the link between protein structure and function.

5.1 Impact of E163R cTnT mutation on myofilament response to Ca^{2+}.

A frequent finding among HCM mutations is increased myofilament Ca^{2+} sensitivity. This likely provides a molecular basis for hypercontractility that is commonly observed in human patients and in studies with TG mouse models. Myofilament Ca^{2+} sensitization, by affecting cytosolic Ca^{2+} buffering (Schober et al, 2012) alters the intracellular calcium homeostasis and generates several immediate downstream effects. An increased myofilament Ca^{2+} sensitivity, could impair mechanics (positive inotropic, negative lusitropic effect), energy demand and may contribute to the proarrhythmic effect (Huke S. &. Knollmann B.C, 2010).
In E163R trabeculae vs WT although there was no significant difference in Ca^{2+} activated maximal tension, at all submaximal activating [Ca^{2+}] there was a significant increase in the tension development and ATPase activity compared to WT i.e. an increase in calcium sensitivity. This result is in agreement with previous studies on recombinant human cardiac TnT (HCTnT) mutants incorporated into porcine cardiac skinned fibers together with HCTnI and HCTnC, where both E163R and E163K mutation on cTnT induced an increase in Ca^{2+} sensitivity (Szczesna D., 2000; Harada & Potter, 2004). Furthermore, single E163R myofibrils showed no change in maximal isometric tension (P_0) but the duration of the slow phase of relaxation was prolonged compared to WT. The prolonged duration of slow phase of relaxation has been shown to correlate with the increase in myofilament Ca^{2+} sensitivity as in presence of a reduction of Ca^{2+} k_{off}. (Kreutziger KL et al 2011).
Similarly, no modification of maximal Ca^{2+} activated tension and an enhanced myofilament Ca^{2+} sensitivity have been also found in R92Q cTnT mutation compared to WT and in other missense mutations on codon 92 such as R92W and R92L (Chandra M.et al, 2001; Chandra M.et al 2005). Alteration in Ca^{2+} sensitivity of force development might be explained by a direct effect of mutation on the Tn complex, or by an inefficient binding of improperly folded mutant cTnT or, finally, by an impact on actin-Tm. The first demonstration that a HCM-causing TnT mutation alters Ca^{2+} affinity *per se*, was given by a study by Tobacman, reporting the effects of mutations introduced into bovine cardiac TnT via mutagenesis of cDNA isolated from a bovine heart cDNA library. There are strong evidences that D160E mutation on TnT causes an enhanced myofibrillar Ca^{2+} sensitivity by increasing Ca^{2+} affinity of the TnC regulatory site (Tobacman et al, 1999). However, the mechanism by which the R92Q mutation could increases the myofilament response to Ca^{2+} appears to be linked to a decreased threshold for thin filaments Ca^{2+} activation (Chandra et al, 2005). The mechanisms by which E163R cTnT mutation may cause a Ca^{2+} sensitizing effect are still not clear. A recent study on atomistic model of the cTn–Tm complex (Manning et al. 2012) showed that alterations of flexibility or orientation of specific portion of TnT molecule could affect the protein complex and then also the function of the thin filament. This study predicts an increase of the flexibility of TNT1 in presence of E163R cTnT mutation, decreasing cTnC affinity for bound Ca^{2+} i.e. the opposite of our data suggesting an enhanced Ca^{2+} sensitivity. Other studies (Palm et al, 2001) performed in thin filaments containing only a fragment of residues 70–170 cTnT showed that HCM-causing mutations in human cardiac TnT (hcTnT) between residues 92 and 110 (R92L, R92Q, R92W, R94L, A104V, and F110I) impair TM-dependent functions of hcTnT, identifying altered TM binding as a probable cause of disease. This study did not report any difference between ΔE160 and E163K mutants and WT

characteristics, concluding that these mutations "must cause disease by other mechanisms." Thus, to date, the molecular basis for the E163R-induced increase in Ca^{2+} sensitivity of transgenic myofilaments remain controversial.

5.2 Impact of E163R cTnT mutation on tension-dependent ATP consumption.

As discussed in introduction, it has been proposed that sarcomere mutations related to HCM may lead to increased cost of force production through inefficient or excessive ATP usage and that this ultimately results in an energy deficiency that contributes to the pathogenesis of the disease (Ferrantini et al., 2009; Chandra et al, 2005; Frey et al, 2006).

In this work, we tested the hypothesis that the presence of the mutated TnT could alter the cross bridge cycling kinetics by regulating the interaction between myosin-based cross bridges and the thin filament. We simultaneously measured ATPase activity and isometric steady-state force and according to our results Ca^{2+}-activated maximal ATPase activity was significantly increased compared to WT while tension was not altered by the E163R mutation in cTnT. Slopes describing the isometric force-ATPase relationships (tension cost) were significantly different in WT trabecule and in E163R mutation in cTnT. The change in tension cost was significant and averaged a 37% increase in E163R group compared to WT. Our values of the maximum rate of ATP consumption were 680.68±655.52 and 931.27±115.54 pmol $\mu l^{-1}s^{-1}$ for WT and E163R transgenic trabeculae, respectively. These values seem to be higher compared to those previously reported for mouse skinned fibers (approximately from 320 to 371 pmol $\mu l^{-1}s^{-1}$ Wolska BM, 1999; Chandra et al 2000; Chandra et al, 2005). This apparent discrepancy can be justified by the parallel increase in our values of max tension in skinned trabeculae and partially to a different set-up disposition. Assuming that the 95% of Ca^{2+}-activated ATPase activity was due to actomyosin and that the myosin head concentration is 0.16 mM (160 pmol/ml) (Barsotti & Ferenczi, 1988), 4.04 and $5.5s^{-1}$ corresponds to the maximum cycling rate per myosin head for WT and E163R trabeculae, respectively. These values are almost in line to that previously reported in mice (Potma et al. 1994, Kentish and Stienen, 1994, and de Tombe and Stienen, 1995)

According to a simple 2-state model of acto-myosin interactions (Brenner 1988) (**Fig. 5.2**), (i) the formation of force-generating crossbridges occurs via an apparent rate constant f_{app}, (ii) crossbridge detachment occurs with apparent rate constant g_{app}, (iii) the overall crossbridge turnover rate is given by $f_{app}+ g_{app}$,(iiii) tension is proportional to $f_{app}/(f_{app}+ g_{app})$, and (iiiii) the energy cost of tension generation (ATPase/tension ratio) is proportional to g_{app} (Brenner 1988; deTombe & Stienen 2007).

Fig 5.2. 2-state crossbridge scheme. $AM_{no\ force}$ represents all weak binding states (mostly detached) and AM_{force} all strong binding states. The transition from the non-force-generating states to the force-generating states has an apparent rate constant f_{app} whereas g_{app} describes the return to the non-force-generating states by means of ADP release and ATP binding. The apparent rate constant for the reverse transition f'_{app} that depends on [Pi] can be neglected under the conditions of the study.

Thus, our data reporting an increase in tension cost indicate that the E163R mutation in cTnT could alter the intrinsic cross-bridge detachment rates *"g_{app}"* in cardiac myofilaments. To further investigate

this point we performed mechanical and kinetics measurements on single myofibrils isolated from E163R and WT hearts.

It has been shown (Poggesi *et al.* 2005; Stehle et al 2009) that the slow linear force decay of isometric contraction following sudden calcium decrease below the activation threshold occurs while sarcomeres are isometric and its rate constant (slow k_{REL}) is predominantly the apparent rate with which attached crossbridges leave force-generating states or apparent detachment rate (g_{app}). In E163R myofibrils compared to WT we observed that the kinetics of the slow phase of relaxation (slow k_{REL}) tended to be accelerated by approximately ~ 40%.(0.87 ± 0.13 s^{-1} and 1.22 ± 0.20 s^{-1} in WT and E163R mutant myofibrils respectively), Since $k_{REL} \sim g_{app}$ This increase is not significant but it is consistent with the increase in TC observed in E163R skinned trabeculae.

In both E136R and WT myofibrils, k_{ACT} was the same as k_{TR}, suggesting that k_{ACT} is not limited by the rate with which thin filaments are switched on by Ca^{2+}. Albeit a marked trend toward an increase in slow k_{REL} in E163R myofibrils was observed, we did not notice any difference in the activating rate constants k_{ACT} and k_{TR} in E163R myofibrils compared to WT. k_{ACT} reflects isometric crossbridge turnover rates, i.e. the sum of the apparent rates with which crossbridges enter and leave their force generating states (f_{app} + g_{app}). We can assume that, since f_{app} is the major component of k_{ACT} with respect to g_{app}, this not dramatic increase in g_{app} could not affect the overall crossbridge turnover rate (given by f_{app}+ g_{app}).

As regards the kinetics of the exponential phase of relaxation, it was slower in E163R myofibrils compared to WT and in some cases relaxation was incomplete. Of note, the prolongation of the slow relaxation phase combined with a reduction of the fast k_{REL} results in a prolongation of the overall relaxation in E163R compared to WT myofibrils which may significantly affect the twitch kinetics of the intact E163R myocardium (discussed below). We can assume that the mechanisms underlying a prolonged and incomplete relaxation in E163R myofibrils could be linked to a mutation-relate impairment of the "switch off "regulation of the thin filament. In presence of a disrupted or inefficient thin filament inactivation, in absence of Ca^{2+}, Tm would not completely return in its 'blocked state' where sterically blocks the interaction between actin and myosin heads. Another mechanism that can account for an impaired relaxation could be related to the increase in Ca^{2+} sensitivity observed in E163R trabeculae. A prolongation of relaxation could reflect a slower dissociation of Ca^{2+} from the Tn complex. The relaxation behavior of E163R myofibrils, in fact, resembles the relaxation of control myofibrils following sudden decrease in [Ca^{2+}] to levels just above contraction threshold, e.g. pCa 6 instead of pCa 8 (Tesi et al, 2002). This would indicate that residual thin filament activation after Ca^{2+} removal allows recruitment of some new cross-bridges and is responsible for slowing down myofibril force decay and for the increase in resting tension observed. This last data is in agreement with our measures of ATPase activity in resting conditions. E163R, in fact, showed a significant increase of resting ATPase compared to WT trabeculae. The increase in ATP consumption even in resting condition suggests an overall higher rate of ATP hydrolysis in E163R sarcomeres compared to WT and consistently support the data of impaired and incomplete relaxation.

5.3 Cardiomyopathy associated E163R and R92Q cardiac troponin T mutation causes specific E-C coupling alterations and pro-arrhythmogenic changes.

In this study, structural ventricular remodeling, Ca^{2+} handling abnormalities, E-C coupling and pro-arrhythmogenic changes were also examined.

The assessment of the phenotypic characteristics, heart size and chambers dimensions, of this mouse model is particularly important given the limited availability of clinical information in literature on this mutation (Koga et al, 1996). On gross examination, heterozygous mice carrying the E163R mutation did not present any significant alteration of the gross heart morphology compared to WT littermates and showed neither hypertrophic phenotype nor ventricular dilation. Though, ultrastructural analysis of left ventricle tissue carried out by J. Tardiff group (Tucson, University of Arizona, personal communication) showed significant abnormalities in sarcomeric structure compared to WT with misregistration of thin filament orientation at Z- disk, myofibrillar lysis and disarray that could account for mechanical alteration observed in intact multicellular preparations. Contrarily, in R92Q mice the ventricular mass was decreased by approximately 18%. A progressive atrial hypertrophy over time was also observed in R92Q mice, with a proportional increase with transgenic protein levels. Ultrastructural examination of cardiac tissues revealed areas of disorganization with lipid deposition, and mitochondrial degeneration but sarcomere structure was preserved (Tardiff et al, 1999). It has been suggested that a chronic mismatch between ATP synthesis and ATP consumption related to an increase in basal sarcomeric activation could account for the observed changes in lipid content and mitochondrial morphology observed in R92Q myocardium (Chandra M. et al, 2001).

Regarding the presence of α to β shift in myosin isoforms, 6 month old E163R mice did not present any (excluding this as a potential mechanism for the mechanical changes we observed), while R92Q mice showed a progressive β-myosin induction over time, with late onset.

We have performed mechanical measurements on isometrically contracting trabeculae. No alterations were found in twitch amplitude in basal condition, at high pacing rates and under inotropic challenge in E163R compared do WT. A preserved contractile reserve in E163R was expected from our data obtained in skinned trabeculae and single myofibrils but in intact preparations it was ensured by no alterations in the Ca^{2+} transient (CaT) amplitude compared to WT. Although the peak isometric twitch tension was preserved, the kinetics of force development and relaxation was markedly affected by E163R mutation. Two possible mechanisms could be responsible for a prolongation of twitch kinetics: (i) a prolongation of Ca^{2+} transient kinetics and an altered balance between SERCA vs NCX activity, or (iii) a primary impact of the mutation E163R at sarcomeric level, i.e. the overall prolongation of myofibrils relaxation.

Interestingly, CaT kinetics such as time to peak, decay time to 50% and decay time to 90% was significantly faster compared to WT. Accelerated CaT kinetics, both time to peak and decay time cannot account for the prolongation of twitch kinetics, but are likely related to the Ca^{2+} sensitizing effect of E163R mutation. In fact, the increased myofilament Ca^{2+} sensitivity, by enhancing the static intracellular Ca^{2+} buffering capacity, can account for the faster CaT kinetics (Bers et al, 2003).

Furthermore, the preserved decay phase of CaT would suggest a maintained SERCA function, evaluated by the assessment of Ca^{2+} recirculation fraction (RF). At basal conditions and under Isoproterenol, RF was similar in WT and E163R trabeculae, supporting that SERCA function, and its response to PKA, is substantially maintained in E163R mice. Hence, the faster CaT kinetics with a preserved SERCA function together with the inability of isoproterenol to restore twitch relaxation kinetics to WT levels strongly support the idea that relaxation is affected by the primary effect at sarcomeric level of the mutation E163R. In the absence of any abnormalities in the Ca^{2+}-handling system of the myocyte, increased Ca^{2+} sensitivity of myofilaments could play a significant role in slowing the rate of relaxation.

The prolongation of the twitch time to peak in E163R, instead, is hard to be explained, since CaT rise was not prolonged and myofibrils activation kinetics was unchanged in E163R versus WT. We can

hypothesize that the severe degree of structural remodeling in E163R myocardium including myofibril disarray within the cells and myocytes misalignment within the tissue, by increasing non homogeneity of muscle contraction, could slow down the kinetics of force development in E163R trabeculae (Ter Keurs et al, 2008).

In contrast, the secondary remodeling observed in R92Q myocardium seems to be more complex. R92Q trabeculae presented a depression of the ascending limb of the force frequency relationship and a significantly reduction of tension under inotropic challenge (high pacing rates, long stimulation pauses and Isoproterenol administration), unveiling a reduction of contractile reserve in R92Q myocardium compared to WT and E163R. In support of our results, a previous work reported that R92Q hearts demonstrated systolic dysfunction at both the whole heart and myocyte levels (Rice R et al, 2009). The reduction of contractile reserve observed in R92Q trabecualae, likely follows the lower R92Q CaT amplitude observed when compared to WT.

The kinetics of force relaxation was markedly affected by R92Q mutation compared to WT likewise in E163R, while time to peak was not affected. In Rice R et al, measurements of unloaded shortening on single cells showed a similar behaviour with decreased amplitude and a prolongation of relaxation. However, at variance with isometric twitching trabeculae, single cells showed a prolonged peak rate of contraction. This apparent discrepancy could be, at least partially, related to the different loading conditions (Iribe et al, 2006; Monasky et al, 2008). In this case, the prolongation of twitch kinetics is associated with slower CaT kinetics, decay time to 50% and decay time to 90% of the CaT were significantly slower in R92Q myocytes compared to WT, while time to peak was not affected. Of note, a previous work by Rice R et al reported prolonged rates of both CaT decay and rise, the letter, at present, remains in contrast with our results.

In contrast with what has been found in E163R trabecualae, the prolongation of relaxation in R92Q trabeculae and the slower rate of CaT decay are likely related to a reduced SERCA activity as indicated by a significantly lower SERCA2a expression in R92Q when compared to WT in presence of normal levels of PLB. Furthermore, Ca^{2+} recirculation fraction was markedly reduced, indicating an increased NCX vs. SERCA function. In agreement with these observations, direct measurements of SERCA activity performed with a spectroscopic method showed a reduction of the maximum velocity of SR Ca^{2+} uptake (Rice et al, 2010), paralleled by a reduced levels of SERCA protein expression and a reduction of SERCA/ PLB ratio.

A common feature observed in both E163R and R92Q was a pro-arrhythmogenic phenotype. Compared to WT both groups showed spontaneous activity during pauses, in the form of either irregular premature contractions or run of regular spontaneous beating. Additionally, in both mutants we observed after-contractions and premature beats not only during stimulation pauses but even during the regular stimulation. In the R92Q group was observed an increase in the occurrence of spontaneous beats with an increment of pause duration, but this behavior was not observed in the in E163R group where the occurrence did not depend on pause duration. In a previous study on mouse models has shown that Δ160E and R92Q, which both exhibit clinically severe phenotypes in patients, lead to alteration in heart rate (RT) regulation, with no alterations in β- adrenergic receptor density. ECG signals, recorded using a telemetry receiver showed an increased occurrence of aftercontractions after isoproterenol injection and higher HR in R92Q mice (Jimenez J et al, 2010). Spontaneous aftercontractions and beats observed in E163R and R92Q muticellular preparations were paralled by spontaneous Ca^{2+} fluxes in sigle cardiomyocytes. In basal condition, the occurrence of spontaneous Ca^{2+} waves was higher in both E163R and R92Q cardiomyocytes compared to WT, though E163R cardiomyocytes exhibited a much higher occurrence (approximately double) compared to R92Q. Under β-adrenergic stimulation, both E163R and R92Q showed a comparable higher occurrence of spontaneous events compared to WT, unvailing that the effect of Iso was more pronouced in R92Q.

However, the occurrence of spontaneous Ca transient (CaT) was significantly higher in both E163R and in R92Q when compared to WT and significantly augmented under administration of Iso. Of note, while the occurrence of Ca^{2+}waves was higher in E163R compared to R92Q, the occurrence of

spontaneous CaT was similar in the two mutants. This result could indicate that the likelihood of Ca^{2+} waves to propagate and generate a global CaT is lower in E163R than in R92Q. We can hypothesize that the presence of sarcolemmal remodeling (including increased NCX function) in R92Q, but not in E163R, could promote generation of delayed after depolarization and premature action potential, inducing a global Ca^{2+} release.

We tested the potential reversal of these alterations in contractile function and Ca^{2+}_i handling observed in intact trabeculae and single cardiomyocytes of the selective inhibition of late Na^+ current (I_{NaL}), Ranolazine. Ranolazine 10 μM applied on top of isoproterenol (Iso) significantly reduced the occurrence of aftercontractions and premature beats below basal levels in both E163R and R92Q trabeculae. The application of Ranolazine reversed to basal levels in both R92Q and E163R the enhancement of spontaneous Ca^{2+} waves induced by Iso, with a quantitatively larger effect in R92Q (-54%), milder effect in E163R (-17%). Furthermore, Ranolazine reversed almost completely the higher occurrence of spontaneous CaT under Iso administration in both mutants, exerting negligible effect on WT.

To better understand the mechanism underling these pro arrhythmogenic spontaneous events we employed Ca^{2+} recirculation fraction (RF) and mechanical restitution protocols to investigate NCX and RyR2 function, respectively. As mentioned above, RF was similar in WT and E163R trabeculae but markedly reduced in R92Q indicating an increased role of NCX versus SERCA for cytosolc Ca^{2+} removal in R92Q. Under Iso, RF increases in all groups. Administration of Ran completely reversed the RF enhancement to baseline values in R92Q and partially in E163R but not in WT. The more pronounced effect of Ran on R92Q group is likely related to an increase role of NCX in this mouse line compared to E163R. In fact, Ran by reducing intracellular [Na^+] and [Ca^{2+}] indirectly promote forward NCX function (Coppini et al, 2013). While at baseline mechanical restitution was faster in both mutants, including R92Q where it has been shown a reduced SERCA activity, acceleration of mechanical restitution induced by Iso was fully reversed in both mutants upon addition of Ran while this effect was negligible in WT. This would indicate that shorter RyR2 refractoriness which could contribute to generate spontaneous Ca^{2+} waves and CaT, may be a mechanism underlying spontaneous activity in both R92Q and E163R. The beneficial effect of Ran on mechanical restitution may support an additional effect of Ran on RyR2 function other than its notorious effects as I_{NaL} blocker, which have been previously described (Parikh et al, 2012). Finally, preliminary current clamp measurements on R92Q cardiomyocytes revealed a prolongation of action potential duration (APD) compared to WT. This was paralleled, for istance, by a significant reduction of mRNA expression of primary and secondary subunits of potassium current (I_{to}). Specifically, Kv4.3 and KChip2 mRNA gene expression relative to GAPDH were 0.70± 0.08 and 0.49± 0.06 respectively, versus 1.01± 0.07 and 1.14± 0.02 in WT. Reduction of repolarizing outward currents could account for the prolongation of the APD. An increase in depolarizing inward currents could also contribute to prolong APD and it is still under investigation. Of note, preliminary assessment in E163R did not reveal any of the sarcolemmal alterations observed in R92Q. These observations together would suggest that as in human HCM, the beneficial effects of ranolazine on R92Q cells and trabeculae are likely mediated by the consequences of late Na^+ current inhibition, i.e. reduction of intracellular Na^+, enhancement of NCX forward function and reduction of Ca^{2+} overload. In E163R cardiac tissue, myocardial arrhythmogeneicity is not accompanied by remodeling of ion currents or changes of SERCA/NCX function, and thus appear to be a direct consequence of increased myofilaments Ca^{2+} sensitivity and changes of RyR2 function.

6. Conclusions

In this thesis, we investigated myofilament response to Ca^{2+} and crossbridge cycling kinetics in heterozygous transgenic mice carrying E163R cTnT mutation. We also characterize the E-C coupling and pro-arrhythmogenic changes occurring in E163R myocardium, clarifying how they concur with primary effects of the mutation to determine the contractile performance of intact E163R myocardium. We compare these Ca^{2+} handling abnormalities to those identified in widely described cTnT mouse model carrying R92Q mutation, and finally we tested the effects of specific pharmacological interventions, which may be effective to acutely reverse some of the E-C coupling and mechanical alterations observed.

Dr. Jil Tardiff and collaborators have validated transgenic mouse lines carrying different cTnT mutations (Δ160E, R92Q, R92L, R92W) which well reproduce human disease, representing an ideal model to better understand myocardial abnormalities related with thin-filament HCM and to screen the effects of novel compounds such as ranolazine. The relative rarity of thin filament mutations combined with the lower tendency to develop obstruction in thin-filament patients reduces the possibility to directly investigate on human myocardium harvested from patients underwent myectomy.

Many studies on R92Q mouse model have previously characterized the abnormalities that are present both at cardiomyocytes and whole heart level in these models (Tardiff et al, 1999, Chandra et al 2001, Chandra et al 2005, Rice R et al 2009). However, in our work we tried to elucidate the relative contribution of primary mutation-driven sarcomeric dysfunction and secondary remodeling-induced cellular abnormalities to the abnormal contraction seen in mutant mice.

We observed that primary myofilament changes in R92Q are associated with a large spectrum of EC-coupling and sarcolemmal alterations, which appear to be the major contributor to the observed mechanical dysfunction and arrhythmogeneicity in this mouse line, resembling advanced human disease. In E163R instead, in the absence of major EC-coupling changes, the impairment of myofilament function appear to be the leading element determining mechanical abnormalities. The increased arrhythmogeneicity in E163R myocardium may be thus a direct consequence of the increased myofilaments Ca^{2+} sensitivity.

Although some phenotypic similarities exist between E163R and R92Q, including diastolic dysfunction, a lack of overt cardiac hypertrophy, increased Ca^{2+} sensitivity and cardiomyocyte disarray, the mutations cause disease via distinct molecular mechanisms. In fact, the two mutations are localized at opposite ends of the TNT1 tail domain, and are supposed to cause different effect on TNT1flexibility (P Manning et al, 2012).

Finally, detecting the molecular and cellular abnormalities driving the HCM-related phenotype, we could help identifying specific therapeutic options. This could be a future perspective, to confirm whereas ranolazine could be able to prevent or delay phenotype development in transgenic mice.

REFERENCES

Adabag AS, Maron BJ, Appelbaum E, Harrigan CJ, Buros JL, Gibson CM, Lesser JR, Hanna CA, Udelson JE, Manning WJ, Maron MS (2008) Occurrence and frequency of arrhythmias in hypertrophic cardiomyopathy in relation to delayed enhancement on cardiovascular magnetic resonance. Journal of the American College of Cardiology 51: 1369-1374

Alcalai R, Seidman JG, Seidman CE (2008) Genetic basis of hypertrophic cardiomyopathy: from bench to the clinics. Journal of cardiovascular electrophysiology 19: 104-110

Ashrafian H, Redwood C, Blair E, Watkins H (2003) Hypertrophic cardiomyopathy:a paradigm for myocardial energy depletion. Trends in genetics : TIG 19: 263-268

Banijamali HS, Gao WD, MacIntosh BR, ter Keurs HE (1991) Force-interval relations of twitches and cold contractures in rat cardiac trabeculae. Effect of ryanodine. Circulation research 69: 937-948

Barsotti RJ, Ferenczi MA (1988) Kinetics of ATP hydrolysis and tension production in skinned cardiac muscle of the guinea pig. The Journal of biological chemistry 263: 16750-16756

Bassani, R. A., Ferraz, S. A., Bassani J.W.M. 2001. Estimation of Ca^{2+} recirculating fraction in rat ventricle: Influence of the methodological approach. Brazilian Journal of Biomedical Enginnering. 17,2: 63-67.

Basso C, Thiene G, Corrado D, Buja G, Melacini P, Nava A (2000) Hypertrophic cardiomyopathy and sudden death in the young: pathologic evidence of myocardial ischemia. Human pathology 31: 988-998

Baudenbacher F, Schober T, Pinto JR, Sidorov VY, Hilliard F, Solaro RJ, Potter JD, Knollmann BC (2008) Myofilament Ca2+ sensitization causes susceptibility to cardiac arrhythmia in mice. The Journal of clinical investigation 118: 3893-3903

Baudino TA, Carver W, Giles W, Borg TK (2006) Cardiac fibroblasts: friend or foe? American journal of physiology Heart and circulatory physiology 291: H1015-1026

Belus A, Piroddi N, Scellini B, Tesi C, D'Amati G, Girolami F, Yacoub M, Cecchi F, Olivotto I, Poggesi C (2008) The familial hypertrophic cardiomyopathy-associated myosin mutation R403Q accelerates tension generation and relaxation of human cardiac myofibrils. The Journal of physiology 586: 3639-3644

Bers DM (2002) Cardiac excitation–contraction coupling. Review Article. Macmillan Magazines Ltd.

Bers DM, Eisner DA, Valdivia HH (2003) Sarcoplasmic reticulum Ca2+ and heart failure: roles of diastolic leak and Ca2+ transport. Circulation research 93: 487-490

Bottinelli R, Canepari M, Reggiani C, Stienen GJ (1994) Myofibrillar ATPase activity during isometric contraction and isomyosin composition in rat single skinned muscle fibres. The Journal of physiology 481 (Pt 3): 663-675

Brenner B (1988) Effect of Ca2+ on cross-bridge turnover kinetics in skinned single rabbit psoas fibers: implications for regulation of muscle contraction. Proceedings of the National Academy of Sciences of the United States of America 85: 3265-3269

Camici PG, Crea F (2007) Coronary microvascular dysfunction. The New England journal of medicine 356: 830-840

Chandra M, Rundell VL, Tardiff JC, Leinwand LA, De Tombe PP, Solaro RJ (2001) Ca(2+) activation of myofilaments from transgenic mouse hearts expressing R92Q mutant cardiac troponin T. American journal of physiology Heart and circulatory physiology 280: H705-713

Chandra M, Tschirgi ML, Tardiff JC (2005) Increase in tension-dependent ATP consumption induced by cardiac troponin T mutation. American journal of physiology Heart and circulatory physiology 289: H2112-2119

Cooke R (1995) The actomyosin engine. FASEB journal : official publication of the Federation of American Societies for Experimental Biology 9: 636-642

Coppini R, Ferrantini C, Yao L, Fan P, Del Lungo M, Stillitano F, Sartiani L, Tosi B, Suffredini S, Tesi C, Yacoub M, Olivotto I, Belardinelli L, Poggesi C, Cerbai E, Mugelli A (2013) Late sodium current inhibition reverses electromechanical dysfunction in human hypertrophic cardiomyopathy. Circulation 127: 575-584

Crilley JG, Boehm EA, Blair E, Rajagopalan B, Blamire AM, Styles P, McKenna WJ, Ostman-Smith I, Clarke K, Watkins H (2003) Hypertrophic cardiomyopathy due to sarcomeric gene mutations is characterized by impaired energy metabolism irrespective of the degree of hypertrophy. Journal of the American College of Cardiology 41: 1776-1782

Cuda G, Fananapazir L, Zhu WS, Sellers JR, Epstein ND (1993) Skeletal muscle expression and abnormal function of beta-myosin in hypertrophic cardiomyopathy. The Journal of clinical investigation 91: 2861-2865

de Tombe PP, Stienen GJ (1995) Protein kinase A does not alter economy of force maintenance in skinned rat cardiac trabeculae. Circulation research 76: 734-741

de Tombe PP, ter Keurs HE (1990) Force and velocity of sarcomere shortening in trabeculae from rat heart. Effects of temperature. Circulation research 66: 1239-1254

DeAnda A, Jr., Komeda M, Moon MR, Green GR, Bolger AF, Nikolic SD, Daughters GT, 2nd, Miller DC (1998) Estimation of regional left ventricular wall stresses in intact canine hearts. The American journal of physiology 275: H1879-1885

Doolan A, Tebo M, Ingles J, Nguyen L, Tsoutsman T, Lam L, Chiu C, Chung J, Weintraub RG, Semsarian C (2005) Cardiac troponin I mutations in Australian families with hypertrophic cardiomyopathy: clinical, genetic and functional consequences. Journal of molecular and cellular cardiology 38: 387-393

Egorova MV, Afanas'ev SA, Popov SV (2005) A simple method for isolation of cardiomyocytes from adult rat heart. Bulletin of experimental biology and medicine 140: 370-373

Ertz-Berger BR, He H, Dowell C, Factor SM, Haim TE, Nunez S, Schwartz SD, Ingwall JS, Tardiff JC (2005) Changes in the chemical and dynamic properties of cardiac troponin T cause discrete cardiomyopathies in transgenic mice. Proceedings of the National Academy of Sciences of the United States of America 102: 18219-18224

Ferrantini C, Belus A, Piroddi N, Scellini B, Tesi C, Poggesi C (2009) Mechanical and energetic consequences of HCM-causing mutations. Journal of cardiovascular translational research 2: 441-451

Ford LE, Huxley AF, Simmons RM (1977) Tension responses to sudden length change in stimulated frog muscle fibres near slack length. The Journal of physiology 269: 441-515

Frey N, Brixius K, Schwinger RH, Benis T, Karpowski A, Lorenzen HP, Luedde M, Katus HA, Franz WM (2006) Alterations of tension-dependent ATP utilization in a transgenic rat model of hypertrophic cardiomyopathy. The Journal of biological chemistry 281: 29575-29582

Frey N, Franz WM, Gloeckner K, Degenhardt M, Muller M, Muller O, Merz H, Katus HA (2000) Transgenic rat hearts expressing a human cardiac troponin T deletion reveal diastolic dysfunction and ventricular arrhythmias. Cardiovascular research 47: 254-264

Fujita H, Sugiura S, Momomura S, Omata M, Sugi H, Sutoh K (1997) Characterization of mutant myosins of Dictyostelium discoideum equivalent to human familial hypertrophic cardiomyopathy mutants. Molecular force level of mutant myosins may have a prognostic implication. The Journal of clinical investigation 99: 1010-1015

Gagne SM, Tsuda S, Li MX, Smillie LB, Sykes BD (1995) Structures of the troponin C regulatory domains in the apo and calcium-saturated states. Nature structural biology 2: 784-789

Geisterfer-Lowrance AA, Kass S, Tanigawa G, Vosberg HP, McKenna W, Seidman CE, Seidman JG (1990) A molecular basis for familial hypertrophic cardiomyopathy: a beta cardiac myosin heavy chain gene missense mutation. Cell 62: 999-1006

Gersh BJ, Maron BJ, Bonow RO, Dearani JA, Fifer MA, Link MS, Naidu SS, Nishimura RA, Ommen SR, Rakowski H, Seidman CE, Towbin JA, Udelson JE, Yancy CW, American College of Cardiology Foundation/American Heart Association Task Force on Practice G, American Association for Thoracic S, American Society of E, American Society of Nuclear C, Heart Failure Society of A, Heart Rhythm S, Society for Cardiovascular A, Interventions, Society of Thoracic S (2011) 2011 ACCF/AHA guideline for the diagnosis and treatment of hypertrophic cardiomyopathy: a report of the American College of Cardiology Foundation/American Heart Association Task Force on Practice Guidelines. Circulation 124: e783-831

Glyn H, Sleep J (1985) Dependence of adenosine triphosphatase activity of rabbit psoas muscle fibres and myofibrils on substrate concentration. The Journal of physiology 365: 259-276

Goldman Y.E & Simmons R.M. (1984) Control of sarcomere length in skinned muscle fibres of rana temporaria during mechanical transients. J. Physiol. 350, pp. 497-518

Gomes AV, Venkatraman G, Davis JP, Tikunova SB, Engel P, Solaro RJ, Potter JD (2004) Cardiac troponin T isoforms affect the Ca(2+) sensitivity of force development in the presence of slow skeletal troponin I: insights into the role of troponin T isoforms in the fetal heart. The Journal of biological chemistry 279: 49579-49587

Gordon AM, Homsher E, Regnier M (2000) Regulation of contraction in striated muscle. Physiological reviews 80: 853-924

Gregorio CC, Antin PB (2000) To the heart of myofibril assembly. Trends in cell biology 10: 355-362

Guinto PJ, Haim TE, Dowell-Martino CC, Sibinga N, Tardiff JC (2009) Temporal and mutation-specific alterations in Ca2+ homeostasis differentially determine the progression of cTnT-related cardiomyopathies in murine models. American journal of physiology Heart and circulatory physiology 297: H614-626

Haim TE, Dowell C, Diamanti T, Scheuer J, Tardiff JC (2007) Independent FHC-related cardiac troponin T mutations exhibit specific alterations in myocellular contractility and calcium kinetics. Journal of molecular and cellular cardiology 42: 1098-1110

Hanley PJ, Young AA, LeGrice IJ, Edgar SG, Loiselle DS (1999) 3-Dimensional configuration of perimysial collagen fibres in rat cardiac muscle at resting and extended sarcomere lengths. The Journal of physiology 517 (Pt 3): 831-837

Harada K, Potter JD (2004) Familial hypertrophic cardiomyopathy mutations from different functional regions of troponin T result in different effects on the pH and Ca2+ sensitivity of cardiac muscle contraction. The Journal of biological chemistry 279: 14488-14495

Harada K, Takahashi-Yanaga F, Minakami R, Morimoto S, Ohtsuki I (2000) Functional consequences of the deletion mutation deltaGlu160 in human cardiac troponin T. Journal of biochemistry 127: 263-268

Harris S, Foord SM (2000) Transgenic gene knock-outs: functional genomics and therapeutic target selection. Pharmacogenomics 1: 433-443

Hasenfuss G, Schillinger W, Lehnart SE, Preuss M, Pieske B, Maier LS, Prestle J, Minami K, Just H (1999) Relationship between Na+-Ca2+-exchanger protein levels and diastolic function of failing human myocardium. Circulation 99: 641-648

He H, Javadpour MM, Latif F, Tardiff JC, Ingwall JS (2007) R-92L and R-92W mutations in cardiac troponin T lead to distinct energetic phenotypes in intact mouse hearts. Biophysical journal 93: 1834-1844

Hernandez OM, Housmans PR, Potter JD (2001) Invited Review: pathophysiology of cardiac muscle contraction and relaxation as a result of alterations in thin filament regulation. Journal of applied physiology 90: 1125-1136

Ho CY, Sweitzer NK, McDonough B, Maron BJ, Casey SA, Seidman JG, Seidman CE, Solomon SD (2002) Assessment of diastolic function with Doppler tissue imaging to predict genotype in preclinical hypertrophic cardiomyopathy. Circulation 105: 2992-2997

Ho CY, Sweitzer NK, McDonough B, Maron BJ, Casey SA, Seidman JG, Seidman CE, Solomon SD (2002) Assessment of diastolic function with Doppler tissue imaging to predict genotype in preclinical hypertrophic cardiomyopathy. Circulation 105: 2992-2997

Holmes KC, Popp D, Gebhard W, Kabsch W (1990) Atomic model of the actin filament. Nature 347: 44-49

Homsher E, Lee DM, Morris C, Pavlov D, Tobacman LS (2000) Regulation of force and unloaded sliding speed in single thin filaments: effects of regulatory proteins and calcium. The Journal of physiology 524 Pt 1: 233-243

Huke S, Knollmann BC (2010) Increased myofilament Ca2+-sensitivity and arrhythmia susceptibility. Journal of molecular and cellular cardiology 48: 824-833

Huxley AF (1957) Muscle structure and theories of contraction. Progress in biophysics and biophysical chemistry 7: 255-318

Huxley HE (1969) The mechanism of muscular contraction. Science 164: 1356-1365

Iribe G, Kohl P, Noble D (2006) Modulatory effect of calmodulin-dependent kinase II (CaMKII) on sarcoplasmic reticulum Ca2+ handling and interval-force relations: a modelling study. Philosophical transactions Series A, Mathematical, physical, and engineering sciences 364: 1107-1133

Javadpour MM, Tardiff JC, Pinz I, Ingwall JS (2003) Decreased energetics in murine hearts bearing the R92Q mutation in cardiac troponin T. The Journal of clinical investigation 112: 768-775

Jimenez J, Tardiff JC (2011) Abnormal heart rate regulation in murine hearts with familial hypertrophic cardiomyopathy-related cardiac troponin T mutations. American journal of physiology Heart and circulatory physiology 300: H627-635

Jin JP, Chong SM (2010) Localization of the two tropomyosin-binding sites of troponin T. Archives of biochemistry and biophysics 500: 144-150

Jung WI, Sieverding L, Breuer J, Hoess T, Widmaier S, Schmidt O, Bunse M, van Erckelens F, Apitz J, Lutz O, Dietze GJ (1998) 31P NMR spectroscopy detects metabolic abnormalities in asymptomatic patients with hypertrophic cardiomyopathy. Circulation 97: 2536-2542

Karibe A, Tobacman LS, Strand J, Butters C, Back N, Bachinski LL, Arai AE, Ortiz A, Roberts R, Homsher E, Fananapazir L (2001) Hypertrophic cardiomyopathy caused by a novel alpha-tropomyosin mutation (V95A) is associated with mild cardiac phenotype, abnormal calcium binding to troponin, abnormal myosin cycling, and poor prognosis. Circulation 103: 65-71

Kentish JC, Stienen GJ (1994) Differential effects of length on maximum force production and myofibrillar ATPase activity in rat skinned cardiac muscle. The Journal of physiology 475: 175-184

Knollmann BC, Kirchhof P, Sirenko SG, Degen H, Greene AE, Schober T, Mackow JC, Fabritz L, Potter JD, Morad M (2003) Familial hypertrophic cardiomyopathy-linked mutant troponin T causes stress-induced ventricular tachycardia and Ca2+-dependent action potential remodeling. Circulation research 92: 428-436

Knollmann BC, Potter JD (2001) Altered regulation of cardiac muscle contraction by troponin T mutations that cause familial hypertrophic cardiomyopathy. Trends in cardiovascular medicine 11: 206-212

Knollmann BC, Roden DM (2008) A genetic framework for improving arrhythmia therapy. Nature 451: 929-936

Kobayashi T, Solaro RJ (2005) Calcium, thin filaments, and the integrative biology of cardiac contractility. Annual review of physiology 67: 39-67

Kobayashi T, Solaro RJ (2006) Increased Ca2+ affinity of cardiac thin filaments reconstituted with cardiomyopathy-related mutant cardiac troponin I. The Journal of biological chemistry 281: 13471-13477

Koga Y, Toshima H, Kimura A, Harada H, Koyanagi T, Nishi H, Nakata M, Imaizumi T (1996) Clinical manifestations of hypertrophic cardiomyopathy with mutations in the cardiac beta-myosin heavy chain gene or cardiac troponin T gene. Journal of cardiac failure 2: S97-103

Kokado H, Shimizu M, Yoshio H, Ino H, Okeie K, Emoto Y, Matsuyama T, Yamaguchi M, Yasuda T, Fujino N, Ito H, Mabuchi H (2000) Clinical features of hypertrophic cardiomyopathy caused by a Lys183 deletion mutation in the cardiac troponin I gene. Circulation 102: 663-669

Kreutziger KL, Piroddi N, McMichael JT, Tesi C, Poggesi C, Regnier M (2011) Calcium binding kinetics of troponin C strongly modulate cooperative activation and tension kinetics in cardiac muscle. Journal of molecular and cellular cardiology 50: 165-174

Labeit S, Barlow DP, Gautel M, Gibson T, Holt J, Hsieh CL, Francke U, Leonard K, Wardale J, Whiting A, et al. (1990) A regular pattern of two types of 100-residue motif in the sequence of titin. Nature 345: 273-276

Lankford EB, Epstein ND, Fananapazir L, Sweeney HL (1995) Abnormal contractile properties of muscle fibers expressing beta-myosin heavy chain gene mutations in patients with hypertrophic cardiomyopathy. The Journal of clinical investigation 95: 1409-1414

Lehman W, Craig R, Vibert P (1994) Ca(2+)-induced tropomyosin movement in Limulus thin filaments revealed by three-dimensional reconstruction. Nature 368: 65-67

Lehman W, Hatch V, Korman V, Rosol M, Thomas L, Maytum R, Geeves MA, Van Eyk JE, Tobacman LS, Craig R (2000) Tropomyosin and actin isoforms modulate the localization of tropomyosin strands on actin filaments. Journal of molecular biology 302: 593-606

Lehman W, Vibert P, Craig R (1997) Visualization of caldesmon on smooth muscle thin filaments. Journal of molecular biology 274: 310-317

Lehman W, Vibert P, Uman P, Craig R (1995) Steric-blocking by tropomyosin visualized in relaxed vertebrate muscle thin filaments. Journal of molecular biology 251: 191-196

Lehrer SS, Geeves MA (1998) The muscle thin filament as a classical cooperative/allosteric regulatory system. Journal of molecular biology 277: 1081-1089

LeWinter MM, Granzier H (2010) Cardiac titin: a multifunctional giant. Circulation 121: 2137-2145

LeWinter MM, Wu Y, Labeit S, Granzier H (2007) Cardiac titin: structure, functions and role in disease. Clinica chimica acta; international journal of clinical chemistry 375: 1-9

Lin D, Bobkova A, Homsher E, Tobacman LS (1996) Altered cardiac troponin T in vitro function in the presence of a mutation implicated in familial hypertrophic cardiomyopathy. The Journal of clinical investigation 97: 2842-2848

Linke WA, Bartoo ML, Pollack GH (1993) Spontaneous sarcomeric oscillations at intermediate activation levels in single isolated cardiac myofibrils. Circulation research 73: 724-734

Luedde M, Flogel U, Knorr M, Grundt C, Hippe HJ, Brors B, Frank D, Haselmann U, Antony C, Voelkers M, Schrader J, Most P, Lemmer B, Katus HA, Frey N (2009) Decreased contractility due to energy deprivation in a transgenic rat model of hypertrophic cardiomyopathy. Journal of molecular medicine 87: 411-422

Lyon AR, MacLeod KT, Zhang Y, Garcia E, Kanda GK, Lab MJ, Korchev YE, Harding SE, Gorelik J (2009) Loss of T-tubules and other changes to surface topography in ventricular myocytes from failing human and rat heart. Proceedings of the National Academy of Sciences of the United States of America 106: 6854-6859

Manning EP, Guinto PJ, Tardiff JC (2012) Correlation of molecular and functional effects of mutations in cardiac troponin T linked to familial hypertrophic cardiomyopathy: an integrative in silico/in vitro approach. The Journal of biological chemistry 287: 14515-14523

Marian AJ (2000) Pathogenesis of diverse clinical and pathological phenotypes in hypertrophic cardiomyopathy. Lancet 355: 58-60

Marian AJ (2008) Genetic determinants of cardiac hypertrophy. Current opinion in cardiology 23: 199-205

Marian AJ, Roberts R (2001) The molecular genetic basis for hypertrophic cardiomyopathy. Journal of molecular and cellular cardiology 33: 655-670

Maron BJ (2000) Ventricular arrhythmias, sudden death, and prevention in patients with hypertrophic cardiomyopathy. Current cardiology reports 2: 522-528

Maron BJ (2002) Hypertrophic cardiomyopathy: a systematic review. JAMA : the journal of the American Medical Association 287: 1308-1320

Maron BJ (2003) Contemporary considerations for risk stratification, sudden death and prevention in hypertrophic cardiomyopathy. Heart 89: 977-978

Maron BJ, Spirito P, Shen WK, Haas TS, Formisano F, Link MS, Epstein AE, Almquist AK, Daubert JP, Lawrenz T, Boriani G, Estes NA, 3rd, Favale S, Piccininno M, Winters SL, Santini M, Betocchi S, Arribas F, Sherrid MV, Buja G, Semsarian C, Bruzzi P (2007) Implantable cardioverter-defibrillators and prevention of sudden cardiac death in hypertrophic cardiomyopathy. JAMA : the journal of the American Medical Association 298: 405-412

Maron MS, Maron BJ, Harrigan C, Buros J, Gibson CM, Olivotto I, Biller L, Lesser JR, Udelson JE, Manning WJ, Appelbaum E (2009) Hypertrophic cardiomyopathy phenotype revisited after 50 years with cardiovascular magnetic resonance. Journal of the American College of Cardiology 54: 220-228

Marston SB (2011) How do mutations in contractile proteins cause the primary familial cardiomyopathies? Journal of cardiovascular translational research 4: 245-255

Maytum R, Lehrer SS, Geeves MA (1999) Cooperativity and switching within the three-state model of muscle regulation. Biochemistry 38: 1102-1110

McKillop DF, Geeves MA (1993) Regulation of the interaction between actin and myosin subfragment 1: evidence for three states of the thin filament. Biophysical journal 65: 693-701

McLeod CJ, Ackerman MJ, Nishimura RA, Tajik AJ, Gersh BJ, Ommen SR (2009) Outcome of patients with hypertrophic cardiomyopathy and a normal electrocardiogram. Journal of the American College of Cardiology 54: 229-233

McTaggart DR (2004) Diltiazem reverses tissue Doppler velocity abnormalities in pre-clinical hypertrophic cardiomyopathy. Heart, lung & circulation 13: 39-40

Miller T, Szczesna D, Housmans PR, Zhao J, de Freitas F, Gomes AV, Culbreath L, McCue J, Wang Y, Xu Y, Kerrick WG, Potter JD (2001) Abnormal contractile function in transgenic mice expressing a familial hypertrophic cardiomyopathy-linked troponin T (I79N) mutation. The Journal of biological chemistry 276: 3743-3755

Monasky MM, Varian KD, Davis JP, Janssen PM (2008) Dissociation of force decline from calcium decline by preload in isolated rabbit myocardium. Pflugers Archiv : European journal of physiology 456: 267-276

Montgomery DE, Tardiff JC, Chandra M (2001) Cardiac troponin T mutations: correlation between the type of mutation and the nature of myofilament dysfunction in transgenic mice. The Journal of physiology 536: 583-592

Moolman JC, Corfield VA, Posen B, Ngumbela K, Seidman C, Brink PA, Watkins H (1997) Sudden death due to troponin T mutations. Journal of the American College of Cardiology 29: 549-555

Moolman-Smook J, Flashman E, de Lange W, Li Z, Corfield V, Redwood C, Watkins H (2002) Identification of novel interactions between domains of Myosin binding protein-C that are modulated by hypertrophic cardiomyopathy missense mutations. Circulation research 91: 704-711

Moolman-Smook JC, De Lange WJ, Bruwer EC, Brink PA, Corfield VA (1999) The origins of hypertrophic cardiomyopathy-causing mutations in two South African subpopulations: a unique profile of both independent and founder events. American journal of human genetics 65: 1308-1320

Moore RK, Grinspan LT, Jimenez J, Guinto PJ, Ertz-Berger B, Tardiff JC (2013) HCM-linked 160E cardiac troponin T mutation causes unique progressive structural and molecular ventricular remodeling in transgenic mice. Journal of molecular and cellular cardiology 58: 188-198

Morimoto S, Yanaga F, Minakami R, Ohtsuki I (1998) Ca2+-sensitizing effects of the mutations at Ile-79 and Arg-92 of troponin T in hypertrophic cardiomyopathy. The American journal of physiology 275: C200-207

Nagueh SF, McFalls J, Meyer D, Hill R, Zoghbi WA, Tam JW, Quinones MA, Roberts R, Marian AJ (2003) Tissue Doppler imaging predicts the development of hypertrophic cardiomyopathy in subjects with subclinical disease. Circulation 108: 395-398

Niimura H, Bachinski LL, Sangwatanaroj S, Watkins H, Chudley AE, McKenna W, Kristinsson A, Roberts R, Sole M, Maron BJ, Seidman JG, Seidman CE (1998) Mutations in the gene for cardiac myosin-binding protein C and late-onset familial hypertrophic cardiomyopathy. The New England journal of medicine 338: 1248-1257

Nistri S, Olivotto I, Betocchi S, Losi MA, Valsecchi G, Pinamonti B, Conte MR, Casazza F, Galderisi M, Maron BJ, Cecchi F (2006) Prognostic significance of left atrial size in patients with hypertrophic cardiomyopathy (from the Italian Registry for Hypertrophic Cardiomyopathy). The American journal of cardiology 98: 960-965

Oakley CE, Hambly BD, Curmi PM, Brown LJ (2004) Myosin binding protein C: structural abnormalities in familial hypertrophic cardiomyopathy. Cell research 14: 95-110

Obayashi M, Xiao B, Stuyvers BD, Davidoff AW, Mei J, Chen SR, ter Keurs HE (2006) Spontaneous diastolic contractions and phosphorylation of the cardiac ryanodine receptor at serine-2808 in congestive heart failure in rat. Cardiovascular research 69: 140-151

Ohtsuki I (1979) Molecular arrangement of troponin-T in the thin filament. Journal of biochemistry 86: 491-497

Olivotto I, Cecchi F (2003) The epidemiologic evolution and present perception of hypertrophic cardiomyopathy. Italian heart journal : official journal of the Italian Federation of Cardiology 4: 596-601

Olivotto I, Cecchi F, Gistri R, Lorenzoni R, Chiriatti G, Girolami F, Torricelli F, Camici PG (2006) Relevance of coronary microvascular flow impairment to long-term remodeling and systolic dysfunction in hypertrophic cardiomyopathy. Journal of the American College of Cardiology 47: 1043-1048

Olivotto I, Cecchi F, Poggesi C, Yacoub MH (2012) Patterns of disease progression in hypertrophic cardiomyopathy: an individualized approach to clinical staging. Circulation Heart failure 5: 535-546

Olivotto I, Girolami F, Ackerman MJ, Nistri S, Bos JM, Zachara E, Ommen SR, Theis JL, Vaubel RA, Re F, Armentano C, Poggesi C, Torricelli F, Cecchi F (2008) Myofilament protein gene mutation screening and outcome of patients with hypertrophic cardiomyopathy. Mayo Clinic proceedings 83: 630-638

Olivotto I, Girolami F, Sciagra R, Ackerman MJ, Sotgia B, Bos JM, Nistri S, Sgalambro A, Grifoni C, Torricelli F, Camici PG, Cecchi F (2011) Microvascular function is selectively impaired in patients with hypertrophic cardiomyopathy and sarcomere myofilament gene mutations. Journal of the American College of Cardiology 58: 839-848

Ommen SR, Shah PM, Tajik AJ (2008) Left ventricular outflow tract obstruction in hypertrophic cardiomyopathy: past, present and future. Heart 94: 1276-1281

Orchard CH, Pasek M, Brette F (2009) The role of mammalian cardiac t-tubules in excitation-contraction coupling: experimental and computational approaches. Experimental physiology 94: 509-519

Ostman-Smith I, Wettrell G, Riesenfeld T (1999) A cohort study of childhood hypertrophic cardiomyopathy: improved survival following high-dose beta-adrenoceptor antagonist treatment. Journal of the American College of Cardiology 34: 1813-1822

Palm T, Graboski S, Hitchcock-DeGregori SE, Greenfield NJ (2001) Disease-causing mutations in cardiac troponin T: identification of a critical tropomyosin-binding region. Biophysical journal 81: 2827-2837

Pappas CT, Bliss KT, Zieseniss A, Gregorio CC (2011) The Nebulin family: an actin support group. Trends in cell biology 21: 29-37

Parikh A, Mantravadi R, Kozhevnikov D, Roche MA, Ye Y, Owen LJ, Puglisi JL, Abramson JJ, Salama G (2012) Ranolazine stabilizes cardiac ryanodine receptors: a novel mechanism for the suppression of early afterdepolarization and torsades de pointes in long QT type 2. Heart rhythm : the official journal of the Heart Rhythm Society 9: 953-960

Pasek M, Brette F, Nelson A, Pearce C, Qaiser A, Christe G, Orchard CH (2008) Quantification of t-tubule area and protein distribution in rat cardiac ventricular myocytes. Progress in biophysics and molecular biology 96: 244-257

Pasquale F, Syrris P, Kaski JP, Mogensen J, McKenna WJ, Elliott P (2012) Long-term outcomes in hypertrophic cardiomyopathy caused by mutations in the cardiac troponin T gene. Circulation Cardiovascular genetics 5: 10-17

Piroddi N, Belus A, Eiras S, Tesi C, van der Velden J, Poggesi C, Stienen GJ (2006) No direct effect of creatine phosphate on the cross-bridge cycle in cardiac myofibrils. Pflugers Archiv : European journal of physiology 452: 3-6

Piroddi N, Belus A, Scellini B, Tesi C, Giunti G, Cerbai E, Mugelli A, Poggesi C (2007) Tension generation and relaxation in single myofibrils from human atrial and ventricular myocardium. Pflugers Archiv : European journal of physiology 454: 63-73

Poggesi C, Tesi C, Stehle R (2005) Sarcomeric determinants of striated muscle relaxation kinetics. Pflugers Archiv : European journal of physiology 449: 505-517

Potma EJ, Stienen GJ, Barends JP, Elzinga G (1994) Myofibrillar ATPase activity and mechanical performance of skinned fibres from rabbit psoas muscle. The Journal of physiology 474: 303-317

Potter JD, Gergely J (1975) The regulatory system of the actin-myosin interaction. Recent advances in studies on cardiac structure and metabolism 5: 235-244

Redwood C, Lohmann K, Bing W, Esposito GM, Elliott K, Abdulrazzak H, Knott A, Purcell I, Marston S, Watkins H (2000) Investigation of a truncated cardiac troponin T that causes familial hypertrophic cardiomyopathy: Ca(2+) regulatory properties of reconstituted thin filaments depend on the ratio of mutant to wild-type protein. Circulation research 86: 1146-1152

Reiser PJ, Kline WO (1998) Electrophoretic separation and quantitation of cardiac myosin heavy chain isoforms in eight mammalian species. The American journal of physiology 274: H1048-1053

Rice R, Guinto P, Dowell-Martino C, He H, Hoyer K, Krenz M, Robbins J, Ingwall JS, Tardiff JC (2010) Cardiac myosin heavy chain isoform exchange alters the phenotype of cTnT-related cardiomyopathies in mouse hearts. Journal of molecular and cellular cardiology 48: 979-988

Roopnarine O, Leinwand LA (1998) Functional analysis of myosin mutations that cause familial hypertrophic cardiomyopathy. Biophysical journal 75: 3023-3030

Sata M, Ikebe M (1996) Functional analysis of the mutations in the human cardiac beta-myosin that are responsible for familial hypertrophic cardiomyopathy. Implication for the clinical outcome. The Journal of clinical investigation 98: 2866-2873

Schiaffino S, Reggiani C (1996) Molecular diversity of myofibrillar proteins: gene regulation and functional significance. Physiological reviews 76: 371-423

Schober T, Huke S, Venkataraman R, Gryshchenko O, Kryshtal D, Hwang HS, Baudenbacher FJ, Knollmann BC (2012) Myofilament Ca sensitization increases cytosolic Ca binding affinity, alters intracellular Ca homeostasis, and causes pause-dependent Ca-triggered arrhythmia. Circulation research 111: 170-179

Seidman JG, Seidman C (2001) The genetic basis for cardiomyopathy: from mutation identification to mechanistic paradigms. Cell 104: 557-567

Semsarian C, Ahmad I, Giewat M, Georgakopoulos D, Schmitt JP, McConnell BK, Reiken S, Mende U, Marks AR, Kass DA, Seidman CE, Seidman JG (2002) The L-type calcium channel inhibitor diltiazem prevents cardiomyopathy in a mouse model. The Journal of clinical investigation 109: 1013-1020

Sequeira V, Wijnker PJ, Nijenkamp LL, Kuster DW, Najafi A, Witjas-Paalberends ER, Regan JA, Boontje N, Ten Cate FJ, Germans T, Carrier L, Sadayappan S, van Slegtenhorst MA, Zaremba R, Foster DB, Murphy AM, Poggesi C, Dos Remedios C, Stienen GJ, Ho CY, Michels M, van der Velden J (2013) Perturbed length-dependent activation in human hypertrophic cardiomyopathy with missense sarcomeric gene mutations. Circulation research 112: 1491-1505

Sherrid MV, Barac I, McKenna WJ, Elliott PM, Dickie S, Chojnowska L, Casey S, Maron BJ (2005) Multicenter study of the efficacy and safety of disopyramide in obstructive hypertrophic cardiomyopathy. Journal of the American College of Cardiology 45: 1251-1258

Shiner JS, Solaro RJ (1984) The hill coefficient for the Ca2+-activation of striated muscle contraction. Biophysical journal 46: 541-543

Shiner JS, Solaro RJ (1984) The hill coefficient for the Ca2+-activation of striated muscle contraction. Biophysical journal 46: 541-543

Slupsky CM, Sykes BD (1995) NMR solution structure of calcium-saturated skeletal muscle troponin C. Biochemistry 34: 15953-15964

Solaro RJ, Moir AJ, Perry SV (1976) Phosphorylation of troponin I and the inotropic effect of adrenaline in the perfused rabbit heart. Nature 262: 615-617

Spindler M, Saupe KW, Ingwall JS (1998) MR spectroscopy of transgenic mice. Magma 6: 109-110

Spoladore R, Maron MS, D'Amato R, Camici PG, Olivotto I (2012) Pharmacological treatment options for hypertrophic cardiomyopathy: high time for evidence. European heart journal 33: 1724-1733

Squire JM (1997) Architecture and function in the muscle sarcomere. Current opinion in structural biology 7: 247-257

Squire JM, Luther PK, Knupp C (2003) Structural evidence for the interaction of C-protein (MyBP-C) with actin and sequence identification of a possible actin-binding domain. Journal of molecular biology 331: 713-724

Stehle R, Kruger M, Scherer P, Brixius K, Schwinger RH, Pfitzer G (2002) Isometric force kinetics upon rapid activation and relaxation of mouse, guinea pig and human heart muscle studied on the subcellular myofibrillar level. Basic research in cardiology 97 Suppl 1: I127-135

Stehle R, Solzin J, Iorga B, Poggesi C (2009) Insights into the kinetics of Ca2+-regulated contraction and relaxation from myofibril studies. Pflugers Archiv : European journal of physiology 458: 337-357

Stelzer JE, Dunning SB, Moss RL (2006) Ablation of cardiac myosin-binding protein-C accelerates stretch activation in murine skinned myocardium. Circulation research 98: 1212-1218

Stienen GJ, Papp Z, Elzinga G (1993) Calcium modulates the influence of length changes on the myofibrillar adenosine triphosphatase activity in rat skinned cardiac trabeculae. Pflugers Archiv : European journal of physiology 425: 199-207

Stienen GJ, Roosemalen MC, Wilson MG, Elzinga G (1990) Depression of force by phosphate in skinned skeletal muscle fibers of the frog. The American journal of physiology 259: C349-357

Stuyvers BD, McCulloch AD, Guo J, Duff HJ, ter Keurs HE (2002) Effect of stimulation rate, sarcomere length and Ca(2+) on force generation by mouse cardiac muscle. The Journal of physiology 544: 817-830

Swartz DR, Moss RL (1992) Influence of a strong-binding myosin analogue on calcium-sensitive mechanical properties of skinned skeletal muscle fibers. The Journal of biological chemistry 267: 20497-20506

Sweeney HL, Straceski AJ, Leinwand LA, Tikunov BA, Faust L (1994) Heterologous expression of a cardiomyopathic myosin that is defective in its actin interaction. The Journal of biological chemistry 269: 1603-1605

Szczesna D, Zhang R, Zhao J, Jones M, Guzman G, Potter JD (2000) Altered regulation of cardiac muscle contraction by troponin T mutations that cause familial hypertrophic cardiomyopathy. The Journal of biological chemistry 275: 624-630

Szczesna-Cordary D, Jones M, Moore JR, Watt J, Kerrick WG, Xu Y, Wang Y, Wagg C, Lopaschuk GD (2007) Myosin regulatory light chain E22K mutation results in decreased cardiac intracellular calcium and force transients. FASEB journal : official publication of the Federation of American Societies for Experimental Biology 21: 3974-3985

Takeda S, Yamashita A, Maeda K, Maeda Y. Structure of the core domain of human cardiac troponin in the Ca2+-saturated form. Nature. 2003;424:35–41.

Takimoto E, Soergel DG, Janssen PM, Stull LB, Kass DA, Murphy AM (2004) Frequency- and afterload-dependent cardiac modulation in vivo by troponin I with constitutively active protein kinase A phosphorylation sites. Circulation research 94: 496-504

Talmadge RJ, Roy RR (1993) Electrophoretic separation of rat skeletal muscle myosin heavy-chain isoforms. Journal of applied physiology 75: 2337-2340

Tardiff JC (2011) Thin filament mutations: developing an integrative approach to a complex disorder. Circulation research 108: 765-782

Tardiff JC, Factor SM, Tompkins BD, Hewett TE, Palmer BM, Moore RL, Schwartz S, Robbins J, Leinwand LA (1998) A truncated cardiac troponin T molecule in transgenic mice suggests multiple cellular mechanisms for familial hypertrophic cardiomyopathy. The Journal of clinical investigation 101: 2800-2811

Tardiff JC, Hewett TE, Palmer BM, Olsson C, Factor SM, Moore RL, Robbins J, Leinwand LA (1999) Cardiac troponin T mutations result in allele-specific phenotypes in a mouse model for hypertrophic cardiomyopathy. The Journal of clinical investigation 104: 469-481

Ter Keurs HE, Shinozaki T, Zhang YM, Wakayama Y, Sugai Y, Kagaya Y, Miura M, Boyden PA, Stuyvers BD, Landesberg A (2008) Sarcomere mechanics in uniform and nonuniform cardiac muscle: a link between pump function and arrhythmias. Annals of the New York Academy of Sciences 1123: 79-95

Tesi C, Colomo F, Piroddi N, Poggesi C (2002) Characterization of the cross-bridge force-generating step using inorganic phosphate and BDM in myofibrils from rabbit skeletal muscles. The Journal of physiology 541: 187-199

Thierfelder L, Watkins H, MacRae C, Lamas R, McKenna W, Vosberg HP, Seidman JG, Seidman CE (1994) Alpha-tropomyosin and cardiac troponin T mutations cause familial hypertrophic cardiomyopathy: a disease of the sarcomere. Cell 77: 701-712

Tobacman LS, Butters CA (2000) A new model of cooperative myosin-thin filament binding. The Journal of biological chemistry 275: 27587-27593

Tobacman LS, Lin D, Butters C, Landis C, Back N, Pavlov D, Homsher E (1999) Functional consequences of troponin T mutations found in hypertrophic cardiomyopathy. The Journal of biological chemistry 274: 28363-28370

Toniolo L, Maccatrozzo L, Patruno M, Caliaro F, Mascarello F, Reggiani C (2005) Expression of eight distinct MHC isoforms in bovine striated muscles: evidence for MHC-2B presence only in extraocular muscles. The Journal of experimental biology 208: 4243-4253

van Dijk SJ, Dooijes D, dos Remedios C, Michels M, Lamers JM, Winegrad S, Schlossarek S, Carrier L, ten Cate FJ, Stienen GJ, van der Velden J (2009) Cardiac myosin-binding protein C mutations and hypertrophic cardiomyopathy: haploinsufficiency, deranged phosphorylation, and cardiomyocyte dysfunction. Circulation 119: 1473-1483

Van Driest SL, Ackerman MJ, Ommen SR, Shakur R, Will ML, Nishimura RA, Tajik AJ, Gersh BJ (2002) Prevalence and severity of "benign" mutations in the beta-myosin heavy chain, cardiac troponin T, and alpha-tropomyosin genes in hypertrophic cardiomyopathy. Circulation 106: 3085-3090

Van Driest SL, Ellsworth EG, Ommen SR, Tajik AJ, Gersh BJ, Ackerman MJ (2003) Prevalence and spectrum of thin filament mutations in an outpatient referral population with hypertrophic cardiomyopathy. Circulation 108: 445-451

Varnava AM, Elliott PM, Baboonian C, Davison F, Davies MJ, McKenna WJ (2001) Hypertrophic cardiomyopathy: histopathological features of sudden death in cardiac troponin T disease. Circulation 104: 1380-1384

Wang Y, Xu Y, Kerrick WG, Wang Y, Guzman G, Diaz-Perez Z, Szczesna-Cordary D (2006) Prolonged Ca2+ and force transients in myosin RLC transgenic mouse fibers expressing malignant and benign FHC mutations. Journal of molecular biology 361: 286-299

Watkins H, McKenna WJ, Thierfelder L, Suk HJ, Anan R, O'Donoghue A, Spirito P, Matsumori A, Moravec CS, Seidman JG, et al. (1995) Mutations in the genes for cardiac troponin T and alpha-tropomyosin in hypertrophic cardiomyopathy. The New England journal of medicine 332: 1058-1064

Whitten AE, Jeffries CM, Harris SP, Trewhella J (2008) Cardiac myosin-binding protein C decorates F-actin: implications for cardiac function. Proceedings of the National Academy of Sciences of the United States of America 105: 18360-18365

Witjas-Paalberends ER, Piroddi N, Stam K, van Dijk SJ, Oliviera VS, Ferrara C, Scellini B, Hazebroek M, ten Cate FJ, van Slegtenhorst M, dos Remedios C, Niessen HW, Tesi C, Stienen GJ, Heymans S, Michels M, Poggesi C, van der Velden J (2013) Mutations in MYH7 reduce the force generating capacity of sarcomeres in human familial hypertrophic cardiomyopathy. Cardiovascular research 99: 432-441

Wolska BM, Keller RS, Evans CC, Palmiter KA, Phillips RM, Muthuchamy M, Oehlenschlager J, Wieczorek DF, de Tombe PP, Solaro RJ (1999) Correlation between myofilament response to Ca2+ and altered dynamics of contraction and relaxation in transgenic cardiac cells that express beta-tropomyosin. Circulation research 84: 745-751

Wolska BM, Wieczorek DM (2003) The role of tropomyosin in the regulation of myocardial contraction and relaxation. Pflugers Archiv : European journal of physiology 446: 1-8

Xu C, Craig R, Tobacman L, Horowitz R, Lehman W (1999) Tropomyosin positions in regulated thin filaments revealed by cryoelectron microscopy. Biophysical journal 77: 985-992

Yang Z, Pascarel C, Steele DS, Komukai K, Brette F & Orchard CH (2002). Na+-Ca2+ exchange activity is localized in the T-tubules of rat ventricular myocytes. Circ Res 91, 315–322.

Zhang R, Zhao J, Mandveno A, Potter JD (1995) Cardiac troponin I phosphorylation increases the rate of cardiac muscle relaxation. Circulation research 76: 1028-1035